

Letter to the Editor

ACP Discussions doi: 10.5194/acp-2018-1193

(Editor - Martin Dameris)

‘Mechanism of ozone loss under enhanced water vapour conditions in the mid-latitude lower stratosphere in summer’

Dear Martin Daneris,

many thanks for handling our manuscript. We prepared and submitted a revised version of our manuscript and are confident that we have satisfactorily addressed all comments of referee #1 and #2. A detailed point-by-point response to all referee comments is attached. Further, a document specifying all changes in the revised manuscript compared to the ACPD version is added.

Best wishes,

Sabine Robrecht

Author Comment to Referee #1: page 2-4

Author Comment to Referee #2: page 5-26

All Changes: page 27-74

Author Comment to Referee #1

ACP Discussions doi: 10.5194/acp-2018-1193

(Editor - Martin Dameris)

‘Mechanism of ozone loss under enhanced water vapour conditions in the mid-latitude lower stratosphere in summer’

We thank Referee #1 for guidance on how to revise our paper. Following the reviewers advice we shortend the description of chemical processes and refer to a potential change of stratospheric dynamics due to an enhancement of the stratospheric sulphur abundance. Our reply to the reviewer comments is listed in detail below. Questions and comments of the referee are shown in italics. Passages from the revised version of the manuscript are shown in blue.

This paper presents a detailed chemical study for a potentially significant ozone depletion in the lowermost stratosphere, using a chemical box-model, with 7-day and 19-day back-trajectory analysis. The study is conducted under conditions of low temperatures (<205 K) and an elevated water vapour mixing ratio, up to 20 ppmv (resulting from convective overshooting events, rather frequent for summertime mid-latitude conditions). These convective events can transport ice crystals into the lowermost stratosphere, where the ice evaporates leading to a local water vapour increase. The sensitivity to high Cl_{ly} mixing ratios is also addressed. The authors analyze with plenty of details the catalytic chemical cycles involving ClO_x, NO_x, HO_x and leading to a perturbed balance of ozone production and destruction taking place in the lowermost stratosphere. The study takes inspiration from previous published works (Anderson et al., 2012; Anderson and Clapp, 2018); the authors conclude that the combined effects of temperature, water vapour and chlorine on the ozone loss process are consistent in their study with respect to these previous ones. I think that this study may help clarify important points regarding the ozone sensitivity to elevated water vapour conditions in the lowermost stratosphere and for this reason I recommend publication on ACP. In my opinion, a few improvements could be made in the manuscript, mainly for completeness and for improving readability.

Specific Comments

(1) Chemical cycles are essentially those leading to polar ozone depletion and widely described in previous literature. For this reason, I suggest moving large part of chemical details from the main text to a specific Appendix or in supplementary material. In particular, section 3.2.2 is in my opinion way too detailed and should be simplified focusing of the evidences of Fig. 5 (which is clear and exhaustive).

As proposed, we decided to shorten following aspects to focus on the analysis of lowermost stratospheric ozone chemistry occurring under enhanced water vapour conditions:

- We removed the chemical formulation of the ClO-Dimer-Cycle and the ClO-BrO-cycle in the description of ozone loss cycles leading to polar ozone loss and moved the formulation of cycle C3 from the introduction to section 3.2.2.
- The description of ozone formation at low water vapour mixing ratios is shortened by removing the formulation of ozone chemistry and NO reactions in Section 3.1.
- The detailed explanations of the water vapour dependence of R12 ($\text{OH}+\text{O}_3$) and R19 ($\text{OH}+\text{CO}$) in Section 3.2.2 (P.17,l.18-26, ACPD version of the manuscript) is removed.
- The description of the maintenance of activated chlorine is simplified by moving the chemical formulation of cycle C7 and C8 to the appendix. They are substituted by a new scheme (see Fig. 1 of this reply), which illustrates the important relations for the maintenance of elevated chlorine.

(2) The authors clearly state that their box-model ignores mixing with outside air poorer of water vapour, so that their calculated ozone losses should be interpreted as an extreme case. They also suggest a possible use of their findings in global modelling of the atmosphere for future experiment of sulphate geoengineering under changing climate conditions, or in case of major volcanic eruptions. It should be mentioned that in these cases the large scale

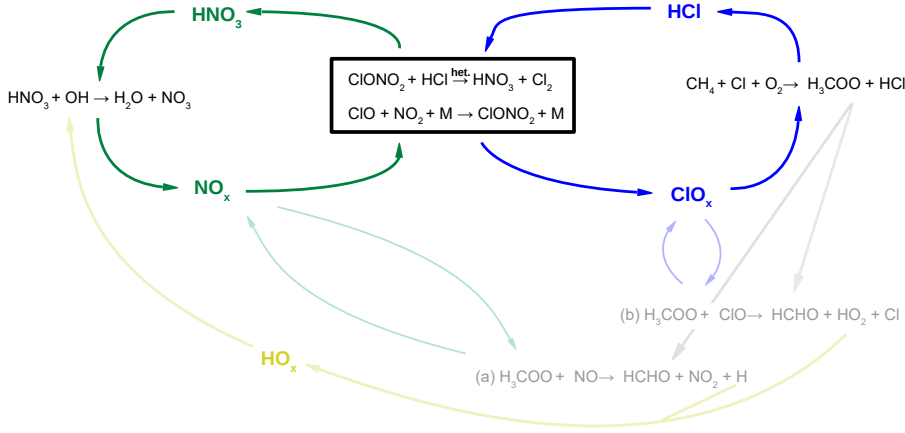


Figure 1: Scheme to illustrate the balance between chlorine activation and chlorine deactivation (blue, right) and NO_x activation and deactivation (green, left). The heterogeneous reaction $\text{ClONO}_2 + \text{HCl}$ (R1) links both cycles. Additional reaction pathways balancing radicals are shown in light colour.

latitudinal mixing of atmospheric tracers in the lower branch of the Brewer-Dobson circulation could be significantly affected in sulphate-perturbed conditions due to geoengineering or major tropical eruptions, both leading to a different level of isolation of the tropical pipe with the mid-latitudes. Eddy heat fluxes could also be perturbed, thus affecting mid-latitude temperatures in the lower stratosphere. Recent works have addressed these specific points (e.g., Visoni et al., 2017).

Visoni, D., et al. : Sulphate Geoengineering Impact on Methane Transport and Lifetime: Results from the Geoengineering Model Intercomparison Project (GeoMIP), Atmos. Chem. Phys., 17, 11209-11226, doi:10.5194/acp-17-11209-2017, 2017.

We mention the effect of sulphate geoengineering on lowermost stratospheric dynamics in Section 6 (P.27, 1.27–31, revised version of the manuscript). We added the following paragraph.

Applying solar geoengineering would also affect the temperature in the lower-most stratosphere by perturbing the Eddy-heat fluxes and would change the lower stratospheric dynamic (Visioni et al., 2017). It would affect large scale latitudinal mixing of atmospheric tracers in the lower branch of the Brewer-Dobson-Circulation leading to a different level of isolation of the tropical pipe with mid-latitudes and would result in a different chemical composition of the lower mid-latitude stratosphere.

References

Visioni, D., Pitari, G., Aquila, V., Tilmes, S., Cionni, I., Di Genova, G., and Mancini, E.: Sulfate geoengineering impact on methane transport and lifetime: results from the Geoengineering Model Intercomparison Project (GeoMIP), *Atmos. Chem. Phys.*, 17, 11 209–11 226, doi: 10.5194/acp-17-11209-2017, 2017.

Author Comment to Referee #2

ACP Discussions doi: 10.5194/acp-2018-1193

(Editor - Martin Dameris)

‘Mechanism of ozone loss under enhanced water vapour conditions in the mid-latitude lower stratosphere in summer’

We thank Referee #2 for comprehensive guidance on how to revise our paper. Following the reviewers advice we shortened parts of the paper to improve the readability. Our reply to the reviewer comments is listed in detail below. Questions and comments of the referee are shown in italics. Passages from the revised version of the manuscript are shown in blue.

General comments: The paper by Robrecht et al. investigates a potential ozone loss mechanism in the mid-latitude lower stratosphere under enhanced water vapour conditions and low temperatures, initiated by heterogeneous chlorine activation on liquid aerosol particles. For that purpose the authors conducted box model simulations along 7(19)-days backward trajectories with the CLaMS model. Besides a detailed chemical analysis of their standard case, they investigated the sensitivity of the proposed ozone loss mechanism to water vapour, mixing ratios of Cl_y , NO_y , and Bry , sulphate content and temperature. Overall, I have no doubts that the applied methods and presented findings are valid and of wider interest for the scientific community, and therefore, I recommend this paper for publication in ACP. However, the paper is rather lengthy and the presentation of so many different case studies and sensitivity simulations does not increase the readability of the manuscript. Below I tried to make some suggestions for clarifications. Furthermore, I would like to encourage the authors to address or discuss the overall importance of the discussed ozone depletion mechanism. At the very end it is written that for observed conditions no ozone depletion was simulated, but it would be great to put the presented results more into a global and climatological perspective

Specific Comments

- Abstract: It is a bit weird that the abstract does not clearly mention that the discussed ozone loss mechanism is initiated by heterogeneous chlorine activation on binary (ternary?) solution droplets. There are only hints in this direction, namely the impact of volcanic eruptions, geoengineering etc.

Following the reviewer's advice, we mention chlorine activation as initial step for the ozone destruction process in the abstract.

The associated potential ozone loss process requires low temperatures and an elevated water vapour mixing ratio. Since this process is initiated by heterogeneous chlorine activation on liquid aerosols, an increase in sulphate aerosol surface area due to a volcanic eruption or geoengineering could increase its likelihood of occurrence.

Introduction: Again, it would be good to clearly state that the ozone loss process proposed by Anderson et al. involves sulphate aerosol particles. This would put the subsequent description of heterogeneous chlorine activation and catalytic ozone loss cycles much more into perspective.

We revised the first part of the introduction to mention that the mechanism proposed by Anderson et al. involves sulphate aerosols and to make clear, that it is initiated by heterogeneous chlorine activation.

Anderson et al. (2012) proposed a potential ozone depletion in the mid-latitude stratosphere in summer on liquid sulphate aerosols under conditions of enhanced water vapour and low temperatures. They proposed this chemical ozone loss to be initiated through heterogeneous chlorine activation and to be driven by catalytic ozone loss cycles related to ozone loss known from polar regions in early spring (e.g. Grooß et al., 2011; Solomon, 1999; Vogel et al., 2011).

P2, l15: Is the ClOx definition used here not a bit odd? Why is Cl₂ not included? This would also facilitate the understanding of Fig.4f, because then it would be clear where the chlorine released from HCl during the first phase did go. Alternatively, one could also show Cl₂ in Fig. 4.

Many thanks for this comment. We added Cl_2 to the definition of ClO_x and adapted Fig. 4. The sentence discussing the delay between HCl reduction and ClO_x formation (P. 13 l. 11-12 in the ACPD version of this manuscript) is removed.

- *P3, l17/18: By how much has water vapour to be enhanced to allow Cl activation at higher temperatures? Can you provide a number?*

One question of our study is to estimate how much water vapour has to be enhanced to allow chlorine activation at higher temperatures. For our standard case 10.6 ppmv H_2O are necessary for the occurrence of chlorine activation. To clarify that in the text, we added the following sentence to the introduction.

An aim of our study is to investigate how much water vapour has to be enhanced for chlorine activation to occur at these higher temperatures.

- *Model set-up: Why do you neglect NAT and ice in this study? NAT is probably not an issue, but how about ice? Especially since you mention a potential impact of ice particles on the water vapour threshold for Cl activation on liquid aerosol particles due to different heterogeneous reactivities (p32, l3-5).*

We decided to calculate heterogeneous chemistry only on liquid particles to have a better comparability with the studies of Anderson et al. (2012) and Anderson and Clapp (2018). In their studies, they investigate the impact of binary $\text{H}_2\text{O}/\text{sulphate}$ aerosols on mid-latitude ozone chemistry. To clarify this in the text, we added the following sentence to Sec. 2 (Model Setup).

In contrast to the setup in Grooß et al. (2011), Müller et al. (2018) and Zafar et al. (2018), only formation of liquid particles (both binary $\text{H}_2\text{O}/\text{H}_2\text{SO}_4$ and ternary $\text{HNO}_3/\text{H}_2\text{O}/\text{H}_2\text{SO}_4$ solutions) is allowed (i.e. no NAT or ice particles are formed in this model setup) to enable a better comparability with the studies of Anderson et al. (2012, 2017) and Anderson and Clapp (2018).

In our study, we mention that chlorine activation on ice has been observed and analysed in former studies (p.31 l. 29-31, p.33, l.12–15, ACPD version). We decided to not insert a further case study, which additionally shows the

impact of ice formation, to provide a better readability. We think that to reasonably show the impact of ice formation on the ozone process, however a comprehensive study would be necessary, which is beyond the scope of our current study.

- Model set-up: Could provide a short description of the treatment of liquid aerosol particles in your model? In Table 1 you provide the gas phase equivalent H₂SO₄ mixing ratio and Fig. 4 ff show the surface area density, but some more information would be great. For example, which H₂SO₄ wt% in the liquid aerosol particles is reached under the assumed high water vapour/low temperature conditions?

As proposed, we included a description of liquid aerosol treatment in Sec. 2 (P.4, l. 8, revised version of the manuscript).

For heterogeneous particle formation, the initial liquid aerosol number density ($N_0=10.0\text{ cm}^{-3}$), the standard deviation of the logarithmic normal distribution of the particle size ($\sigma=1.8$), and the gas phase equivalent of the amount of sulfuric acid in the aerosol (for chosen values see Tab. 1) are set prior to the simulation. The gas phase equivalent is used to calculate the density of liquid particles as described in the study of Shi et al. (2001) (binary solutions) and Luo et al. (1996) (ternary solutions). Particle size and surface area density are calculated based on the density of liquid particles, the areosol number density, and the standard deviation.

Furthermore, we added an additional plot (in Fig. 8, revised version of the manuscript) as shown in Fig. 1 of this reply, which presents the H₂SO₄ wt% depending on the water vapour mixing ratio. The following description is included in Section 4.2 (p.19, l.19 revised version of the manuscript).

The particles H₂SO₄ wt% decreases for all cases with increasing water vapour from more than 50 wt% at 5 ppmv H₂O to around 20 wt% at 20 ppmv H₂O due to an increasing uptake of H₂O in the thermodynamic equilibrium.

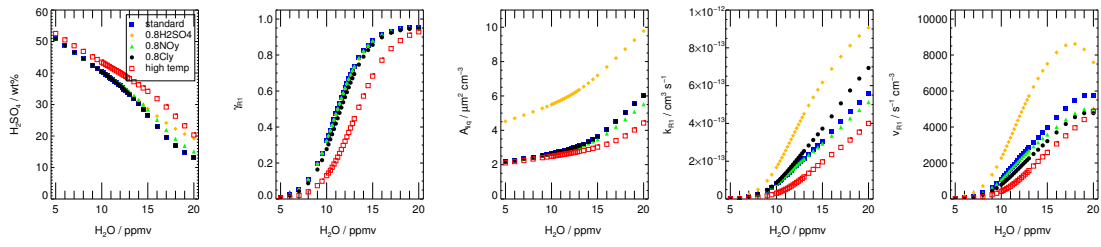


Figure 1: Dependence on water vapour of the rate of the the main heterogeneous chlorine activation reaction $R1$, the rate coefficient (k_{R1}), the γ -value γ_{R1} , the liquid surface area density A_{liq} , and the H_2SO_4 weight %. Presented parameters correspond to the values after the first chemistry time step of the box-model simulation. Additionally the impact of an enhanced sulphate content (0.8 ppbv H_2SO_4 , yellow), reduced NO_y (0.8 NO_y , green), reduced Cl_y (0.8 Cl_y , black) and enhanced temperatures (red) is shown. The standard case is shown as blue squares.

- P5, l32/33: What was the overall background H_2O mixing ratio for the calculated trajectories? And temperature? By how much are the selected trajectories colder?

In the Figure 2 of this reply, we illustrate the water vapour and temperature conditions of the SEAC⁴RS measurements and the calculated backwards tra-

jectories. The top panel shows the distribution of measured water vapour and temperature during the SEAC⁴RS campaign at a pressure of less than 100 hPa of all flights. This pressure range was chosen to select stratospheric measurements. The overall background water vapour is around 6–7 ppmv. We calculated trajectories starting at the location of the measurements with enhanced water vapour of at least 10 ppmv H₂O. The temperature along these backward trajectories (in total 294) is shown in the bottom panels. The left panel shows the mean temperature and the right panel the minimal temperature of each calculated trajectory. The temperature of our standard trajectory is marked with a red arrow. Most of the trajectories have a mean temperature of 201–202 K and a minimal temperature of 199–200 K. Our standard trajectory has a mean temperature of 199 K and a minimal temperature of 197 K. In total, 28 trajectories with similar low temperatures were calculated. Most of these trajectories correspond to higher measured CH₄ mixing ratios and thus very low Cl_y mixing ratios. Only three of the trajectories with very low temperatures and enhanced water vapour correspond to measurements with chlorine high enough to show a visible impact on ozone chemistry.

We added in Sec. 2.2 (p.5, l.1–4, revised version of the manuscript) as follow that Cl_y was a criteria for choosing our standard trajectory in addition to the water vapour mixing ratio and temperature.

A selected example of calculated trajectories is shown in Fig. 1 (revised version). This trajectory was chosen for the chemical analysis, because its initial conditions exhibited enhanced water vapour relative to the overall background, low temperatures and enhanced Cl_y (higher than for comparable water vapour and temperature conditions). Cl_y was calculated from tracer-tracer correlations (see Sec. 2.3).

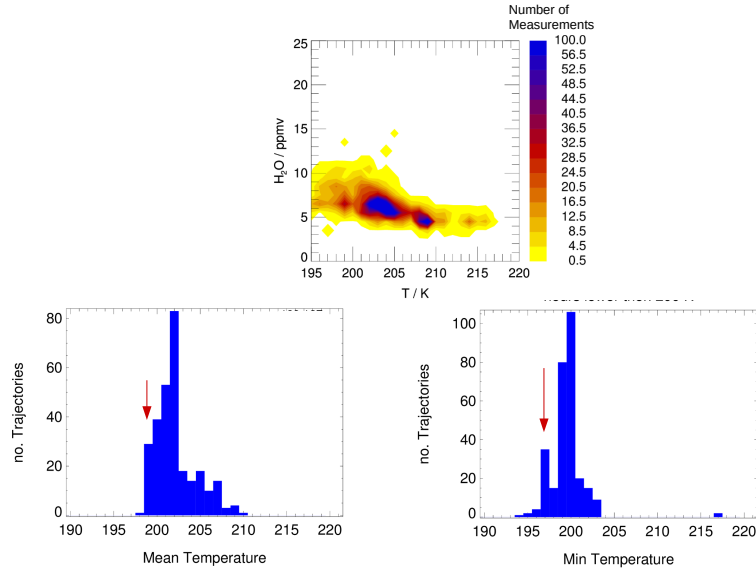


Figure 2: Top panel: Frequency distribution of water vapour mixing ratios and temperature measured during all flights of the SEAC⁴RS campaign at a pressure level of less than 100 hPa. The colour scheme shows the number of measurements in that temperature- and water vapour regime. Bottom panels: Temperature along all backward trajectories (calculated) started at the location of a measurement with a water vapour mixing ratio larger than 10 ppmv. On the y-axis, the total number of trajectories in that temperature regime is plotted. The mean temperature (left) and the minimum temperature (right) of each trajectory is shown.

- Sect. 2.3 Initialization: In Table 1 it is mentioned that the ClO_x species were initialized with 0. Ok, in the mid-latitude lower stratosphere most chlorine is deactivated, but I am wondering how your initial phase in Fig. 4 would look like, if the trajectories had started with non-zero ClO_x? Maybe you could add a short discussion.

We conducted a further simulation, assuming ClO_x counts 1% of total Cl_y. This yields slightly more ClO_x in the initial phase. But it changes neither the rate of R1 nor the water vapour threshold or the time, when ozone destruction starts significantly. We added a small discussion in Sec. 2.3.1 after

the sequence about Cl_y initialization (P.6, l.13–15, revised version of the manuscript).

Since most Cl_y is deactivated in the mid-latitude lowermost stratosphere, the initial mixing ratio of ClO_x species is assumed to be zero. A simulation assuming a ClO mixing ratio of 1% of total Cl_y , does not yield a significant difference to our standard case.

- Sect. 2.3.3: I do not really see the point of discussing the MACPEX case. In my view it is just another special case that could be covered by the sensitivity simulations. For the sake of clarity, I would suggest to leave it away.

We agree with the reviewer, that the discussion of the MACPEX case is neither enhancing the readability of the paper nor leading to other results than our standard case based on SEAC⁴RS measurements. However, we think that presenting a further case, which yields similar sensitivities as the SEAC⁴RS simulations, complements our results. Hence, we decided to present the MACPEX case in the appendix and adapted the figures and the text in Sec. 2. In Section 4.1, the last sequence (P. 18, l. 4–8, revised version of the manuscript) was changed, but still refers to the MACPEX case:

As a further example for an event with high stratospheric water vapour mixing ratios based on airborne measurements, simulations based on measurements during the Mid-latitude Airborne Cirrus Properties Experiments (MACPEX) were conducted. This campaign was based in Texas during springtime 2011 and hence prior to the formation of the North American Monsoon (NAM). A detailed description of this MACPEX case is given in the appendix (A1). For the MACPEX case, changes in sulphate, Cl_y and NO_y mixing ratios affect the water vapour threshold similarly to that observed for the SEAC⁴RS trajectory. Thus, the MACPEX results confirm the SEAC⁴RS findings. Therefore, we conclude that in the considered temperature range (~ 197 – 202 K), an ozone reduction occurs after exceeding a water vapour threshold and that this threshold varies with Cl_y , NO_y , sulphate content and temperature.

- Fig. 2: What is the rationale behind the chosen H_2O mixing ratios of 5 and 15 ppmv? This choice seems a bit arbitrary to me. Why do you not use the 10.6 ppmv H_2O of your standard case?

This study is aimed to investigate the sensitivity of mid-latitude lowermost stratospheric ozone chemistry to water vapour and to analyse the chemical mechanisms in detail. The best way to show the differences between the ozone chemistry at low and high water vapour mixing ratios is to choose water vapour mixing ratios, which are clearly in that water vapour regime. To be able to show the chlorine activation phase, we decided to take a water vapour mixing ratio of 15 ppmv instead of 20 ppmv. At 20 ppmv chlorine activation is very fast and reaction rates and mixing ratios are changing strongly. Since the mixing ratio of 10.6 ppmv H_2O of the realistic case is elevated comparing to the overall background conditions and close to the threshold, we decided against taking this case to illustrate the chemistry in a low water vapour regime.

To clarify this decision we added the following sentence in Sec. 3 (P.8, L.12, revised version of the manuscript).

These water vapour mixing ratios are chosen, because they are clearly in the regime of the low water vapour background (5 ppmv) of the lower mid-latitude stratosphere and of enhanced water vapour (15 ppmv) as it can be reached through convective overshooting events.

Furthermore, we clarified that choice in the description of Fig.2.

These water vapour mixing ratios are chosen, because they are clearly in the regime of low (5 ppmv) and elevated (15 ppmv) water vapour.

- P10, discussion of Fig. 3: In line 3-5 the water vapour threshold is defined as H_2O mixing ratio “at which the end ozone value clearly falls below the end ozone that is reached for low water vapour amounts.” What is meant by “clearly”? That sounds a bit vague. Can you be a bit more quantitative? Furthermore, it is stated that “by 12 ppmv of water vapour, the system is clearly in an ozone destruction regime.” But is 12 ppmv not just the water vapour mixing ratio at which the transition between ozone production to ozone destruction occurs? At lower H_2O values, end ozone is higher than initial ozone.

We agree with the reviewer that the description of the threshold is vague formulated. To make the formulation of the threshold more clear, we de-

terminated the lowest water vapour mixing ratio at which chlorine activation occurs to be the threshold. We changed the discussion of Fig. 3 as follows:

Blue squares lying above that line are cases with ozone production, those lying below that line are cases with ozone destruction. The decrease of final ozone with higher water vapour mixing ratios is related to chlorine activation. The time until chlorine activation occurs in the simulation is plotted in Fig. 3 as violet triangles, assuming that chlorine activation occurs when the ClO_x mixing ratio exceeds 10% of total Cl_y (Drdla and Müller, 2012). Shown is the time when chlorine activation first occurs in the model. Since the ClO_x/Cl_y ratio is dependent on the diurnal cycle, the 24-hours mean value of the ClO_x mixing ratio was used to determine the chlorine activation time. For low water vapour mixing ratios, no chlorine activation time is plotted, because no chlorine activation occurs. For chlorine activation to occur, a threshold in water vapour has to be reached. Here, we determine the lowest water vapour mixing ratio at which chlorine activation occurs as water vapour threshold (marked by a blue arrow in Fig. 3). In our standard case, this threshold is reached at a water vapour mixing ratio of 10.6 ppmv. Between 10.6 and 12 ppmv H_2O , chlorine activation leads not to an ozone destruction during the 7-day simulation. For 10.6 to 11.2 ppmv H_2O , chlorine only remains activated for up to 28 h, because of increasing temperatures, and almost no impact on final ozone is observable. By 12 ppmv of water vapour, chlorine activation yields ozone destruction within the 7-day simulation. Near the water vapour threshold, the activation time is 24 to 36 hours and it decreases with increasing water vapour mixing ratios. It requires only 5 hours at 20 ppmv H_2O .

-Fig. 4b: Where does the first sharp peak in the light blue line ($\text{ClONO}_2 + \text{HCl}$) come from?

In the chosen standard case (15 ppmv), the chlorine activation reaction R1 already occurs significantly within the first diurnal cycle. This would yield an increase in ClO_x . Since the NO_x mixing ratio is high at the same time, every formed ClO_x leads to the formation of ClONO_2 . Hence, the ClONO_2 mixing ratio increases (Fig. 4f) and thus the rate of R1 ($\text{ClONO}_2 + \text{HCl}$). The chlorine activation chain (P.13, l. 3–7, ACPD version of the manuscript) requires light to transform Cl_2 to Cl-radicals. During night ClO_x is accumulated in Cl_2 and Cl_2O_2 . Hence, there is no ClO from which ClONO_2 could be formed

and the rate of R1 decreases rapidly. This yields the first sharp peak in the light blue line in Fig. 4b. For a better readability, we decided to not add this discussion to the paper.

- P13, l20ff: *Shouldn't this sentence read: Dependent on temperature and water vapour content, the HNO₃ formed remains in the condensed phase.? And further down: ... 64% of the HNO₃ remains in the condensed phase on the day with the lowest temperature, while at higher temperatures... 85% of HNO₃ are released to the gas phase.... Is the HNO₃ shown in Fig. 4d gas-phase only or total HNO₃?*

As the reviewer recommended, we revised the text as follows:

Dependent on temperature and water vapour content, the HNO₃ formed remains in the condensed particles. In the standard simulation using 15 ppmv H₂O, 64% of HNO₃ remains in the condensed phase on the day with the lowest temperature (197.3 K, 2 Aug 2013), while at higher temperatures (4–7 August 2013) 85% of HNO₃ are released to the gas phase.

To clarify that HNO₃ in Fig. 4d is total HNO₃ (gas phase + condensed), we revised the description of Fig. 4.

Panels (d), mixing ratio of HNO₃ (gas phase + condensed), NO_x and ClONO₂,
...

- P18/19 cycles C7 and C8: *I have a hard time to follow the construction of these reaction cycles. My impression is that the authors combined different reactions until they ended up with the intended net reaction. For example: In R29 NO₂ is formed, which in the next step photolyses (R15). Lower down another NO₂ is formed (R32), but this time it reacts with ClO to ClONO₂ (R22).*

We revised the part about the maintenance of activated chlorine in Sec. 3.2.2. The detailed description of the pathways C7 and C8 is moved to the appendix. In Sec. 3.2.2, it is substituted by a scheme, which focuses on the main reactions to balance chlorine activation and deactivation as well as HNO₃ and NO_x. This scheme is shown in Fig. 3 of this reply.

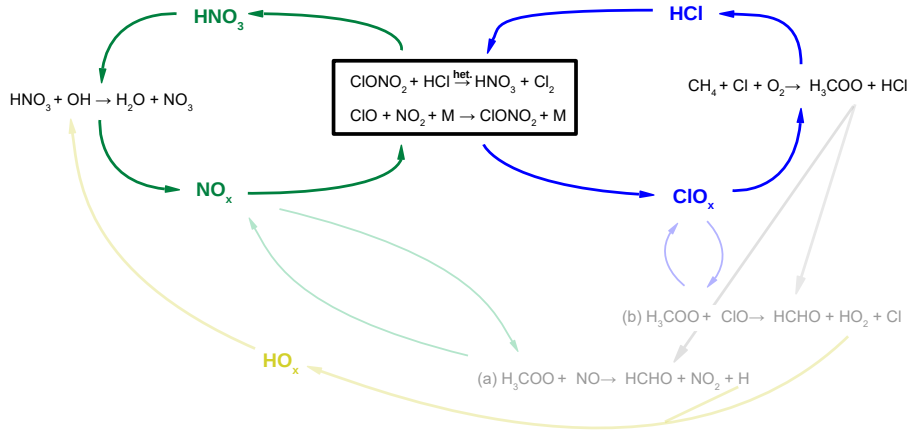


Figure 3: Reaction scheme to illustrate the balance between chlorine activation and chlorine deactivation (blue, right) and NO_x activation and deactivation (green, left). The heterogeneous reaction $\text{CIONO}_2 + \text{HCl}$ (R1) links both cycles. Additional reaction pathways, which balance radicals are shown in light colours.

- P20, l 14-16: I think it would be helpful to mention the reason for the lower H_2O threshold under enhanced sulphate conditions, namely the increased SAD. In general, the presentation of the model results would benefit from some more explanation of the underlying processes. This holds also for Sect. 4.2 and the sensitivity of the uptake coefficient to H_2O or temperature. By the way, why is the $10\text{xH}_2\text{SO}_4$ case not shown in Fig. 7?

The sensitivity of the water vapour threshold to temperature, sulphate, Cl_y and NO_y is described in Sec. 4.1 and explained in Sec. 4.2. To clarify this, we added a reference to Section 4.2 in Sec. 4.1 (P.18, l.2, revised version of the manuscript).

The sensitivity of the water vapour threshold to temperature, sulphate abundance and Cl_y and NO_y mixing ratio is explained in Section 4.2.

... In general, the presentation of the model results would benefit from some more explanation of the underlying processes. This holds also for Sect. 4.2

and the sensitivity of the uptake coefficient to H_2O or temperature. ...

To go into the underlying processes, we mention that the γ -value depends on the weight-% on sulphuric acid in the particles (which is known from laboratory studies). Therefore a further panel illustrating the dependence of the H_2SO_4 wt% on the water vapour mixing ratio was included in Fig. 8 of the revised version of the manuscript (Fig. 1 of this reply). We revised the text in Sec. 4.2 (p.19, l.11–23, revised version of the manuscript):

The γ -value describes the uptake of $ClONO_2$ into liquid particles due to the decomposition of $ClONO_2$ during reaction R1 and is thus a measure of the probability of the occurrence of this heterogeneous reaction (Shi et al., 2001). Laboratory studies showed a dependence of γ_{R1} on the solubility of HCl in the droplet, which generally increases for a lower H_2SO_4 fraction in the particle (H_2SO_4 wt%) (Elrod et al., 1995; Hanson, 1998; Zhang et al., 1994; Hanson and Ravishankara, 1994). From Eq. 2 it is obvious that a large surface area A_{liq} and a high γ -value γ_{R1} increase k_{R1} and thus the heterogeneous reaction rate v_{R1} .

In Figure 8, the impact of the water vapour content on the H_2SO_4 weight-percent, γ_{R1} , A_{liq} , k_{R1} and the reaction rate v_{R1} is shown. To avoid the influence of R1 itself on these parameters as much as possible, these parameters are selected for 1 August 2013 at 13:00 UTC. This point in time corresponds to the values after the first chemistry time step during the chemical simulation. The particles H_2SO_4 wt% decreases for all cases with increasing water vapour from more than 50 wt% at 5 ppmv H_2O to around 20 wt% at 20 ppmv H_2O due to an increasing uptake of H_2O in the thermodynamic equilibrium. The standard case is illustrated in blue squares (Fig. 8) and exhibits a strongly increasing gamma value especially for water vapour mixing ratios between 9 and 14 ppmv due to a lower H_2SO_4 wt%. In the same water vapour range, the liquid surface area density A_{liq} increases slightly. It increases more for higher water vapour mixing ratios because of HNO_3 uptake into the particles.

...By the way, why is the 10x H_2SO_4 case not shown in Fig. 7?

The aim of Fig. 7 (ACPD version of the manuscript, Fig. 8 of revised version of the manuscript, Fig 1 in this reply) is to illustrate the sensitivity of the water vapour threshold. To focus on this processes, we decided to not

show the 10xH₂SO₄ case here. The 10xH₂SO₄ case yields higher values for the surface area, the reaction rate and the rate constant. If we would show also the 10xH₂SO₄ case, the detailed discussion in Sec. 4.2 would not benefit from Fig. 7 (ACPD version of the manuscript, Fig. 8 of revised version of the manuscript).

- P20, discussion of Fig. 6b: I do not understand the statement that similar conclusions as for the SEAC⁴RS trajectory hold for the MACPEX trajectory. For almost all cases final O₃ is higher than initial O₃. And why is there only a subset of sensitivities shown for the MACPEX trajectory? Why not also +1K and 10xH₂SO₄?

The statement refers to the sensitivity of the water vapour threshold (and thus chlorine activation) to Cl_y, NO_y, temperature and sulphate. This sensitivity is similar in the MACPEX and SEAC⁴RS case. In the MACPEX case, final ozone is higher than initial ozone because of the low Cl_y mixing ratio (~55 pptv). Hence, the catalytic ozone loss cycles have lower rates and ozone is destroyed slower. We added the 10xH₂SO₄ and +1 K case to Fig. 6b (ACPD version of the manuscript, Fig. B2 in the revised version of the manuscript).

- Fig. 6: What is the rationale for the 3xH₂SO₄ case?

The 3× H₂SO₄ case is shown here as well, because it is the lowest H₂SO₄ amount, which would yield ozone destruction in the realistic case (see Sec. 5.2).

- P25, l3-5: I do not fully understand this argumentation. Do you mean that there is no longer enough ClONO₂ available to react with the HCl taken up by the condensed particles and that therefore the enhanced HCl uptake does not lead to further chlorine activation and ozone loss?

This argumentation only refers to ozone destruction, not also chlorine activation. After chlorine activation occurred, ozone loss is driven by chlorine catalysed ozone loss cycles. The more chlorine is available in the gas phase, the more ozone can be destroyed by these cycles. An uptake of HCl into the condensed particles reduces gas phase chlorine. Hence, also the chlorine catalysed ozone loss cycles have lower rates and less ozone is destroyed.

- Fig. 8: This figure nicely shows the different ozone regimes as a function of temperature and H₂O for two different sulphate conditions. Would it possible to provide such figure also for Cly, Bry, NO_y sensitivities? I am aware that this is a multi-dimensional problem, but I think it would be really helpful to get an overview under which conditions ozone formation and ozone depletion occurs. This would also help to get a better understand of the importance of this mechanism on larger scales.

We did the same plot for the 0.8 Cl_y, 0.8 NO_y and 0.5Br_y case (see Fig. 5 of this reply). Only minor differences regarding the standard case are observable. For the 0.8 Cl_y and the 0.5 Br_y case, less ozone is destroyed if chlorine activation occurs and the chlorine activation line is slightly shifted. Assuming the 0.8 NO_y case yields a minor shift of the chlorine activation line. Since these tendencies are rather small, we think they are more clear in Fig. 7 of the revised version of the manuscript. Hence, we decided against showing these plots in the paper.

We agree with the reviewer that it would be helpful to apply the processes analysed here on a larger scale also showing the climatological perspective. Therefore, we started a second comprehensive study looking on the likelihood of the occurrence of ozone loss in the WACCM model at mid-latitudes in the lowermost stratosphere that is beyond the scope of our current study. The study here is mainly focused on the mechanisms itself. To enable here already an estimation for the relevance of this process under further conditions, we conducted the sensitivity studies (0.8Cl_y, 0.8NO_y, 0.5 Br_y, several H₂SO₄ abundances and temperatures) and case studies (other time duration, observed SEAC⁴RS conditions, MACPAX case). These additional studies give an estimation for extending the results of this study to a larger scale.

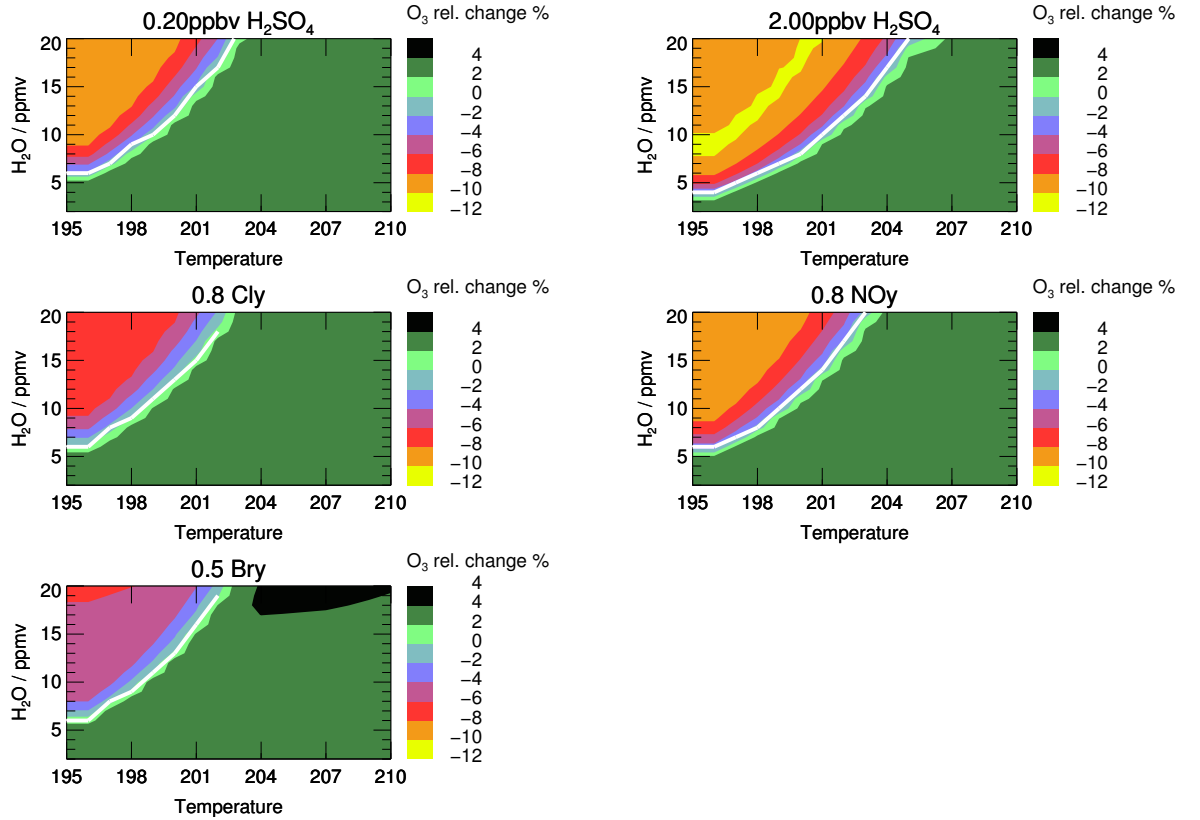


Figure 4: Relative ozone change during the 7-day simulation along the standard trajectory dependent on temperature and H_2O mixing ratio for several conditions. The white line corresponds to the water and temperature dependent chlorine activation threshold. In the top-panels, climatological non enhanced (left panel) and enhanced (right panel) sulphate conditions are shown. In the middle panels the impact of a reduction of Cl_y (left) and NO_y (right) and in the bottom panel of Br_y on the ozone change are shown.

- Sect. 5: As mentioned above I think the case studies are too much and do not help to provide further insights into the main chemical mechanism. Its rather confusing to distinguish the various atmospheric compositions assumed for the individual model simulations. In particular the 19-days case seems

trivial to me: longer time under cold and humid conditions, more ozone loss.

We agree that the sensitivity studies are very detailed and comprehensive. But we think, that they give an insight in the sensitivities of the ozone loss processes and thus enable to apply this processes on a larger scale of realistic conditions than only the chosen example. To make this part less excessive, we moved the chemical details of the ‘Case of high Cl_y ’, the ‘Reduced Br_y case’ and the ‘19-day Simulation’ to supplemental material. We only show the effect of these cases on the water vapour threshold in a new Figure (see Fig. 5 of this reply, Fig. 11 of the revised version of the manuscript). We did not change the ‘Case based on observations’.

Technical corrections:

- P3, l19: *hypothesis hat* → *hypothesis that*
- P4, l8: *ans* → *and*
- P4, l20: $\text{HNO}_3 + 2\text{N}_2\text{O}_5$
- P8, l3: N_2O , 2 should be subscript
- P9, l28: ClO_x , x should be subscript
- P16, l3: *simultaneous* → *simultaneous*
- P17, l29: *HCl-formating* → *HCl-forming*
- P34, l19: *and extreme* → *an extreme*

As the reviewer recommended, we revised these sequences in the text.

- *Units: The text is a mixture of ppb/ppt and ppbv/pptv. I assume it is always volume mixing ratio?*

We revised the text to use only the volume mixing ratio.

- *Chemical reactions: It would be nice to mark heterogeneous reactions as such.*

In the revised version of the manuscript, heterogeneous reactions are marked ().

- *Table 1: I would suggest to add Cl_y and NO_y for completeness. And are 0.6 ppbv and 2.0 ppbv H_2SO_4 not also sensitivity simulations?*

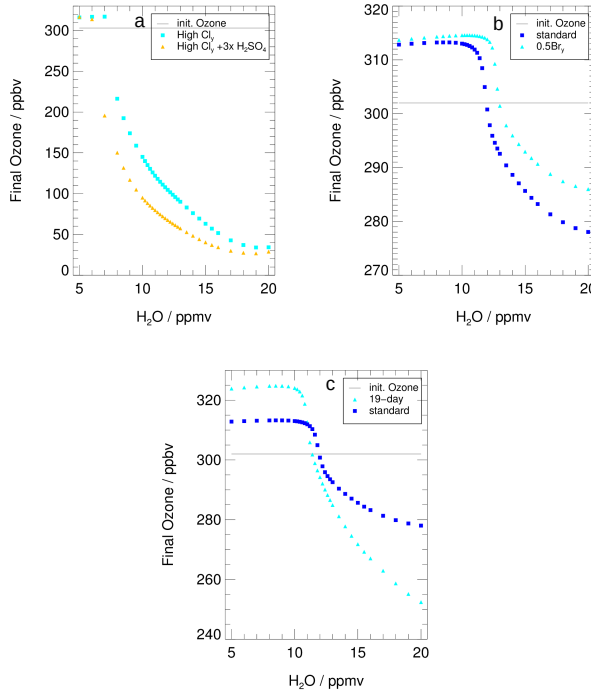


Figure 5: The water dependent final ozone value is shown for (a) the “Case of high Cl_y ” (see Tab. 1 for NO_y and Cl_y initialisation) assuming background aerosol (light blue) and tripled H_2SO_4 (yellow), (b) reduced Br_y (light blue, “Reduced Br_y case”), and (c) an extended time period of activated chlorine (light blue, “19-day simulation”). In panel (b) and (c) also final ozone of the standard case is shown (blue). Initial ozone is marked with a grey line. Note that the scale of all y-axis differ.

As proposed by the reviewer, we added Cl_y and NO_y to Table 1 and moved the initialisations with enhanced H_2SO_4 (0.6 and 2.0 H_2SO_4) to the column, which presents the sensitivity studies.

- Fig 1.: It would be nice to mark the time of measurement by a red square or a vertical line also to the left panels. And maybe the tropopause altitude at the location of the air parcel could also be added to the left panel.

As recommended by the reviewer, we mark the time of measurement in the left panels of Fig. 1 with a vertical red line as well as the tropopause at the location of the air parcel with a horizontal grey line.

- Fig. 4, 9, 10, 11, 12: Which time of day do the x-axis tick marks refer to? One can infer night-/day-time from the reactions with OH, but it would be helpful to provide this information, e.g., in the caption.

In the ACPD version of the manuscript, the x-axis tick marks refer to 00:00 UTC. In the revised version of the manuscript, they refer to 00:00 local time, which corresponds to 06:00 UTC on that day. To clarify this in the text, we added the following sentence to the caption of that figures.

The x-axis ticks refer to 00:00 local time (06:00 UTC).

- Fig. 7: units (y-axis) are missing

We added the units in Fig. 7 in the ACPD version of the manuscript (Fig. 8 of the revised version of the manuscript, Fig. 1 in this reply). The γ -value has no unit.

References

Anderson, J. G. and Clapp, C. E.: Coupling free radical catalysis, climate change, and human health, *Phys. Chem. Chem. Phys.*, 20, 10 569–10 587, doi:10.1039/C7CP08331A, 2018.

Anderson, J. G., Wilmouth, D. M., Smith, J. B., and Sayres, D. S.: UV Dosage Levels in Summer: Increased Risk of Ozone Loss from Convectively Injected Water Vapor, *Science*, 337, 835–839, doi:10.1126/science.1222978, 2012.

Anderson, J. G., Weisenstein, D. K., Bowman, K. P., Homeyer, C. R., Smith, J. B., Wilmouth, D. M., Sayres, D. S., Klobas, J. E., Leroy, S. S., Dykema, J. A., and Wofsy, S. C.: Stratospheric ozone over the United States in summer linked to observations of convection and temperature via chlorine

and bromine catalysis, Proc. Natl. Acad. Sci., 114, E4905–E4913, doi: 10.1073/pnas.1619318114, 2017.

Drdla, K. and Müller, R.: Temperature thresholds for chlorine activation and ozone loss in the polar stratosphere, Ann. Geophys., 30, 1055–1073, doi:10.5194/angeo-30-1055-2012, 2012.

Elrod, M. J., Koch, R. E., Kim, J. E., and Molina, M.: HCl vapour pressures and reaction probabilities for $\text{ClONO}_2 + \text{HCl}$ on liquid $\text{H}_2\text{SO}_4\text{-HNO}_3\text{-HCl-H}_2\text{O}$ solutions, Faraday Discuss., 100, 269–278, 1995.

Groß, J.-U., Brautzsch, K., Pommrich, R., Solomon, S., and Müller, R.: Stratospheric ozone chemistry in the Antarctic: What controls the lowest values that can be reached and their recovery?, Atmos. Chem. Phys., 11, 12 217–12 226, doi:10.5194/acp-11-12217-2011, 2011.

Hanson, D. R.: Reaction of ClONO_2 with H_2O and HCl in sulfuric acid and $\text{HNO}_3/\text{H}_2\text{SO}_4/\text{H}_2\text{O}$ mixtures, J. Phys. Chem. A, 102, 4794–4807, 1998.

Hanson, D. R. and Ravishankara, A. R.: Reactive Uptake of ClONO_2 onto Sulfuric Acid Due to Reaction with HCl and H_2O , J. Phys. Chem., 98, 5728–5735, 1994.

Luo, B., Krieger, U. K., and Peter, T.: Densities and refractive indices of $\text{H}_2\text{SO}_4\text{/HNO}_3\text{/H}_2\text{O}$ solutions to stratospheric temperatures, Geophys. Res. Lett., 23, 3707–3710, doi:10.1029/96GL03581, 1996.

Müller, R., Groß, J.-U., Zafar, A., Robrecht, S., and Lehmann, R.: The maintenance of elevated active chlorine levels in the Antarctic lower stratosphere through HCl null cycles, Atmos. Chem. Phys., 18, 2985–2997, doi: 10.5194/acp-18-2985-2018, 2018.

Shi, Q., Jayne, J. T., Kolb, C. E., Worsnop, D. R., and Davidovits, P.: Kinetic model for reaction of ClONO_2 with H_2O and HCl and HOCl with HCl in sulfuric acid solutions, J. Geophys. Res., 106, 24 259–24 274, doi: 10.1029/2000JD000181, 2001.

Solomon, S.: Stratospheric ozone depletion: A review of concepts and history, Rev. Geophys., 37, 275–316, doi:10.1029/1999RG900008, 1999.

Vogel, B., Feck, T., and Grooß, J.-U.: Impact of stratospheric water vapor enhancements caused by CH₄ and H₂ increase on polar ozone loss, *J. Geophys. Res.*, 116, D05301, doi:10.1029/2010JD014234, 2011.

Zafar, A. M., Müller, R., Grooß, J.-U., Robrecht, S., Vogel, B., and Lehmann, R.: The relevance of reactions of the methyl peroxy radical (CH₃O₂) and methylhypochlorite (CH₃OCl) for Antarctic chlorine activation and ozone loss, *Tellus B*, 70, 1507391, doi:10.1080/16000889.2018.1507391, 2018.

Zhang, R., Jayne, J. T., and Molina, M. J.: Heterogeneous interactions of ClONO₂ and HCl with sulfuric acid tetrahydrate: Implications for the stratosphere, *J Phys Chem*, 98, 867–874, 1994.

Mechanism of ozone loss under enhanced water vapour conditions in the mid-latitude lower stratosphere in summer

Sabine Robrecht¹, Bärbel Vogel¹, Jens-Uwe Groß¹, Karen Rosenlof², Troy Thornberry^{2,3}, Andrew Rollins², Martina Krämer¹, Lance Christensen⁴, and Rolf Müller¹

¹Forschungszentrum Jülich, Institute of Energy and Climate Research (IEK-7), Jülich, Germany

²NOAA Earth System Research Laboratory (ESRL) Chemical Sciences Division, Boulder, CO 80305 USA

³University of Colorado, Cooperative Institute for Research in Environmental Sciences, Boulder, CO 80309 USA

⁴California Institute of Technology, Jet Propulsion Laboratory, Pasadena, CA 91125 USA

Correspondence to: Sabine Robrecht (sa.robrecht@fz-juelich.de)

Abstract. Water vapour convectively injected into the mid-latitude lowermost stratosphere could affect stratospheric ozone.

The associated potential ozone loss process requires low temperatures ~~and an together with~~ elevated water vapour mixing ~~ratio-~~

~~An-ratios. Since this ozone loss is initiated by heterogeneous chlorine activation on liquid aerosols, an~~ increase in sulphate aerosol surface area due to a volcanic eruption or geoengineering could increase the likelihood of ~~occurrence of this process~~its occurrence

5 However, the chemical mechanism of this ozone loss process has not yet been analysed in sufficient detail and its sensitivity to various conditions is not yet clear. Under conditions of climate change associated with an increase in greenhouse gases, both a stratospheric cooling and an increase in water vapour convectively injected into the stratosphere is expected. Understanding the influence of low temperatures, elevated water vapour and enhanced sulphate particles on this ozone loss mechanism is a key step in estimating the impact of climate change and potential sulphate geoengineering on mid-latitude

10 ozone.

Here, we analyse the ozone loss mechanism and its sensitivity to various stratospheric conditions in detail. Conducting a box-model study with the Chemical Lagrangian Model of the Stratosphere (CLaMS), chemistry was simulated along a 7-day backward trajectory. This trajectory was calculated neglecting mixing of neighbouring air masses. Chemical simulations were initialized using measurements taken during the Study of Emissions and atmospheric Composition, Clouds and Climate

15 Coupling by Regional Surveys (SEAC⁴RS) aircraft campaign (2013, Texas), which encountered an elevated water vapour mixing ratio of 10.6 ppmv at a pressure level around 100 hPa. We present a detailed analysis of the ozone loss mechanism, including the chlorine activation, chlorine catalysed ozone loss cycles, maintenance of activated chlorine and the role of active nitrogen oxide radicals (NO_x). Focussing on a realistic trajectory in a temperature range from ~~197–203~~197–202 K, a threshold in water vapour of ~~41.0–41.6~~10.6 ppmv has to be exceeded and maintained for stratospheric ozone loss to occur. We investigated

20 the sensitivity of the water vapour threshold to temperature, sulphate content, inorganic chlorine (Cl_y), inorganic nitrogen (NO_y) and inorganic bromine (Br_y). The water vapour threshold is mainly determined by the temperature and sulphate content. However, the amount of ozone loss depends on Cl_y, Br_y and the duration of the time period over which chlorine activation can be maintained. NO_y affects both the potential of ozone formation and the balance between reactions yielding chlorine activation and -deactivation, which determines the water vapour threshold. Our results show that in order to deplete ozone, a

chlorine activation time of 24 to 36 hours for conditions of the water vapour threshold with low temperatures ~~and high water vapour mixing ratios~~ must be maintained. A maximum ozone loss of 9% was found for a 20 ppmv water vapour mixing ratio ~~at using~~ North American Monsoon (NAM) tropopause standard conditions with ~~the model run a chemical box-model simulation~~ along a realistic trajectory. For the same trajectory, using observed conditions (of 10.6 ppmv ~~), whether ozone loss occurs was simulated~~ H_2O), ~~the occurrence of simulated ozone loss was~~ dependent on the sulphate amount assumed. Detailed analysis of current and future possibilities is needed to assess whether enhanced water vapour conditions in the summertime mid-latitude lower stratosphere ~~leads~~~~lead~~ to significant ozone loss.

1 Introduction

The impact of water vapour convectively injected into the lowermost stratosphere on the mid-latitude ozone layer is a matter of current debate (Anderson et al., 2012, 2017; Ravishankara, 2012; Schwartz et al., 2013). ~~Borrmann et al. (1996, 1997) and Solomon et al. (1997) investigated~~ While Anderson et al. (2012) focused on the heterogeneous chemistry of cold liquid sulfate aerosol, earlier studies have focussed on the influence of cirrus clouds on ozone chemistry in the lowermost stratosphere (Borrmann et al., 1996, 1997; Solomon et al., 1997; von Hobe et al., 2011). Anderson et al. (2012) proposed a potential ozone depletion in the mid-latitude stratosphere in summer ~~on liquid sulphate aerosols~~ under conditions of enhanced water vapour and low temperatures. They proposed ~~this~~ chemical ozone loss to ~~occur under these conditions through processes be initiated through heterogeneous chlorine activation and to be driven by catalytic ozone loss cycles~~ related to ozone loss known from polar regions ~~in~~ early spring (e.g. Groß et al., 2011; Solomon, 1999; Vogel et al., 2011). Here, we present a detailed analysis of this ozone loss mechanism and an extensive investigation of its sensitivity to a variety of conditions.

In the bulk and on the surface of cold condensed stratospheric particles, such as binary $\text{H}_2\text{SO}_4/\text{H}_2\text{O}$ solutions, ternary solutions, NAT (Nitric Acid Trihydrate) and ice particles (e.g. Spang et al., 2018), inactive chlorine species (HCl , ClONO_2) can be converted to active chlorine ($\text{ClO}_x = \text{Cl} + \text{ClO} + 2 \times \text{Cl}_2\text{O}_2 + 2 \times \text{Cl}_2$) through the heterogeneous reactions R1, R2 and R3 (Solomon et al., 1986; Prather, 1992; Crutzen et al., 1992) and the subsequent photolysis of Cl_2 and HOCl .



The heterogeneous reactions R1 and R2 drive the conversion of active nitrogen-oxides ($\text{NO}_x = \text{NO} + \text{NO}_2 + \text{NO}_3 + 2 \times \text{N}_2\text{O}_5$) into HNO_3 . After chlorine activation, catalytic ozone loss cycles can occur, such as the ClO -dimer-cycle (~~Molina and Molina, 1987, ??~~) (~~Molina and Molina, 1987~~) and the ClO - BrO -cycle (~~McElroy et al., 1986, ??~~) (~~McElroy et al., 1986~~). These cycles are responsible for the rapid ozone loss observed in Antarctic spring (e.g. Solomon, 1999). ~~ClO -Dimer-Cycle (??):~~ $\text{++} \rightarrow \text{++} \text{hv} \rightarrow \text{++} \rightarrow \text{++} 2 \times (\text{++} \rightarrow \text{++})$ net: $2 \rightarrow 3$

~~ClO - BrO -Cycle (??):~~ $\text{++} \rightarrow \text{++} \rightarrow \text{++} \rightarrow \text{++} \rightarrow \text{++}$ net: $2 \rightarrow 3$ A third cycle with ClO and HO_2 (see Sec. In a third catalytic ozone loss cycle, C2 , HOCl is formed and subsequently photolysed yielding OH and Cl radicals leading to stratospheric ozone

~~destruction~~³) proposed by Solomon et al. (1986) would be expected to play a role in ozone loss in the mid-latitude lower stratosphere (e.g. Daniel et al., 1999; Ward and Rowley, 2016). This cycle was originally proposed by Solomon et al. (1986) as an ozone depleting cycle in the Antarctic lower stratosphere, but for polar ozone destruction, this cycle turned out to be of minor importance (Solomon, 1999). Nevertheless, C2 would be expected to play a role in ozone loss in the mid-latitude lower stratosphere (e.g. Daniel et al., 1999; Ward and Rowley, 2016). + → + + → + + → + + → +

5 net: ~~2 + → 3~~ Under the very dry conditions in the polar stratosphere, very low temperatures (below \sim 195 K) are required for heterogeneous chlorine activation through reactions R1–R3 (Solomon, 1999; Shi et al., 2001). An enhancement of water vapour above background values would allow chlorine activation at higher temperatures (200–205 K) (Drdla and Müller, 2012), which led to the hypothesis ~~hat that~~ chlorine activation and subsequent ozone loss could occur at mid-latitudes in summer in the lower-10 most stratosphere (Anderson et al., 2012, 2017; Anderson and Clapp, 2018). The aim of our study is to investigate for a variety of conditions by how much water vapour has to be enhanced for chlorine activation to occur at these higher temperatures. An enhanced stratospheric sulphate aerosol content increases heterogeneous chlorine activation by increasing the surface area of the condensed particles (Drdla and Müller, 2012; Solomon, 1999). As an example, the aerosol surface area density in the lower stratosphere ranges between \sim 0.5 and $1.5 \mu\text{m}^2\text{cm}^{-3}$ under non-volcanic conditions (Thomason and Peter, 2006), while 15 the perturbation of Mt. Pinatubo yielded peak values of more than $40 \mu\text{m}^2\text{cm}^{-3}$ (Thomason et al., 1997). In the stratosphere, water vapour increases with altitude, primarily due to methane oxidation (LeTexier et al., 1988; Rohs et al., 2006). The upper branch of the Brewer Dobson circulation (BDC) transports higher stratospheric water vapour mixing ratios down to lower altitudes at mid to high latitudes, and this air mixes with the low water vapour containing air from the tropics that has moved pole-ward in the lower branch of the BDC (e.g. ~~Brewer, 1949; Randel et al., 2004; Schwartz et al., 2013; Konopka et al., 2015; Poshyvailo et al.~~ 20 (e.g. Brewer, 1949; Randel et al., 2004; Poshyvailo et al., 2018), giving typical mid-latitude lowermost stratosphere values of 2–6 ppmv H_2O . However, above North America in summer ~~enhanced~~ enhanced water vapour mixing ratios of 10–18 ppmv at an altitude of \sim 16.5 km (380 K potential temperature, \sim 100 hPa) (Smith et al., 2017) have been observed, which were connected with deep convective storm systems penetrating the tropopause (Homeyer et al., 2014; Herman et al., 2017; Smith et al., 2017). These convective overshooting events can transport ice crystals into the lowermost stratosphere, where the ice evaporates leading 25 to a local enhancement of water vapour (Hanisco et al., 2007; Schiller et al., 2009; Herman et al., 2017).

As greenhouse gases increase in the atmosphere, models predict that more water may be convectively transported into the stratosphere (Trapp et al., 2009; Klooster and Roebber, 2009). This increases the ~~possibility~~ probability that the ozone loss process proposed by Anderson et al. (2012) will occur, especially in the case of an additional enhancement of stratospheric sulphate particles caused by volcanic eruptions or sulphate geoengineering. ~~However, the~~ The occurrence of this ozone loss 30 process requires halogens to be present, which are decreasing in the stratosphere due to the Montreal Protocol ~~ans and~~ its amendments and adjustments (WMO, 2014) (WMO, 2018). However, for assessing the impact of geoengineering on the ozone layer, also the impact of very short lived halogens needs to be taken into account (Tilmes et al., 2012). For estimating the impact of both climate change and a possible sulphate geoengineering on the mid-latitude ozone layer, it is necessary to consider the influence of enhanced water vapour and sulphate content on mid-latitude ozone chemistry in the lowermost stratosphere in 35 ~~more~~ detail.

In the study by Anderson et al. (2012), a range of initial mixing ratios for HCl and ClONO₂ with rather high concentrations of 850 pptv HCl and 150 pptv ClONO₂ was assumed. Here, we investigate ozone loss in mid-latitude summer based on measurements from flights by the NASA ER-2 aircraft during the Studies of Emissions and Atmospheric Composition, Clouds and Climate Coupling by Regional Surveys (SEAC⁴RS) campaign, which was based in Houston, Texas in 2013 (Toon et al., 2016).

5 Conducting box-model simulations with the Chemical Lagrangian Model of the Stratosphere (CLaMS, McKenna et al., 2002a, b), the ozone loss mechanism is analysed in greater detail. The model setup is described in Section 2. In Sec. 3, the chlorine activation step, catalytic ozone loss cycles and the maintenance of activated chlorine levels in the mid-latitude stratosphere are investigated in detail. The sensitivity of this mechanism to water vapour, sulphate content, temperature, Cl_y mixing ratio (Cl_y=HCl+ClONO₂+ClO_x), reactive nitrogen (NO_y=NO_x+HNO₃+⁺) and inorganic bromine (Br_y) is explored in Sec. 4. Case 10 studies, which extend the simulated time period and assume conditions based on ~~both~~ SEAC⁴RS and ~~MACPEX (Mid-latitude Airborne Cirrus Properties Experiment)~~ measurements as well as conditions used in the study of Anderson et al. (2012), further illustrate these sensitivities in Sec. 5.

2 Model setup

The simulations presented here were performed with the box-model version of CLaMS (McKenna et al., 2002a, b). Stratospheric chemistry is simulated based on a setup used in previous studies (Groß et al., 2011; Müller et al., 2018; Zafar et al., 2018) for single air parcels along trajectories including diabatic descent and neglecting mixing between neighbouring air masses. A full chemical reaction scheme comprising gas phase and heterogeneous chemistry is applied using the SVODE-solver (Brown et al., 1989). Chemical reaction kinetics are taken from Sander et al. (2011), ~~photolysis rates are calculated for spherical geometry (Becker et al., 2000), and~~ heterogeneous reaction rates for R1–R3 were calculated based on the the 20 study of Shi et al. (2001), ~~and photolysis rates are calculated for spherical geometry (Becker et al., 2000)~~. For heterogeneous particle formation, the initial liquid aerosol number density ($N_0=10.0\text{ cm}^{-3}$), the standard deviation of the logarithmic normal distribution of the particle size ($\sigma=1.8$), and the gas phase equivalent of the amount of sulfuric acid in the aerosol (for chosen values see Tab. 1) are set prior to the simulation. The gas phase equivalent is used to calculate the density of liquid particles as described in the study of Shi et al. (2001) (binary solutions) and Luo et al. (1996) (ternary solutions). Particle size and surface 25 area density are calculated based on the density of liquid particles, the aerosol number density, and the standard deviation. In contrast to the setup in Groß et al. (2011), Müller et al. (2018) and Zafar et al. (2018), only formation of liquid particles (both binary H₂O/H₂SO₄ and ternary HNO₃/H₂O/H₂SO₄ solutions) is allowed (i.e. no NAT or ice particles are formed in this model setup) ~~to enable a better comparability with the studies of Anderson et al. (2012, 2017) and Anderson and Clapp (2018)~~. Note that this is also different from the study of ~~and to the study of~~ Borrmann et al. (1996, 1997), who investigated lowermost 30 stratospheric ozone chemistry on cirrus clouds.

2.1 Measurements

The box model simulations were initialized using water vapour, ozone and CH₄ measurements taken during the SEAC⁴RS aircraft campaign ~~and water vapour, ozone and measurements taken during MACPEX campaign~~ (more information on the chemical initialization is provided in Section 2.3). ~~The investigation of mid-latitude ozone chemistry presented here is primarily based on SEAC⁴RS conditions, while simulations based on MACPEX data were conducted to complement the results of the investigation by showing a further measurement-based example. The SEAC⁴RS campaign took place during the North American summertime, while the MACPEX campaign was in spring, prior to the build up of the North American Monsoon (NAM) anticyclone. The SEAC⁴RS campaign~~ It was based in Houston, Texas, and took place during August and September 2013 (Toon et al., 2016). One aim of this campaign was to investigate the impact of deep convective clouds on the water vapour content and the chemistry in the lowermost stratosphere. We initialized the model using measurements taken on 8 August 2013 by the Harvard Lyman- α photofragment fluorescence hygrometer (HWV, Weinstock et al., 2009), which flew 10 on the NASA ER-2 high altitude research aircraft. Ozone was initialized in our simulations ~~using O₃ measurements from the National Oceanic and Atmospheric Administration (NOAA) UAS-O₃-instrument (Gao et al., 2012)~~. Initial Cl_y and NO_y were determined using tracer-tracer correlations (for more informations see Sec. 2.3) based on methane measurements with the Harvard University Picarro Cavity Ring down Spectrometer (HUPCRS) (Werner et al., 2017). ~~The simulation results initialized with SEAC⁴RS measurements were compared with a ease of enhanced lower stratospheric water sampled during the spring 2011 MACPEX campaign (Rollins et al., 2014) also based in Houston, Texas. The water vapour values used here were measured by the Fast In-situ Stratospheric Hygrometer (FISH), which employs the Lyman- α photofragment fluorescence technique (Meyer et al., 2015). MACPEX ozone was measured by the UAS instrument (Gao et al., 2012). Initial and were assumed based on tracer-tracer correlations with that was measured by the Jet Propulsion Laboratory's Aircraft Laser Infrared Absorption Spectrometer (ALIAS) instrument (Webster et al., 1994).~~

20 2.2 Trajectories

Diabatic trajectories were calculated using wind and temperature data from the ERA-Interim reanalysis (Dee et al., 2011) with 1° × 1° resolution provided by the European Centre for Medium-Range Weather Forecasts (ECMWF). The vertical velocities were calculated from the total diabatic heating rates derived from ERA-Interim data (Ploeger et al., 2010). Trajectories (~~7-day 7-day~~ forward and backward) were initialized at locations during ~~MACPEX and~~ SEAC⁴RS where stratospheric water vapour 25 was over 10 ppmv.

~~Selected examples~~ A selected example of calculated trajectories ~~are is~~ shown in Fig. 1. ~~These trajectories were~~ This trajectory was chosen for the chemical analysis, because ~~their its~~ initial conditions exhibited enhanced water vapour relative to the overall background ~~and the temperatures were very low~~. ~~These are then the~~ low temperatures and enhanced Cl_y (higher than for comparable water vapour and temperature conditions). Cl_y ~~was calculated from tracer-tracer correlations (see Sec. 2.3)~~. ~~This trajectory is then~~ most suitable for the occurrence of the mechanism proposed by Anderson et al. (2012). In the left panel, ~~backward trajectories are~~ a backward trajectory is presented in the range of –7 to 0 days from the time of measurement ~~and~~

forward trajectories (red line) and a forward trajectory in the range from 0 to 7 days. In the right panel, the location of the measurement is shown by a red square. The black trajectory refers to a measurement on 11 April 2011 during the MACPEX campaign. The potential temperature level of this trajectory is around 380 and above the tropopause located at ~ 350 , which was deduced from the temperature profile measured during the flight on 11 April 2011. The backward trajectory reaches very low temperatures with a minimum temperature of 191. The forward trajectory shows a strongly increasing temperature and pressure level due to a decrease in altitude. Coming from the Western Pacific, this air parcel passes the North American continent briefly. For this study numerous water measurements of the MACPEX campaign were analysed, but only few values of more than 10 were observed above the tropopause. The trajectory marked in blue in Fig.

5 The shown trajectories (Fig. 1 is 1, a forward and a backward trajectory) are based on measurements on 8 August 2013 during the SEAC⁴RS campaign. With a potential temperature of 380 to 390 K, this trajectory is these trajectories are above the tropopause of ~ 370 K (Fig. 1 left, grey line), deduced from the temperature profile measured during the flight. Both, the forward and backward trajectories stay in the region of the North American continent. For the SEAC⁴RS campaign, the 10 temperature range of the backward trajectory varies between 197 and 202 K and the forward trajectory exhibits increasing temperatures. In addition, we considered trajectories based on other SEAC⁴RS measurements with enhanced water vapour, however most of them exhibit higher mean temperatures of at least 200 K. Since low temperatures are expected to push stratospheric ozone depletion in mid-latitudes (Anderson et al., 2012) due to faster heterogeneous chemical reactions and thus faster chlorine activation, the SEAC⁴RS backward trajectory (Fig. 1, blue, day -7 to 0) is selected here as the standard trajectory.

15 This trajectory is used to analyse the chemical mechanisms affecting lower stratospheric ozone under various water vapour conditions, and to explore the sensitivity of these processes to different initial conditions.

2.3 Initialization

Important trace gases for ozone chemistry – O₃, Cl_y and NO_y – are initialized based on measurements during the SEAC⁴RS and 5 MACPEX aircraft campaigns over North America (see Sec. 2.1). Ozone and water vapour were measured directly during the aircraft campaigns, Cl_y and NO_y are inferred from tracer-tracer relations using either correlations 10 using CH₄ (SEAC⁴RS) or (MACPEX) measured on the aircraft employed. The initialization of all further trace gases except of water vapour were taken from the full chemistry 3D-CLaMS simulation (Vogel et al., 2015, 2016) for summer 2012 at the location of the measurement. Chemistry was initialized 7 days before the measurement. However, this time shift does not affect the sensitivities and the mechanism investigated here, because the trace gases Cl_y and NO_y were initialized based on measured CH₄ and mixing ratios, which are not significantly changing during a 7-day box-model simulation.

2.3.1 Standard case

In the standard case, the initial values of O₃, Cl_y and NO_y are determined based on an observation with an enhanced water vapour content of 10.6 ppmv (measured by the HWV-instrument) from the SEAC⁴RS (Toon et al., 2016) aircraft campaign. A gas phase equivalent mixing ratio for background sulphuric acid (H₂SO₄) of 0.20 ppbv is assumed. Initial CO (49.6 ppbv) is 15 taken from the 3D-CLaMS simulation (Vogel et al., 2015), which is higher than the measured value of 34.74 ppbv (measured

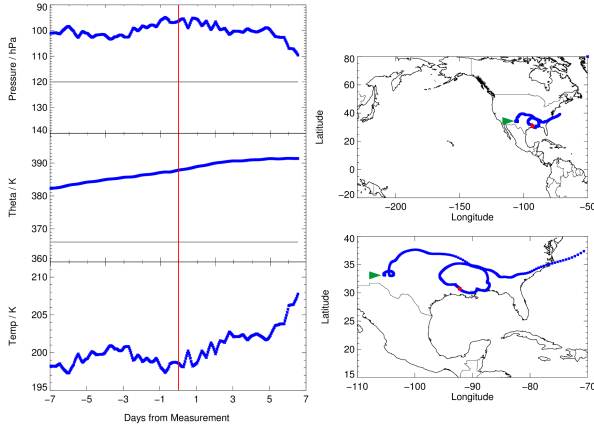


Figure 1. Pressure, potential temperature, temperature and location of the selected 7-day trajectories (forward and backward) calculated based on measurements with enhanced water vapour during the MACPEX (black) and SEAC⁴RS (blue) aircraft campaigns. Red In the left panels, the grey line marks the approximate tropopause altitude, deduced from the temperature profile measured during the flight. The red line (left panel) marks the time of measurement and red squares (right panels) mark the location of the measurement (right). For the right panels, the bottom panel exhibits a zoom from the top panel. In the bottom panel, and the MACPEX trajectory consists of single squares due to a faster movement begin of the air parcel in that region backward-trajectory (1 August) is marked by a green arrow.

by the HUPCRS instrument). Simulations assuming the measured CO mixing ratio showed only a minor difference to the results presented here. The initial values for the main trace gases for the standard case are summarized in Table 1. Note, in the 3D-CLaMS simulation, the mixing ratios of HCl (131 ppt, CLaMS), O₃ (206 ppb, CLaMS) and HNO₃ (354 ppt, CLaMS) are at the location of the SEAC⁴RS measurement lower than in the standard initialization (see Tab. 1).

20 Since Cl_y and NO_y were not measured during the SEAC⁴RS ER2-flights in the lowermost stratosphere, values for Cl_y and NO_y are calculated through tracer-tracer correlations (Groß et al., 2014, see Appendix C for equations) based on a SEAC⁴RS CH₄ measurement (of 1.776 ppmv) on 8 August 2013. The Cl_y-CH₄ correlation was calculated from measurements of the Airborne Chromatograph for Atmospheric Trace Species (ACATS) during flights of the ER-2 aircraft and from measurements by the cryogenic whole air sampler (Triple of the university of Frankfurt (on board of the TRIPLE balloon gondola) during 25 balloon flights at mid and high latitudes in the year 2000 (Groß et al., 2002). Between the year 2000 and 2013 stratospheric CH₄ increased and Cl_y decreased. Hence, the change of both lowermost stratospheric CH₄ and Cl_y has to be taken into account when using this tracer-tracer correlation. The increase in CH₄ was estimated to be equivalent to the growth rate for tropospheric CH₄. This growth rate was calculated to be 45.8 ppb-ppby from the year 2000 to 2013 by determining and adding every annual mean of the tropospheric CH₄ growth rate given in GHG Bulletin (2014). Subtracting this increase of CH₄ from the measured 30 CH₄ mixing ratio yields an equivalent-CH₄ equivalent for the year 2000. From the CH₄ equivalent, an equivalent Cl_y mixing ratio for the year 2000 was calculated using the tracer-tracer correlation (Groß et al., 2014). The annual decrease of Cl_y is assumed to be 0.8% (WMO, 2014) from the year 2000 to 2013, and thus the initial Cl_y is calculated to be 156 ppt. Since most

Cl_y is deactivated in the mid-latitude lowermost stratosphere, the initial mixing ratio of ClO_x species is assumed to be zero. A simulation assuming a ClO mixing ratio of 1% of total Cl_y, does not yield a significant difference to our standard case.
Initial NO_y was calculated through a N₂O correlation. Since no N₂O was measured on the ER2-flights during SEAC⁴RS, stratospheric ~~N₂O~~-N₂O was first estimated through a methane correlation (Groß et al., 2002), which is based on measurements from the year 2000. Hence, the equivalent CH₄ mixing ratio for the year 2000 (see above) was used to calculate an N₂O equivalent. Considering an estimated increase in N₂O of 10.4 ppb~~ppbv~~ from 2000 to 2013, which was determined in the same way as the CH₄ change (GHG Bulletin, 2014), the N₂O mixing ratio related to the time of the measurement in 2013 was calculated. Afterwards NO_y is calculated with a correlation from Groß et al. (2014) to be 782.9 ppt.

This standard case initialization is shown in Table 1. Because of the uncertain conditions in convective overshooting plumes, sensitivity box-model simulations are conducted. Furthermore, testing the impact of various parameters on chemical ozone loss is intended to yield a better understanding of the balance between stratospheric ozone production and ozone loss, which is a key aspect for potential mid-latitude ozone depletion. The assumed water vapour content in a simulation is varied from 5 to 20 ppmv. In addition, simulations assuming the same water vapour range and a constant temperature in a range from 195–220 K are conducted assuming sulphate background conditions with a gas phase equivalent of 0.20 ppbv and 10×enhanced sulphate (2.00 ppbv) for illustrating the dependence of ozone loss on water vapour and temperature. Furthermore, sensitivity simulations are conducted, assuming 80% Cl_y, 80% NO_y or 50% Br_y, and a standard case simulation along a 19-day trajectory is calculated.

2.3.2 Case of high Cl_y

Simulations conducted assuming high Cl_y and NO_y concentrations taken from Fig. 2 in Anderson et al. (2012) are referred to as “Case of high Cl_y”, which constitutes a worst case scenario. In the case of high Cl_y, HNO₃ is determined as 1.19 ppb~~ppbv~~ assuming the same ratio for HNO₃ (63% of total NO_y) and NO+NO₂ (37% of total NO_y) as in the standard case. An overview of the important trace gases in the initialization is given in Tab. 1. The results of the case ~~initialize~~initialized with high Cl_y are compared with the results obtained from standard case simulations.

2.3.3 MACPEX Case

~~Similar to the standard case, a simulation based on measurements during the MACPEX aircraft campaign 2011 (Rollins et al., 2014) was conducted, referred to as “MACPEX Case”. This case presents a further example for an event with high stratospheric water vapour based on airborne measurements and complements the results obtained from the standard case. All trace gases except for ozone, and water vapour are taken from a 3D-CLaMS-simulation (Vogel et al., 2015, 2016). Initial and is calculated based on and tracer-tracer correlations (Groß et al., 2014) with corrections considering a increase from 2009 to 2013 and a increase from 2000 to 2009. is determined using the same correlation with as for the standard case. Therefore is first calculated using measured of 320.28 ppbv and a correlation based on measurements from 2009 (Groß et al., 2014). The increase of stratospheric and is considered as described for the standard case (GHG Bulletin, 2014). First, an increase in of 1.6 ppb from 2009 to 2011 is estimated to adjust . Furthermore calculated is adjusted considering a difference between in 2000 and 2009 of~~

Table 1. Mixing ratios and sources used for initialization of relevant trace gases. The standard initialization is based on SEAC⁴RS measurements. Cl_y and NO_y values were determined based on tracer-tracer correlations (see [text Sec. 2.3.1](#) for the standard and the MACPEX case). The high Cl_y case is based on Fig. 2 from Anderson et al. (2012). Initial mixing ratios of ClO_x species were assumed to be zero for all cases.

	Standard case			Case of high Cl _y		
Species	Value	Source	Sensitivity simulation	Value	Source	Value
O ₃	303.2 ppbv	UAS-O ₃		303.2 ppbv	UAS-O ₃	283.0 ppbv UAS-O ₃
CH ₄	1.76 ppmv	CLaMS-3D		1.76 ppmv	CLaMS-3D	4.68 ppmv CLaMS-3D
CO	49.6 ppbv	CLaMS-3D		49.6 ppbv	CLaMS-3D	49.0 ppbv CLaMS-3D
Cl _y	149.5 156 pptv	tracer corr.	80% Cl _y	850 1.00 pptv ppbv		Anderson et al. (2012)
HCl	52.7 149.5 pptv	tracer corr.		850 pptv		Anderson et al. (2012)
ClONO ₂	6.2 pptv	tracer corr.		150 pptv		Anderson et al. (2012)
NO _y	2.19 782.9 pptv	tracer corr.	80% NO _y	1.89 ppbv		
HNO ₃	439.23 493.2 pptv	tracer corr.	80%	1.19 ppbv	see section 2.3.2	390.3 pptv tracer corr.
NO	144.8 pptv	tracer corr.		325 pptv	Anderson et al. (2012)	114.6 pptv tracer corr.
NO ₂	144.8 pptv	tracer corr.		375 pptv	Anderson et al. (2012)	114.6 pptv tracer corr.
Bry	6.9 pptv	CLaMS-3D	50% Bry	6.9 pptv	CLaMS-3D	1.2 pptv CLaMS-3D
H ₂ O	5–20 ppmv		5–20 ppmv	5–20 ppmv 5–20 ppmv		
H ₂ SO ₄	0.2 ppbv		0.6 ppbv 2.0 ppbv	0.2 ppbv, 0.6 ppbv		
Temperature	195–220 K	standard trajectory	const. temp (195–220 K)			standard trajectory

0.026 ppm. The annual decrease of from 2000 to 2011 is assumed to be 0.8% (WMO, 2014). A summary of the initial values for main tracers assumed in the MACPEX case are given in Table 1.

20 3 Mid-latitude ozone chemistry

Mid-latitude ozone chemistry in the lowermost stratosphere depends on water vapour abundance and temperature. This study focuses on the water vapour dependence of stratospheric ozone chemistry by analysing chemical processes occurring in a box-model simulation along a realistic trajectory in the temperature range from ~~197–203~~ ~~197–202~~ K under several water vapour conditions. In Figure 2, the mixing ratio of ozone, ClO_x and NO_x is shown for two simulations assuming 5 ppmv (dashed line) 25 and 15 ppmv (solid line) H₂O. These water vapour mixing ratios are chosen, because they are clearly in the regime of the low water vapour background (5 ppmv) of the lower mid-latitude stratosphere and of enhanced water vapour (15 ppmv) as it can be reached through convective overshooting events. For the low water vapour (5 ppmv) case, net ozone formation occurs, the ClO_x mixing ratio remains low and the NO_x mixing ratio high. In contrast, assuming a water vapour mixing ratio of 15 ppmv, ozone depletion occurs, accompanied by a decrease in NO_x occurs, and coupled with chlorine activation as indicated by the increasing ClO_x-ClO_x mixing ratio. The sensitivity to variations in water vapour conditions on stratospheric ozone is tested 30

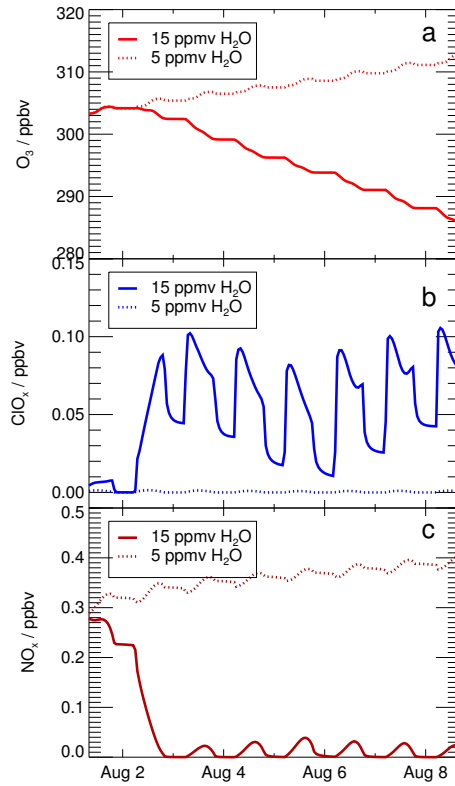


Figure 2. Volume mixing ratio of O_3 (panel-a), ClO_x (panel-b) and NO_x (panel-c) during a simulation with 15 ppmv H_2O and 5 ppmv H_2O . These water vapour mixing ratios are chosen, because they are clearly in the regime of low (5 ppmv) and elevated (15 ppmv) water vapour. The x-axis ticks refer to 00:00 local time (06:00 UTC).

here by conducting simulations with standard conditions but varying the assumed water vapour mixing ratio from 5 to 20 ppmv in varying increments, with the resolution increased near the changeover from ozone production to destruction.

In Figure 3, the ozone values reached at the end of the 7-day simulation (endfinal ozone, blue squares) are plotted as a function of the assumed water vapour mixing ratio. The initial ozone value, of 303.2 ppbv, is shown by the grey line. Blue squares lying above that line are cases with ozone production, those lying below that line are cases with ozone destruction. The thresholdis

5 determined as the water vapour mixing ratio at which the end ozone value clearly falls below the end ozone that is reached for low water vapour amounts. For the standard case shown in Fig. 3, this threshold is reached at a water vapour mixing ratio in the range of 11.0 to 11.6 ppmv. By 12 ppmv of water vapour, the system is clearly in an ozone destruction regime. The occurrence of the water vapour threshold and ozone depletion decrease of final ozone with higher water vapour mixing ratios is related to chlorine activation. The time until chlorine activation occurs in thethis simulation is plotted in Fig. 3 as violet triangles.

10 ~~Assuming, assuming~~ that chlorine activation occurs when the ClO_x mixing ratio exceeds 10% of total Cl_y (Drdla and Müller, 2012), ~~plotted here~~. Shown is the time when chlorine activation first occurs in the model. Since the ClO_x/Cl_y ratio is dependent on the diurnal cycle, the 24-hours mean value of the ClO_x mixing ratio was used to determine the chlorine activation time. For low water vapour mixing ratios, no chlorine activation time is plotted, because no chlorine activation occurs. ~~Chlorine activation only occurs when the~~ ~~For chlorine activation to occur, a threshold in water vapour has to be reached. Here, we determine the~~

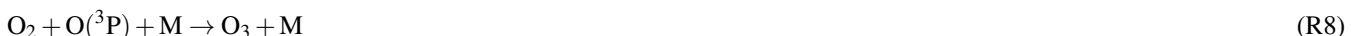
5 ~~lowest water vapour mixing ratio at which chlorine activation occurs as~~ water vapour threshold ~~is exceeded~~ (marked by a blue arrow in Fig. 3). In our standard case, this threshold is reached at a water vapour mixing ratio of 10.6 ppmv. Between 10.6 and 11.8 ppmv H_2O , ~~chlorine activation leads not to an ozone destruction during the 7-day simulation. For 10.6 to 11.2 ppmv~~ H_2O , ~~chlorine only remains activated for up to 28 h, because of increasing temperatures, and almost no impact on final ozone is observable. By 12.0 ppmv of water vapour, chlorine activation yields ozone destruction within the 7-day simulation.~~ Near the water vapour threshold, the activation time is 24 to 36 hours and it decreases with increasing water vapour mixing ratios. It requires 5 hours at 20 ppmv H_2O . The shorter the chlorine activation time, the longer activated chlorine exists during the simulation yielding greater ozone depletion. The processes yielding ozone depletion at high water vapour conditions as well as ozone formation at low water vapour are analysed in detail in the subsequent sections. For this investigation we use the simulated reaction rates for each chemical reaction along the course of the calculation. For high water vapour mixing ratios the roles of both chlorine activation and a decrease in the NO_x mixing ratio (Fig. 2) are discussed.

10

3.1 Ozone formation at low water vapour mixing ratios

At water vapour mixing ratios up to 11.8 ppmv, ~~net~~ ozone formation occurs ~~during the 7-day simulation~~ (see Fig. 3). This ozone formation is mainly driven by the photolysis of O_2 ~~→ and the subsequent reaction → Additionally, photolysis of → followed by~~

5 ~~R8 leads to ozone formation. NO radicals, which are formed in R7, mainly react with ozone as well as ClO and BrO forming Cl and Br radicals. → → Since these radicals react with ozone in reaction R16 () and ?? (), not all of the formed in R7 yields a net ozone formation. However, R7 is part of . Additionally~~ the “Ozone Smog Cycle” (Haagen-Smit, 1952) known from tropospheric chemistry ~~, which has also an impact on stratospheric chemistry~~ ~~can yield ozone formation in the lower stratosphere~~ (Grenfell et al., 2006; Grooß et al., 2011).



The rate of this cycle is determined by reaction R4 at low water vapour mixing ratios, and its net reaction is the oxidation of CO . The ozone formation through this cycle contributes around 40% to the total ozone formation at 5 ppmv in our box model

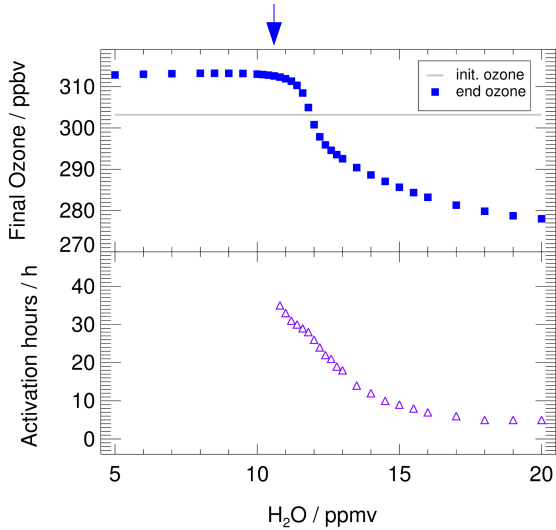


Figure 3. Impact of the water vapour content on the ozone mixing ratio (final ozone, blue squares) reached at the end of the 7-day simulation along the standard trajectory and assuming standard conditions. The initial ozone amount is marked by the grey line. [The arrow marks the water vapour threshold, which has to be exceeded for chlorine activation at standard conditions to occur.](#) In the bottom panel, violet triangles show the time until chlorine activation occurs. For low water vapour mixing ratios no chlorine activation occurs.

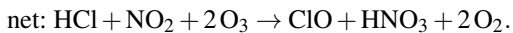
standard simulation. Hence, the ozone formation which occurs in the simulations assuming low water vapour mixing ratios is due to both the photolysis of O_2 and cycle C1.

20 3.2 Ozone loss at high water vapour mixing ratios

For higher water vapour mixing ratios than [11](#) [12](#) ppmv, [net](#) ozone depletion is simulated (Fig. 3) [in the 7-day standard simulation](#). The ozone loss mechanism generally consists of two steps: a chlorine activation step transferring inactive chlorine (HCl) into active ClO_x followed by catalytic ozone loss processes (Anderson et al., 2012). We analyse both the chlorine activation step and subsequent catalytic ozone loss cycles potentially occurring in mid-latitudes in the lower stratosphere under enhanced water vapour conditions. Since ozone depletion is larger at high water vapour mixing ratios, conditions with a water vapour mixing ratio of 15 ppmv are chosen here to analyse the chemical ozone loss mechanism. Figure 4 shows an overview of the development of important mixing ratios and reaction rates during the 7-day simulation. Panel a illustrates temperature (black line) and surface area density of liquid particles (blue line).

The first phase of the ozone loss mechanism (dark grey background in Fig. 4) is dominated by the occurrence of heterogeneous reactions. The most important heterogeneous chlorine activation reaction is R1 (Fig. 4b), which leads to the chlorine activation

chain (von Hobe et al., 2011)



This chlorine activation chain yields a transformation of inactive HCl into active ClO_x as well as of NO_x into HNO_3 . The ozone loss due to this reaction chain is negligible and no depleting effect on ozone occurs during the first phase (Fig. 4c). In 10 Fig. 4ef, the NO_x mixing ratio is seen to decrease and HNO_3 increases due R1. Further, in the first phase the HCl mixing ratio decreases, yielding an increase of ClO_x (Fig. 4f). ~~The delay between HCl reduction and formation (Fig. 4f) is caused by the combination of the diurnal cycle and the accumulation of and during night.~~ Both decreasing NO_x and increasing ClO_x have an impact on ozone during the second phase of the ozone loss mechanism (light grey background in Fig. 4), which is characterized by a decreasing ozone mixing ratio (Fig. 4c). The role of NO_x and ClO_x is discussed in detail in the next sections.

15

3.2.1 Role of NO_x

The transformation of NO_x -radicals into HNO_3 is due to R9 ($\text{ClO} + \text{NO}_2$) and subsequent the occurrence of the heterogeneous reactions R1 ($\text{ClONO}_2 + \text{HCl}$) and R2 ($\text{ClONO}_2 + \text{H}_2\text{O}$), which form HNO_3 . This behaviour was also found in former studies (e.g. Keim et al., 1996; Pitari et al., 2016; Berthet et al., 2017), investigating the impact of volcanic aerosols on stratospheric 20 ozone chemistry. Dependent on temperature and water vapour content, the HNO_3 formed ~~is taken up into remains in the~~ condensed particles. In the standard simulation using 15 ppmv H_2O , ~~an uptake of 64% is reached of~~ HNO_3 ~~remains in the~~ ~~condensed phase~~ on the day with the lowest temperature (197.3 K, 2 Aug 2013), while at higher temperatures (4–7 August 2013) 85% of HNO_3 ~~remain in are released to~~ the gas phase. After the transformation of NO_x into HNO_3 , the NO_x mixing 25 ratio remains low in the second phase of the mechanism (Fig. 4d, light grey region) while the HNO_3 mixing ratio (cond.+gas) remains high.

The transformation of NO_x radicals into HNO_3 , due to the occurrence of heterogeneous reactions at elevated water vapour amounts, affects stratospheric ozone chemistry. In the presence of a high NO_x concentration (as at low water vapour mixing ratios), ozone ~~chemistry is dominated by radicals (see See. 3.1) and the ozone~~ formation in cycle **C1** is determined by the rate of R4 ($\text{OH} + \text{CO}$). But if the NO_x concentration is low (as in the second phase of the mechanism), this ozone formation cycle 30 is rate limited by R6 ($\text{NO} + \text{HO}_2$). For the standard case at 15 ppmv H_2O , both rates are shown in Fig. 4e. In the first phase before NO_x is transferred into HNO_3 , cycle **C1** is limited by R4 ($\text{OH} + \text{CO}$) which peaks on 1 August 2013 with a maximum rate of $1.0 \cdot 10^5 \text{ cm}^{-3} \text{s}^{-1}$. In the second phase at low NO_x concentrations, cycle **C1** is limited by R6 ($\text{NO} + \text{HO}_2$) which peaks

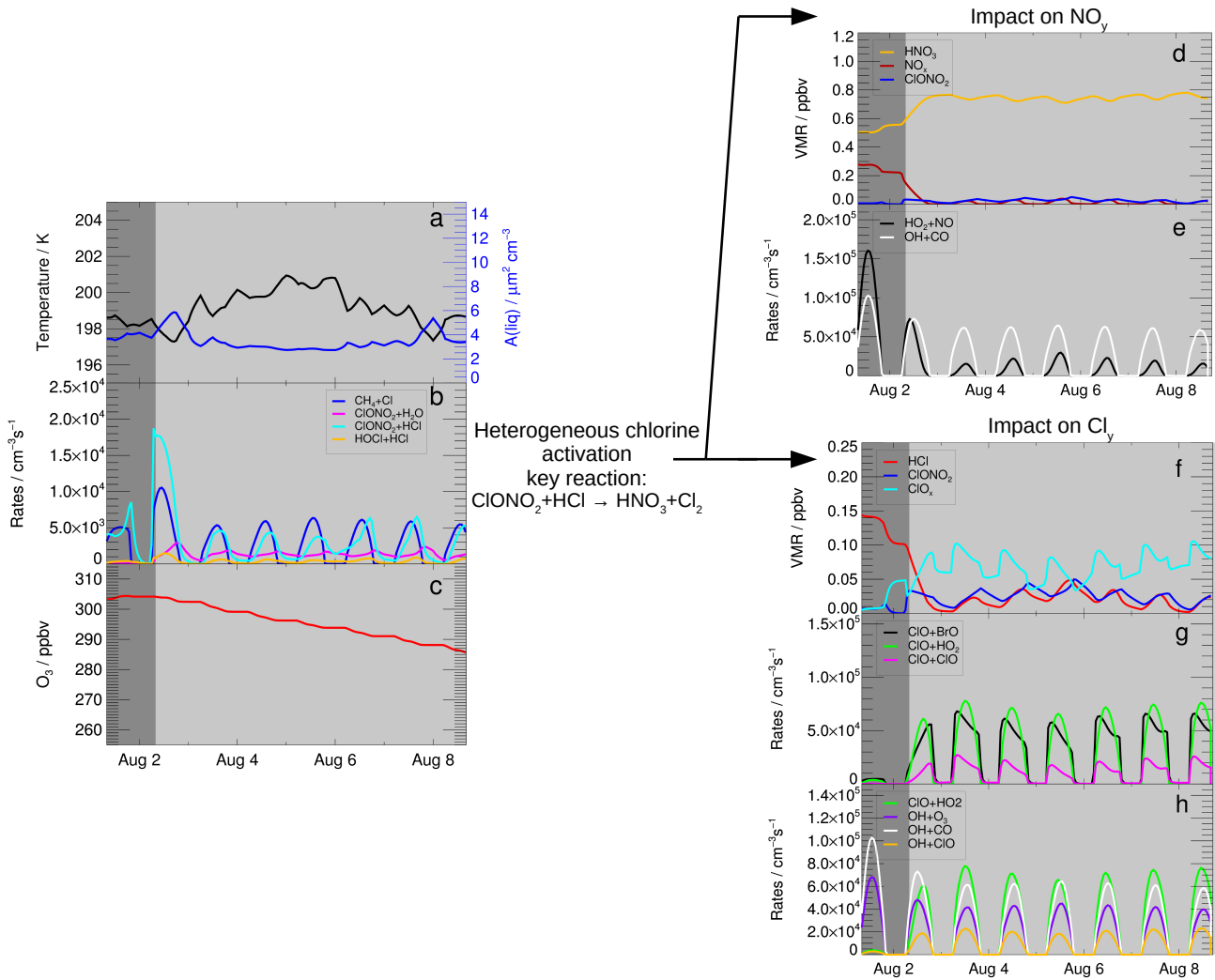


Figure 4. Reaction rates and mixing ratios important for the ozone loss mechanism in the standard simulation using 15 ppmv H₂O. The chlorine activation phase is shaded in dark grey, while the phase of ozone loss has a light grey background. Panel (a) shows the temperature of the trajectory and the liquid surface area density, the ozone mixing ratio is presented in panel (c). Heterogeneous reaction rates are shown in panel (b) as well as the rate of the gas phase reaction CH₄ + Cl. Panels (d), mixing ratio of HNO₃ (gas phase + condensed), NO_x and ClONO₂, and (e) are relevant to show the role of NO_y for the ozone loss process. Reaction R4 (OH+CO, panel e) limits ozone formation in cycle C1 at high NO_x mixing ratios and R6 (HO₂ + NO) at lower NO_x concentrations. Panels (f)–(h) illustrate the role of chlorine for ozone loss by showing the mixing ratio of HCl, ClO_x and ClONO₂ (panel f), main reaction rates (R17 (ClO+ClO), R18 (ClO+BrO), R13 (ClO + HO₂)) for catalytic ozone loss cycles (panel g) and potential reaction pathways for the OH-radical (R4 (OH+CO), R19 (OH+ClO), R15 (OH+O₃)) as possible reaction chains following R13 (ClO+HO₂) (panel h). The x-axis ticks refer to 00:00 o'clock local time (06:00 UTC).

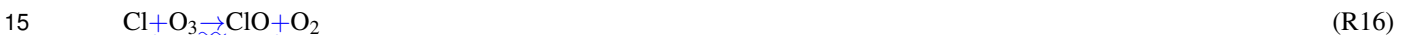
on 3 August 2013 with a maximum rate of $1.5 \cdot 10^4 \text{ cm}^{-3} \text{s}^{-1}$. Hence, due to the occurrence of the heterogeneous reaction R1 the net ozone formation decreases by at least $3.5 \cdot 10^4 \text{ cm}^{-3} \text{s}^{-1}$ from 1 August to 3 August.

3.2.2 Role of ClO_x

5 In the first phase of the mechanism, chlorine activation yields a transformation of inactive chlorine into active ClO_x . Net chlorine activation occurs when the rates of the heterogeneous reactions R1($\text{ClONO}_2 + \text{HCl}$), R2 ($\text{ClONO}_2 + \text{H}_2\text{O}$) and R3 ($\text{HCl} + \text{HOCl}$) exceed the gas phase HCl formation dominated by the reaction



Enhanced ClO_x concentrations induce catalytic ozone loss cycles at low temperatures, as the ClO -Dimer-cycle (??) (Molina et al., 1987), the ClO -BrO-cycle (??) (McElroy et al., 1986) and cycle C2 (Solomon et al., 1986) (McElroy et al., 1986) and the cycle with ClO and HO_2 (C2, Solomon et al., 1986)



Under conditions of low water vapour (stratospheric background) the rate limiting steps of these cycles are the reactions



The rates of the reactions R17, R18 and R13 increase strongly in the second phase of the mechanism (light grey area in Fig. 4g) and thus catalytic ozone loss cycles can occur. Under the assumed conditions, ozone depletion is mainly driven by reaction pathways following both R18 and R13. The reaction rates peak on August 3 with a value of $7.8 \cdot 10^4 \text{ cm}^{-3} \text{s}^{-1}$ for R13 ($\text{ClO} + \text{HO}_2$), $6.8 \cdot 10^4 \text{ cm}^{-3} \text{s}^{-1}$ for R18 ($\text{ClO} + \text{BrO}$) and $2.7 \cdot 10^4 \text{ cm}^{-3} \text{s}^{-1}$ for R17 ($\text{ClO} + \text{ClO}$). In contrast the rate of ozone loss due to the reactions \rightarrow net: \rightarrow 2 are not important here, as the peak values of ?? are only about $0.35 \cdot 10^4$ (not shown). Additionally the sensitivity of various reaction rates to the water vapour mixing ratio was tested. In Figure 5, the mean reaction rates on 3 August are plotted against the water content assumed during the simulation. Panel (a) shows an acceleration of the ozone loss cycles ?? ClO-BrO-cycle (based on R18) and C2 (based on R13) beginning from a water vapour mixing ratio of 11 ppmv. In contrast, the rate determining reaction of ?? (R17, $\text{ClO} + \text{ClO}$ the ClO -Dimer-Cycle (R17)) increases at a higher water vapour mixing ratio. In contrast, the rate of ozone loss due to the reactions between ClO_x and O_x ($\text{O}_x = \text{O}_3, \text{O}$)

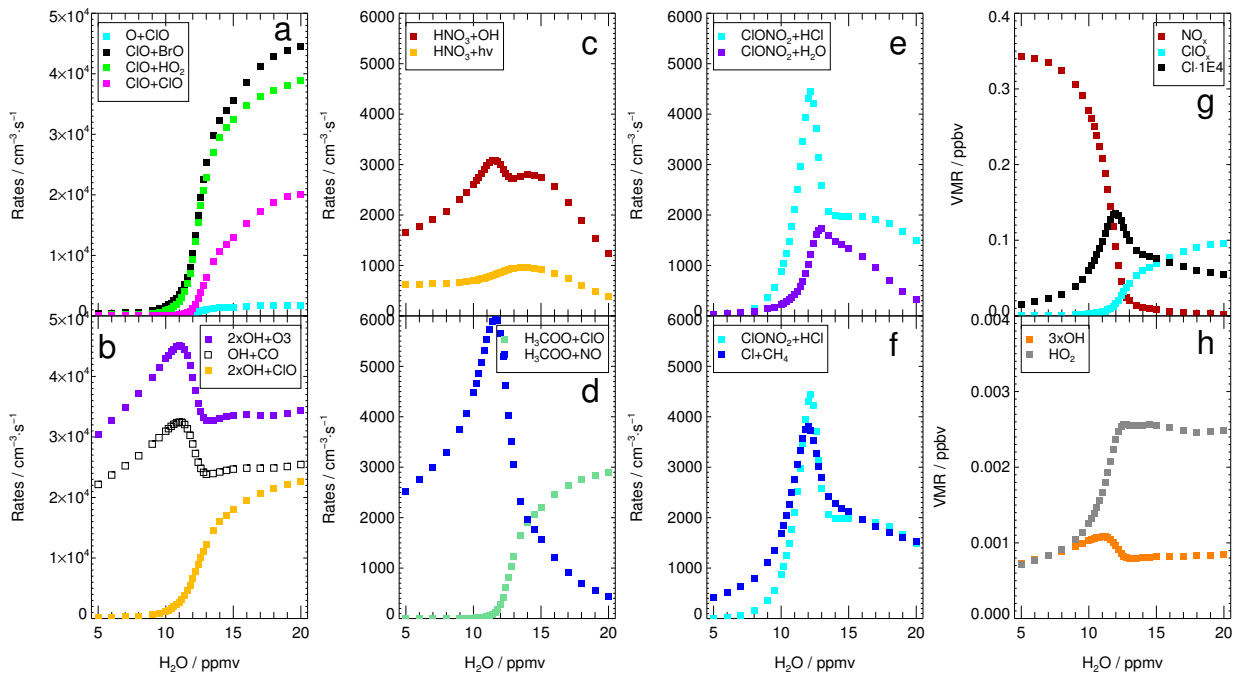
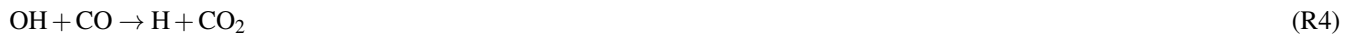


Figure 5. Average reaction rates and volume mixing ratios from the standard simulations on 3rd of August dependent on water vapour content. Panel (a) shows the reaction rates of R17 (ClO+ClO), R18 (ClO+BrO), R13 (ClO + HO₂) and ?? (ClO+O(3P) → Cl + O₂) resulting in ozone reduction, panel (b) possible reaction pathways for the OH radical (R4 (OH+CO), R19 (OH+ClO) and R15 (OH+O₃), panel (c) reactions yielding depletion of HNO₃ (R20 (HNO₃ + OH), R21 (HNO₃ + hν), panel (d) reactions of the H₃COO-radical R23 (H₃COO + ClO) and ?? R22 (H₃COO + NO), panel (e) important heterogeneous reactions (R1 (ClONO₂ + HCl), R2 (ClONO₂ + H₂O)), and panel (f) the balance between R1 (ClONO₂ + HCl) and R12 (CH₄ + Cl). Panel (g) shows the mixing ratios of NO_x, ClO_x and 10·Cl and panel (h) the mixing ratios of OH and HO₂.

species is negligible here (as shown by the low rate of the reaction ClO + O(3P) → Cl + O₂, Fig. 5a).

At stratospheric background conditions with a low water vapour mixing ratio, the rate determining step of cycle **C2** is R13 (Solomon et al., 1986; Ward and Rowley, 2016). For the conditions with enhanced water vapour of 15 ppmv in the standard simulation, the rate of R15 (OH+O₃) is limiting this cycle (Fig. 4f). An investigation of possible reaction pathways of the OH-radical yields that reactions of OH with CO (R4) and ClO (R19) exhibit a rate similar to the reaction with ozone (R15,

Fig. 5b).



5 Based on these reactions, two further reaction chains affecting ozone can be deduced. In cycle **C3**, the OH-radical reacts with CO yielding CO₂ and a hydrogen radical, from which HO₂ is formed. Subsequently HOCl can be formed via R13 (ClO+HO₂) and photolysed in reaction R14. Thus, the net reaction of this pathway is the oxidation of CO to CO₂ and the simultaneous destruction of ozone (**C3**).



15 Furthermore, when the OH-radical reacts with ClO, the products are HO₂ and Cl and thus another catalytic ozone loss cycle **C4** results.



In the cycles **C2** and **C4** two ozone molecules are destroyed, while one ozone molecule is destroyed in **C3**. To assess the effectiveness regarding ozone loss of **C2** and **C3** – **C4**, the rate of R4 (limiting **C3**) is compared with two times the rate of R15 (limiting **C2**) and R19 (limiting **C4**). This comparison shows that cycle **C2** is more relevant for ozone loss than **C3** and **C4** (Fig. 5b). *Reaction R15 (C2) and R4 (C3) accelerate with increasing water vapour mixing ratio, due to an increasing formation of OH (Fig. 5h), and peak in the threshold range of ~11 ppmv. When the threshold region is reached, the OH mixing ratio decreases due to a declining mixing ratio (Fig. 5g) and thus a lower rate of the reaction →. The lower OH concentration results in a decrease of the reaction rates of R15 (OH+) and R4 (OH+CO) shown in Fig. 5b, since R15 (OH+) and R4 (OH+CO) are limited through the OH mixing ratio. The limiting step of cycle **C4** (R19) is negligible for low water amounts and starts to increase in the range of the threshold region due to the strong gain of both and (Fig. 5g-h). Accordingly However, the relevance of **C4** for catalytic ozone destruction increases for higher water vapour mixing ratios.*



(see Fig. 6, green), leading to a steady HNO_3 mixing ratio (Fig. 4d).

A further option to convert HNO_3 into active NO_x ~~may be the~~ HNO_3 -photolysis



25 but the rate of reaction $\text{OH} + (\text{R20}) \text{R20}$ is more than 2.5 times larger than the rate of the HNO_3 photolysis (R21, Fig. 5c). The radical, which is generated in AR4, reacts with ClO (R9) forming , which heterogeneously reacts with HCl (R1). As a consequence the HCl , formed in Hence, the heterogeneous reaction R1 couples two pathways: A pathway balancing HCl -destruction in R1 and HCl -formation in R12 ($\text{Cl} + \text{CH}_4$) and thus maintaining a high ClO_x mixing ratio, and a pathway balancing HNO_3 -formation in R1 and HNO_3 destruction in R20 and thus maintaining a low NO_x mixing ratio.

30 The balance of radical species, which are converted in both pathways, additionally links both pathways (Fig. 6, light colours). In reaction R12, is mainly destroyed in reaction R1 following pathway AC1, which yields the oxidation of as the net reaction. In cycle AC1 the radical reacts with NO (??). As an alternative the besides HCl a methylperoxy radical (H_3COO) is formed,

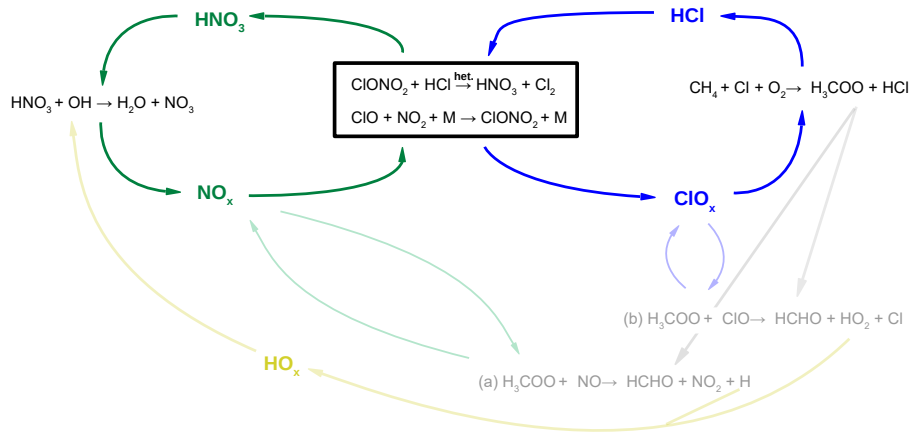


Figure 6. Reaction scheme to illustrate the balance between chlorine activation and chlorine deactivation (blue, right) and NO_x activation and deactivation (green, left). The heterogeneous reaction ClONO₂+HCl (R1) links both cycles. Additional reaction pathways, which balance radicals are shown in light colours.

which reacts either with NO or with ClO leading to HO_x-formation (HO_x=H, OH, HO₂).



Appendix A.

However, in In this example the heterogeneous HCl-destruction ($R1, ClONO_2 + HCl$) does not balance the HCl-formation ($R12, Cl + CH_4$) (Fig. 4b) due to completely, because of increasing temperatures (Fig. 4a). Higher temperatures decelerate the heterogeneous HCl-destruction and thus result in the slightly increasing HCl-mixing ratio from 4 August–7 August 2013 (Fig. 4f). Such temperature fluctuations (Fig. 4a) affect the balance between HCl formation and destruction less at higher water vapour mixing ratios, because the heterogeneous HCl-destruction rate ($R1$) increases for both low temperatures and high water vapour mixing ratios (see Sec. 4). Thus, regarding the balance between HCl formation and HCl destruction (and hence the balance between chlorine deactivation and chlorine activation), a high water vapour mixing ratio can compensate a small range of temperature fluctuations. This balance can be described by the cycles AC1 and AC2 and maintains active maintains activated chlorine levels, which is essential for the catalytic ozone loss cycles ??–C2 and C3–C4 to proceed.

4 Analysis of chlorine activation

In the previous section we showed that in the temperature range of 197–203 K there is a threshold for water vapour, which has to be exceeded to yield chlorine activation and thus enables substantial ozone destruction. Here, we investigate the sensitivity of this threshold on sulphate content, temperature, Cl_y and NO_y mixing ratio.

4.1 Sensitivity of the water vapour threshold

Modifying temperature, sulphate amount or the mixing ratios of Cl_y or NO_y yields a shift of the water vapour threshold. Figure 7 shows the ozone values reached at the end of the 7-day simulation (final ozone) for a variety of sensitivity cases assuming the standard trajectory of the SEAC⁴RS case (left) and the MACPEX trajectory (right). For each case, the water vapour threshold is marked with an arrow in the colour of the corresponding case.

The water vapour dependent final ozone values for the standard case are plotted as blue squares (Fig. 7, left) with a water vapour threshold of 10.6 ppmv (see Sec. 3). Raising the trajectory temperature by 1 K over the standard case leads to a higher water vapour threshold of 13.5–14.0 ppmv (open red squares), while increasing the sulphate content by a factor of 3 results in a lower threshold region of ~9.0–9.5 ppmv (yellow diamonds). An even larger enhancement of the sulphate content (10× H_2SO_4 , magenta diamonds) lowers the water vapour threshold further to a value near 7–8 ppmv. Reducing the NO_y mixing ratio to 80% of the standard case yields a shift of the threshold to a lower water vapour mixing ratio (green filled triangles), while an equivalent reduction in the Cl_y mixing ratio shifts the threshold region to higher water vapour mixing ratios (black circles). A reduction in Cl_y also reduces ozone destruction and hence results in higher ozone mixing ratios at the end of the simulation. While the preceding analysis was based on a single SEAC⁴RS trajectory, similar conclusions are reached when the analysis is conducted using a trajectory from the MACPEX campaign. Results of the analysis using the MACPEX initialization and backward trajectory (Fig. The sensitivity of the water vapour threshold to temperature, sulphate abundance and Cl_y and NO_y mixing ratio is explained in the next Section (Sec. 4, black) are shown in the right panel of Fig. 7. A critical water vapour range of 12–13 ppmv is required to produce a reduction of the final ozone value. In the MACPEX case, the final ozone is mostly for

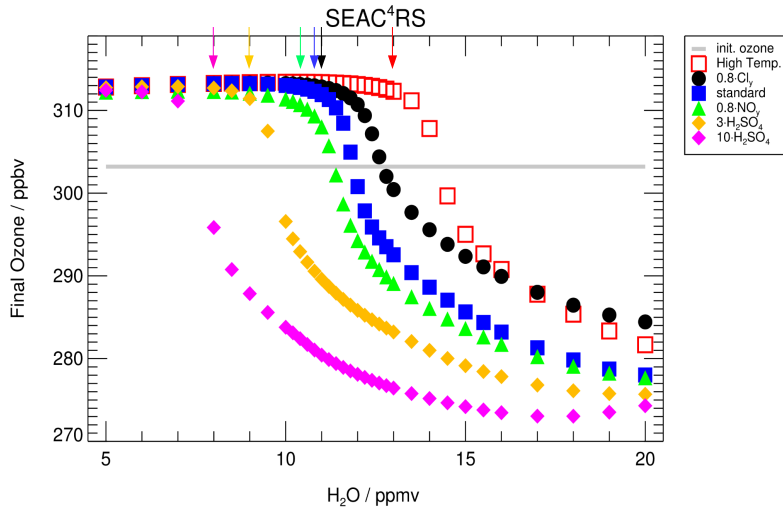


Figure 7. Impact of the water vapour content on the ozone mixing ratio (final ozone) reached at the end of the 7-day simulation along the standard trajectory (SEAC⁴RS, left) and the MACPEX trajectory (right). The standard case is shown in blue and the initial ozone amount is marked by the grey line. An impact on the final ozone mixing ratios is observable after exceeding a critical threshold in water vapour, which is marked with an arrow for the different cases. This threshold changes with a shift in trajectory temperature (+1K, red), the Cl_y mixing ratio to 0.8 Cl_y (black), the NO_y mixing ratio (0.8 NO_y, green) and the sulphate content (3× standard H₂SO₄, yellow and 10× standard H₂SO₄, magenta).

all simulations higher than the initial ozone. This is due to the lower -mixing ratio (~554.2).

As a further example for an event with high stratospheric water vapour mixing ratios based on airborne measurements, simulations based on measurements during the Mid-latitude Airborne Cirrus Properties Experiments (MACPEX) were conducted.

5 This campaign was based in Texas during springtime 2011 and hence prior to the formation of the North American Monsoon (NAM). A detailed description of this MACPEX case is given in the Appendix (App. pptv) assumed in the MACPEX case, which yields lower rates for catalytic ozone loss after chlorine activation occurred B). For the MACPEX case, changes in sulphate (Fig. 7, left, yellow diamonds), Cl_y (black circles) or and NO_y (green triangles) mixing ratios affect the catalytic ozone destruction water vapour threshold similarly to that observed for the SEAC⁴RS trajectory. This yields the conclusion

10 Thus, the MACPEX results confirm the SEC⁴RS findings. Therefore, we conclude that in the considered temperature range (~197–203 K), an ozone reduction occurs after exceeding a water vapour threshold and that this threshold varies with Cl_y, NO_y, sulphate content and temperature.

4.2 Explanation of the water vapour threshold

The sensitivity of the water vapour threshold to Cl_y , NO_y , sulphate loading and temperature is investigated, focussing on the balance between heterogeneous chlorine activation mainly due to R1 ($\text{ClONO}_2 + \text{HCl}$) and gas phase chlorine deactivation

5 mainly due to R12 ($\text{Cl} + \text{CH}_4$). Net chlorine activation takes place when the chlorine activation rate exceeds the chlorine deactivation rate. Reaction R1 is the key reaction in the chlorine activation process. Therefore, in the following, first the **dependency dependence** of R1 on the water vapour content is analysed in detail. Second, the balance between chlorine activation and deactivation is investigated, also considering the impact of Cl_y , NO_y , sulphate and temperature on the **water vapour** threshold.

In general the rate of R1 ($\text{ClONO}_2 + \text{HCl}$) v_{R1} is determined through:

$$10 \quad v_{\text{R1}} = k_{\text{R1}} \cdot c_{\text{ClONO}_2} \cdot c_{\text{HCl}} \quad (1)$$

The concentrations of ClONO_2 c_{ClONO_2} and HCl c_{HCl} are associated with the gas phase mixing ratio and the rate constant k_{R1} , as a measure of the reactivity of the heterogeneous reaction, depends in this case on the γ -value γ_{R1} , the surface area of the liquid particle A_{liq} , the temperature T and c_{HCl} (Eq. 2) (Shi et al., 2001).

$$k_{\text{R1}} \propto \frac{\gamma_{\text{R1}} \cdot A_{\text{liq}} \cdot \sqrt{T}}{1 + c_{\text{HCl}}} \quad (2)$$

15 The γ -value describes the uptake of ClONO_2 into liquid particles due to the decomposition of ClONO_2 during reaction R1 and is thus a measure of the probability of the occurrence of this heterogeneous reaction (Shi et al., 2001). **Laboratory studies showed a dependence of γ_{R1} on the solubility of HCl in the droplet, which generally increases for a lower H_2SO_4 fraction in the particle (H_2SO_4 wt%)** (Elrod et al., 1995; Hanson, 1998; Zhang et al., 1994; Hanson and Ravishankara, 1994). From Eq. 2 it is obvious that a large surface area A_{liq} and a high γ -value γ_{R1} increase k_{R1} and thus the heterogeneous reaction rate v_{R1} .

20 In Figure 8, the impact of the water vapour content on **the H_2SO_4 weight-percent**, γ_{R1} , A_{liq} , k_{R1} and the reaction rate v_{R1} is **plotted shown**. To avoid the influence of R1 itself on these parameters as much as possible, these parameters are selected for 1 August 2013 at 13:00 UTC. This point in time corresponds to the values after the first chemistry time step during the chemical simulation. The **particles H_2SO_4 wt% decreases for all cases with increasing water vapour from more than 50 wt% at 5 ppmv H_2O to around 20 wt% at 20 ppmv H_2O due to an increasing uptake of H_2O in the thermodynamic equilibrium**. The

25 standard case is illustrated in blue squares (Fig.8) and exhibits a strongly increasing gamma value especially for water vapour mixing ratios between 9 and 14 ppmv **as well as an almost constant liquid surface area A_{liq} in due to a lower H_2SO_4 wt%.** **In** the same water vapour range. **The slight increase in, the liquid surface area density A_{liq} is caused by formation in R1 and the subsequent uptake increases slightly. It increases more for higher water vapour mixing ratios because of HNO_3 into the condensed particles, especially for high water values uptake into the particles.** Due to **an** the increasing γ -value with increasing

30 water vapour, the rate constant k_{R1} increases (Shi et al., 2001) and thus induces a larger reaction rate v_{R1} with an increasing water vapour mixing ratio.

At low water vapour mixing ratios, not only the rate of R1 ($\text{ClONO}_2 + \text{HCl}$) but also of R12 ($\text{CH}_4 + \text{Cl}$) increases with an increasing water content (Fig. 5f). An increasing heterogeneous reaction rate (R1) results in both a lower NO_x mixing ratio and

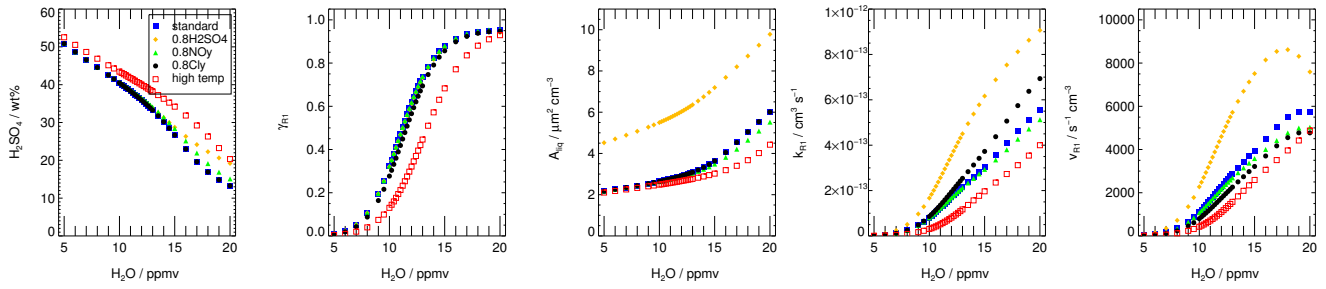


Figure 8. Dependence on water vapour of the rate of the the main heterogeneous chlorine activation reaction R1 v_{R1} , the rate coefficient (k_{R1}), the γ -value γ_{R1} and the liquid surface area density A_{liq} , and the H_2SO_4 weight %. Presented parameters correspond to the values after the first chemistry time step of the box-model simulation. Additionally the impact of an enhanced sulphate content (0.8 ppbv H_2SO_4 , yellow), reduced NO_y (0.8 NO_y , green), reduced Cly (0.8 Cly , black) and enhanced temperatures (red) is shown. The standard case is shown as blue squares.

more HCl converted into ClO_x . A higher ClO_x concentration yields a higher Cl mixing ratio and thus an increase in the rate of R12 ($CH_4 + Cl$). Since both the rates of R1 and R12 increase, no significant net chlorine activation occurs. In-Around the water vapour thresholdregion, the Cl-mixing ratio peaks (Fig. 5g), because less ClO is converted into Cl through **R24 (ClO+NO)**



due to the decreasing NO_x mixing ratio. The lower Cl mixing ratio reduces the HCl formation in R12 ($CH_4 + Cl$). Hence, the increasing heterogeneous reactivity k_{R1} yields a higher rate of R1 and in the same way it impedes R12 by reducing the NO_x

mixing ratio. ~~In the same way, an increase in k_{R1} yields a higher rate of R1.~~ As a consequence the rate of R1 exceeds the rate of R12 and a net chlorine activation takes place, leading to a reduction of HCl. The decline in both HCl and NO_x yields smaller rates of R1 and R12 at high water amounts and thus ~~the a~~ peak of R1 and R12 ~~occurs in the water vapour threshold~~ 5 ~~region~~ (Fig. 5f). Hence, the increasing heterogeneous reactivity (k_{R1}) of R1 ~~promotes destabilizes the balance between chlorine activation and deactivation by promoting the~~ chlorine activation (due to an increasing rate of R1) and ~~impedes impeding~~ chlorine deactivation (due to a reduction of R12). This yields heterogeneous chlorine activation to exceed gas phase HCl-formation in the water vapour threshold region. ~~The increase in k_{R1} yields a net chlorine activation in the water vapour threshold region by destabilizing the balance between chlorine activation and deactivation.~~

10 For an enhanced sulphate content (Fig. 8, yellow diamonds), the particle surface area density (~~illustrated by~~ A_{liq}) is larger, leading to both a stronger increase of the heterogeneous reactivity (k_{R1}) and ~~hence~~ a higher heterogeneous reaction rate than in the standard case. Due to this higher heterogeneous reactivity (k_{R1}), the chlorine activation rate exceeds the chlorine deactivation at a lower water vapour mixing ratio and the net chlorine activation is reached at a lower water vapour threshold. A shift to 15 higher temperatures (Fig. 8, red) yields almost no change in the surface area density (A_{liq}) but a reduced γ -value ~~due to a higher~~ H_2SO_4 ~~fraction in the particles~~ (H_2SO_4 ~~wt%~~) and thus a lower heterogeneous reactivity (k_{R1}). The reduced reactivity causes the net chlorine activation to occur at a higher water vapour threshold.

In contrast, the shift of the threshold for simulations with only 80% of standard NO_y (0.8 NO_y, Fig. 8 green) or Cl_y (0.8 Cl_y, Fig. 8 black) can not be explained only by an increase in k_{R1} . In these cases, further effects on the balance between chlorine activation and chlorine deactivation have to be taken into account. The water vapour threshold in the 0.8 NO_y simulation (green 20 triangles) is shifted to lower water vapour values due to a smaller Cl/ClO-ratio for lower NO_x concentrations. This yields a reduced HCl formation through R12 (CH₄ + Cl) than in the standard case and thus impedes chlorine deactivation. The reduced chlorine deactivation affects the balance between chlorine activation and deactivation in a way that the water vapour threshold region in the 0.8 NO_y case is lower than in the standard case. In the 0.8 Cl_y case (Fig. 8, black), the HCl and ClONO₂ mixing 25 ratios are reduced. This leads to a lower chlorine activation rate v_{R1} than in the standard case, despite of the slight higher heterogeneous reactivity (k_{R1}), which is due to the inverse dependence of k_{R1} on the HCl concentration (Eq. 2). The lower dependence of reaction R12 (Cl+CH₄) than of R1 (HCl + ClONO₂) on the Cl_y mixing ratio would push chlorine deactivation (R12) in the balance between chlorine activation and deactivation and hence shift the water vapour threshold to higher water vapour mixing ratios. Additionally caused by the lower rate of R1 (ClONO₂ + HCl) for reduced Cl_y, the NO_x mixing ratio 30 decreases more slowly. This enhances the rate of R12 compared with the standard case as well, because more NO_x yields a higher Cl/ClO-ratio.

In summary, the ~~water vapour~~ threshold is determined by the balance between chlorine activation and deactivation and is thus in a certain temperature range especially sensitive to the water dependence of the heterogeneous reactivity (k_{R1}) mainly described through the γ -value γ_{R1} and the particle surface A_{liq} . These parameters are dependent on the present temperature and sulphate content. However, further parameters ~~shifting influencing~~ this balance, such as the NO_y and Cl_y mixing ratio, have an impact on the water vapour threshold as well.

4.3 Temperature dependence

The water vapour threshold, which has to be exceeded for chlorine activation and stratospheric ozone loss to occur, is mainly dependent on the temperature. To illustrate the impact of both temperature and water vapour mixing ratio on stratospheric ozone, the relative ozone change occurring after a 7-day simulation, in which a constant temperature and water vapour concentration and the Cl_y and NO_y values of the standard case is assumed, is shown in Fig. 9. In the left panel, ozone change as a function of temperature and water vapour is plotted for non-enhanced sulphate amounts. In the right panel, the relative ozone change is shown for $10\times$ standard sulphate to estimate a potential impact of volcanic eruptions or sulphate geoengineering on stratospheric ozone. Since mixing of neighbouring air parcels is neglected in the box-model study, the relative ozone change calculated corresponds to the largest possible ozone change for the conditions assumed. A mixing of moist tropospheric air with dry stratospheric air is expected to reduce the water vapour mixing ratio during the time period of the 7-day trajectory and hence could stop ozone depletion before the end of the trajectory is reached. In addition to the relative ozone change, the threshold for chlorine activation is shown as a white line in both panels. When temperature is held constant, this threshold corresponds to the water vapour threshold discussed above. Chlorine activation occurs at higher water mixing ratios and lower temperatures relative to the white line plotted. Here, chlorine is defined to be activated, if the ClO_x/Cl_y ratio exceeds 10%. For climatological non-enhanced sulphate amounts (Fig. 9, left), the temperature has to fall below 203 K for chlorine activation to occur, even for high water vapour mixing ratios of 20 ppmv. For the simultaneous presence of high water vapour and low temperatures an ozone loss of 9% (max. 27 ppbv O_3) was found. This maximal ozone loss occurs for a range of low temperatures (195–200 K) and enhanced water vapour mixing ratios (10–20 ppmv), because of a similar time until chlorine activation occurs. If the temperatures are higher and water vapour mixing ratios lower than the chlorine activation line, the ozone mixing ratio increases around 3.5% (~ 10 ppbv O_3). At enhanced sulphate conditions (Fig. 9, right) an ozone loss of max. 10% (30 ppmv O_3) occurs for low temperatures and high water vapour mixing ratios. For a water vapour mixing ratio of 20 ppmv the temperature has to fall below 205 K for ozone loss to occur. If the temperatures are very low (195–200 K) and the water vapour is high (10–20 ppmv) ozone loss is slightly reduced. This turnaround occurs, because at a high sulphate loading in combination with high water and low temperatures more HCl is taken up by condensed particles. This leads to less Cl_y in the gas phase and thus lower rates of catalytic ozone loss.

In summary, the combination of low temperatures, enhanced sulphate concentrations and high water vapour mixing ratios promotes an ozone decrease of up to $\sim 10\%$ (max. corresponding to maximum ~ 30 ppbv O_3) for high water vapour mixing ratios, low temperatures and enhanced sulphate conditions. In comparison to the study of Anderson et al. (2012), the temperatures have to fall below 203 K (here) instead of 205 K (in Anderson et al. (2012)) for non enhanced sulphate conditions and below 205 K instead of 208 K (in Anderson et al. (2012)) for enhanced sulphate conditions and a water vapour mixing ratio of 20 ppmv for chlorine activation and thus ozone loss to occur. Hence, Anderson et al. (2012) found ozone loss in mid-latitudes at high water vapour mixing ratios for temperatures 2 to 3 K higher than in our simulations.

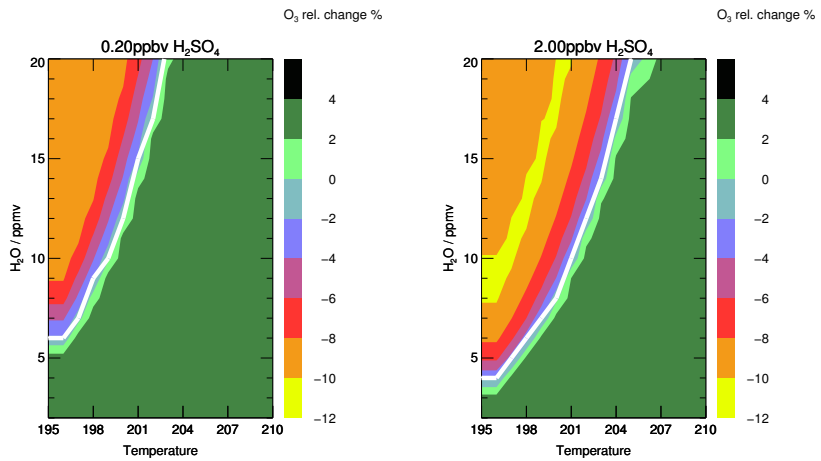


Figure 9. Relative ozone change during the 7-day simulation along the standard trajectory dependent on temperature and H_2O ratio for climatological non enhanced (left panel) and enhanced (right panel) sulphate conditions. The white line corresponds to the water and temperature dependent chlorine activation threshold.

5 Case studies

Case studies were conducted to illustrate the sensitivities described above on ozone loss and to estimate the impact of realistic conditions and an upper boundary on the ozone loss process. ~~As a kind of worst case study (upper boundary), the “Case of high” was simulated using and mixing ratios based on the study of Anderson et al. (2012), which uses and much larger than inferred from tracer-tracer correlations (Table 1).~~ In the “case based on observations”, standard conditions and the measured water vapour mixing ratio of 10.6 ppmv were assumed using both the low sulphate content of the standard case and a slightly enhanced sulphate content, which represents the possible impact of volcanic eruptions or geoengineering conditions. ~~As a kind of worst case study (upper boundary), the “Case of high Cl_y ” was simulated using Cl_y and NO_y mixing ratios based on the study of Anderson et al. (2012), which uses Cl_y and NO_y much larger than inferred from tracer-tracer correlations (Table 1).~~ In the “reduced Br_y case”, standard conditions with a 50% reduced Br_y mixing ratio were assumed to test uncertainties in current observations of stratospheric bromine burden. Additionally the previously noted standard 7-day trajectory was extended to a 19-day trajectory ~~to infer the dependence of ozone loss on the simulated time period~~.

5.1 Case of high-based on observations

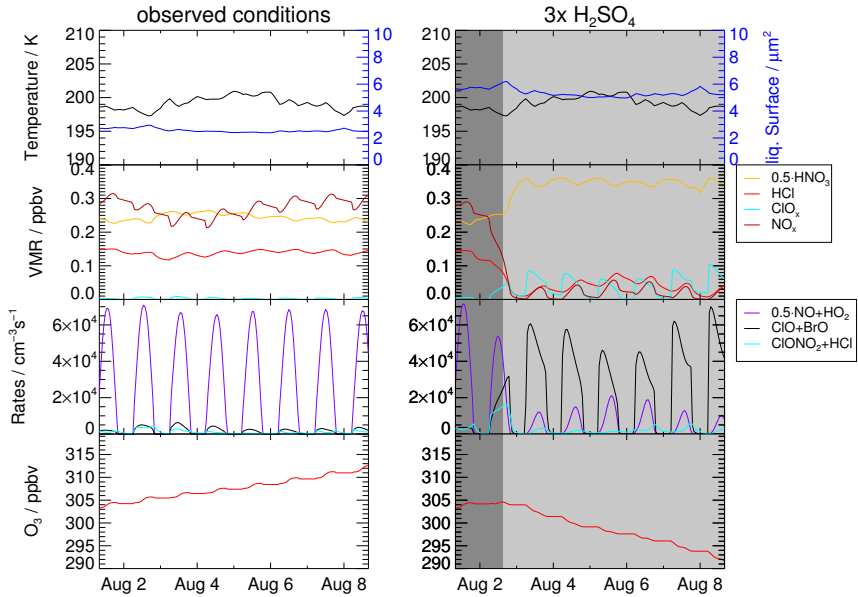


Figure 10. Behaviour under “Case of high” conditions assuming high values for and (see Tab. 1). Left panel shows the dependence of ozone values reached at the end of the 7-day simulation on water vapour for reference (blue) and 3×enhanced sulphate contents (yellow); the grey line corresponds to the initial ozone value. Right panel presents panels present the volume mixing ratio of ozone, temperature, liquid surface area density, ozone mixing ratio, reaction rates of R1 (scaled by 0.5CIONO₂ + HCl, cyan), HClR18 (ClO+BrO, and and reaction rates of reaetions essential black) (as an example for chlorine activation and catalytic ozone loss cycles), R6 (R1 and R18 NO + HO₂, violet) which limits ozone formation at low NO_x concentrations as well as volume mixing ratios of HCl (ClO+BrOred), R17-ClO_x (ClO+ClOlight blue), NO_x (black) and R13-HNO₃ (scaled with 0.5) for the “Case based on observations” with 10.6 ppmv H₂O and 0.20 ppbv H₂SO₄. The panels on the right show the same quantities, but for enhanced sulphate conditions (0.60 ppbv H₂SO₄). The x-axis ticks refer to 00:00 local time (06:00 UTC) of that day.

The simulation of the case based on observations during the SEAC⁴RS aircraft campaign corresponds to the most realistic case for today’s chemical conditions. It is identical to that of the standard case but assumes a fixed water vapour mixing ratio of 10.6 ppmv observed on 8 August 2013. Under these conditions, neither relevant heterogeneous chlorine activation due to R1 (CIONO₂ + HCl) nor catalytic ozone loss cycles (e.g. based on ClO+BrO) can be observed in the simulation (Fig. 10, left). Instead, ozone is formed. In comparison, the same simulation with 0.6 ppbv gas phase equivalent H₂SO₄ instead of 0.2 ppbv was conducted (Fig. 10, right). The enhanced sulphate content yields a larger liquid surface area density and thus an increased heterogeneous reactivity. Hence, reaction R1 occurs in the 3×H₂SO₄ simulation significantly, leading to a slightly increasing ClO_x mixing ratio and a decrease of the NO_x mixing ratio. Both a reduced ozone formation in C1 (which is at decreased NO_x concentrations limited by R6) and ozone loss cycles (e.g. based on the reaction ClO+BrO or ClO+HO₂) can be observed, resulting in a reduction of ozone.

Using initial conditions, the trajectory corresponding to the SEAC⁴RS observations shows ozone loss with sulphate enhanced by a factor of 3. However, we note that this was an unusually cold trajectory. A more common case with higher mean temperatures would require a higher sulphate content to enhance the heterogeneous reactivity that chlorine activation can occur. Thus under current chemical conditions in the UTLS (upper troposphere, lower stratosphere), it is most unlikely to get significant ozone loss by convectively injected water vapour in mid-latitudes.

5.2 Case of high Cl_y

Under conditions of substantially higher initial Cl_y and NO_y mixing ratios (see Tab. 1) than in the standard case used in Anderson et al. (2012), a larger ozone loss up to 265 ppbv during the 7-day simulation is simulated (Fig. ??, left). Since these high Cl_y conditions have been criticised in other studies (e.g. Schwartz et al., 2013; Homeyer et al., 2014) as being unrealistically high, they are assumed here as a worst case scenario. Under high chlorine conditions, and for a high water vapour content (more than \approx 18 ppmv), an almost complete ozone destruction with ~~an end-a final~~ ozone value of less than 50 ppbv is simulated (Fig. ??, left), which corresponds to parcel ozone loss of 85%. During the 3.5-day simulation in the study of Anderson et al. (2012), an ozone loss of 20% with respect to initial ozone occurs for 18 ppmv H₂O. This difference in relative ozone loss for similar conditions here and in the study of Anderson et al. (2012) is caused by a longer assumed ozone destruction period in our simulation. ~~Since the Cl_y-mixing ratio is much higher than in the standard case, the catalytic ozone loss cycles are dominated by the ClO-Dimer cycle (see S1 in the Supplements for chemical details).~~ Assuming the measured water vapour content of 10.6 ppmv for high chlorine conditions would lead to an ozone depletion of 57% during the 7-day simulation. In comparison, in the standard case an ozone loss of 8% is reached when a high water vapour mixing ratio of 20 ppmv is assumed. However, even for the standard trajectory and a high chlorine content, a water vapour amount of 8 ppmv has to be exceeded to yield any ozone reduction. This threshold shifts from 8 ppmv to 7 ppmv for the case where stratospheric sulphate is tripled (Fig. ??, left, yellow triangles). ~~Comparing the standard case and the high case using 15 ppmv water vapour conditions, in the high case more inactive chlorine is converted into active on the first day of the simulation (Fig. ??, right). This higher mixing ratio results in faster catalytic ozone loss cycles with peak values of $3.9 \cdot 10^5$ for R13 (ClO₊), $2.0 \cdot 10^5$ for R18 (ClO+BrO) and $10.9 \cdot 10^5$ for R17 (ClO+ClO) on 3 Aug 2013. Since the mixing ratio is much higher than in the standard case, the catalytic ozone loss cycles are dominated by the ClO-Dimer cycle and result in a much larger ozone loss than in the standard case assuming realistic and mixing ratios.~~

5.3 Case based on observations

The simulation of the case based on observations during the SEAC⁴RS aircraft campaign corresponds to the most realistic case for today's climate. It is identical to that of the standard case but assumes a fixed water vapour mixing ratio of 10.6 ppmv observed on 8 August 2013. Under these conditions, neither heterogeneous chlorine activation due to R1() nor catalytic ozone loss cycles (e.g. based on ClO+BrO) can be observed in the simulation (Fig. 10, left). Instead, ozone is formed due to cycle C1. In comparison, the same simulation with 0.6 gas phase equivalent instead of 0.2 was conducted (Fig. 10, right). The enhanced sulphate content yields a larger liquid surface area density and thus an increased heterogeneous reactivity. Hence, reaction

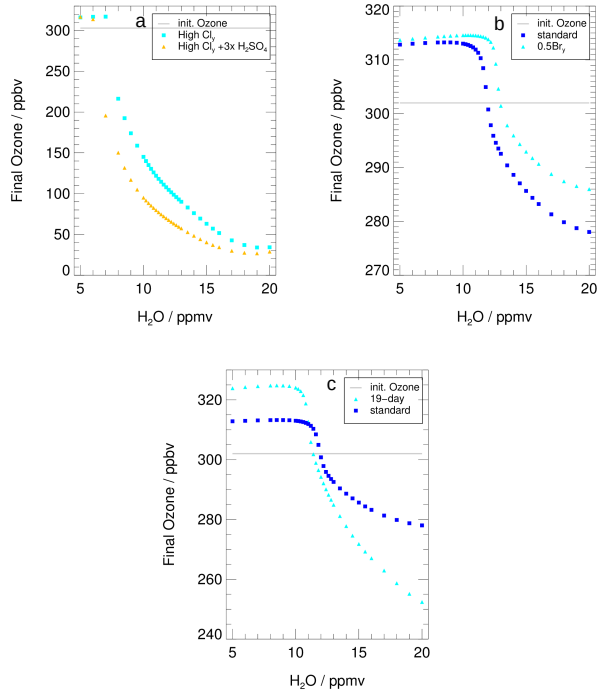


Figure 11. Left panels present the temperature, liquid surface area density, The water dependent final ozone mixing ratio, reaction rates value is shown for (a) the “Case of R1-high Cl_y” (, cyan see Tab. 1 for NO_y and Cl_y initialisation) , R18 assuming background aerosol (ClO+BrO, blacklight blue) and tripled H₂SO₄ (as an example for ozone loss cyclesyellow), R6 (, violet) which limits ozone formation at low concentrations as well as volume mixing ratios of HCl-reduced Br_y (redlight blue, “Reduced Br_y case”), and (c) an extended time period of activated chlorine (light blue), “19-day simulation”). In panel (b) and (c) for conditions also final ozone of the measurement standard case is shown (blue). Initial ozone is marked with 10.6 and 0.20 a grey line. The panels on the right show Note that the same quantities, but for enhanced sulphate conditions (0.60) scale of all y-axis differ.

R1 occurs in the 3×simulation significantly, leading to a slightly increasing mixing ratio and a decrease of the mixing ratio. Both a reduced ozone formation in C1 (which is at decreased concentrations limited by R6) and ozone loss cycles (e.g. based on the reaction ClO+BrO or ClO+) can be observed, resulting in a reduction of ozone. Using initial conditions, the trajectory 5 corresponding to the SEAC⁴RS observations shows ozone loss with sulphate enhanced by a factor of 3. However, we note that this was an unusually cold trajectory. A more common case with higher mean temperatures would require a higher sulphate content to enhance the heterogeneous reactivity enough for chlorine activation to occur.

5.3 Reduced Br_y Case

Impact of a reduction on the water vapour threshold and the ozone loss process. Left panel shows the dependence of ozone values reached at the end of the 7-day simulation on water vapour for the standard case (blue) and a simulation assuming the half of (light blue); the grey line corresponds to the initial ozone value. Right panel presents the volume mixing ratio of ozone, the mixing ratio of (sealed by 0.5), HCl, and and reaction rates of reactions essential for chlorine activation and catalytic ozone loss cycle (R1) and R18 (ClO+BrO), R17 (ClO+ClO) and R13 ()). The mixing ratio of inorganic bromine (Br_y) has a high uncertainty in the lowermost stratosphere due to the influence of very short lived bromine containing substances. For example, during the CONTRAST field campaign (Jan-Feb 2014, western Pacific region), Koenig et al. (2017) observed a Br_y mixing ratio in the lower stratosphere of 5.6–7.3 ppt and the contribution of Br_y , which crosses the tropopause, was estimated to be 2.1 ± 2.1 ppt (Wales et al., 2018). Navarro et al. (2017) found somewhat different bromine partitioning depending on the ozone, NO_2 and Cl_y concentrations, using very short lived bromine species observations in the eastern and western Pacific ocean from the ATTREX campaign. Because our Br_y – Br_y values are not based on measurements for this specific case modeled, we tested the sensitivity to a value that is half of our standard case. The impact of this Br_y reduction is illustrated in Fig. ?? assuming a water vapour mixing ratio of 15 ppmv. Comparing the end ozone value for the 0.5 Br_y simulations (Fig. ??, left, light blue triangles) with those of the standard case (blue squares), a higher water vapour threshold and a reduced ozone loss of about 30% at high water vapour mixing ratios is simulated. The reduction shift of the water vapour threshold is due to the impact of Br_y yields a slightly longer time period of chlorine activation. At high HCl and low mixing ratios at the start of the simulation, the formation of on the NO_2/NO -ratio. Due to the reaction



reduced Br_y yields a smaller NO_2/NO -ratio and hence less ClONO₂ formation in R9 (ClO+NO₂). Since ClONO₂ formation is essential for maintaining the chlorine activation reaction R1. Hence, the chlorine activation is dependent on the formation of chlorine activation in R1 (ClONO₂ and thus on the /NO-ratio (von Hobe et al., 2011). A higher /NO-ratio yields a higher rate of R9 and enhances the rate of R1. A +HCl, reduced Br_y -mixing ratio leads to a smaller /NO-ratio due to R25 (BrO+NO) and thus to yields a lower chlorine activation rate (von Hobe et al., 2011). A reduction of the chlorine activation rate (R1) would change the balance between chlorine activation and chlorine deactivation, which determines and thus a shift of the water vapour threshold region. Thus, this reduction would lead to the shift of the water vapour threshold, which is illustrated in Fig. ?? (left panel). With less to higher water vapour mixing ratios. In the case of reduced Br_y the catalytic, less ozone is destroyed regarding the standard case. The ozone destruction in the ClO-BrO-cycle (??) is reduced (Fig. ??, right panel) is reduced, while the rates of R17 (ClO+ClO) and R13 (ClO+HO₂) are similar to those of the standard case (Fig. 4,e; for chemical details of the reduced Br_y -case see Suppl. S2). This results in the reduced ozone destruction in the 0.5 Br_y case.

5.4 19-day simulation Extended time period

Impact of the simulated time period on ozone loss. Left panel shows the dependence of ozone values reached at the end of the simulation on water vapour for the standard case (7-day, blue) and the 19-day simulation (cyan); the grey line corresponds to

the initial ozone value. Right panel presents temperature, liquid surface area, the mixing ratio of ozone, (sealed by 0.5), HCl, and and reaction rates of reactions essential for chlorine activation and catalytic ozone loss cycles (R1 ()) and R18 (ClO+BrO), R17 (ClO+ClO) and R13 () for the 19-day simulation.

5 Since the occurrence of the ozone loss process analysed in this study is strongly dependent on a variety of parameters, the time period over which the ozone loss might occur is very uncertain. The impact of this time period on ozone loss was tested by extending the 7-day trajectory used in the sections above to span the entire period with temperatures low enough to maintain chlorine activation. ~~The temperature development of this trajectory is shown in Fig. ??.~~ On 27 July 2013, the 19-day simulation starts at a temperature of 208 K (Fig. ??, right), decreasing until 29 July 2013 to lower than ~~In this time extended~~ 10 ~~simulation, temperatures are well below 200 K. The temperatures remain lower than at the begin of the simulation and remain below 201 K until 11 August and increase to over 205 K on for 14 August 2013. Assuming a water vapour mixing ratio of 15 ppmv days. Hence, chlorine activation occurs on 30 July 2013, after the temperatures fall below 200 K (Fig. ??, right). The mixing ratio of remains low and remains high until 11 can be maintained for a longer time period than in the standard case and breaks up due to increasing temperatures (for details regarding chemical processes and temperature development along the~~ 15 ~~extended trajectory see Suppl. August, when the heterogeneous reaction rate of R1 () decreases due to higher temperatures. For this reason chlorine activation cannot anymore be maintained by cycle AC1. Thus, the time span holding a mixing ratio high enough for the occurrence of catalytic ozone loss cycles (??-C2, C3-C4)comprises 14 days and ozone destruction stops on 12 AugustS3).~~

Because of the extended time period, the final ozone values using the enhanced water vapour mixing ratios for ~~19-days the~~ 20 ~~longer trajectory~~ (cyan triangles Fig. ??, left panel ~~11c~~) are much lower than those of the standard 7-day simulation (blue squares). Additionally, more ozone is formed when using low water vapour concentrations. Comparing the water vapour threshold of the 7-day trajectory (~ 11.0 – 11.6 ppmv) and the 19-day simulation (~ 10.6 – 10.2 ppmv), a shift to lower water vapour mixing ratios occurs in the 19-day trajectory. This shift is likely due to an extended time period with a temperature well 25 below 200 K ~~at the begin of this trajectory~~, which allows a chlorine activation to occur even for slightly lower water vapour amounts. Simulations along a trajectory starting on the same day as the 7-day trajectory, but finishing on 15 August, yield the same water vapour threshold as the 7-day simulation (not shown), indicating that the shift in the threshold shown in Fig. ??-11 is associated with the very cold conditions at the start of the 19-day simulation. Hence, the length of the chosen trajectory has no impact on the water vapour threshold, but does effect the final ozone.

6 Discussion

30 Many uncertainties affect the assessment of the extent of ozone loss that occurs in the lowermost stratosphere at mid-latitudes under ~~elevated enhanced~~ water vapour conditions. The number and depth of convective overshooting events as well as the area and duration affected by enhanced water vapour mixing ratios is a subject of recent research (e.g. Homeyer et al., 2014; Smith et al., 2017). The mixing ~~ratio ratios~~ of important trace gases (O₃, Cl_y, Br_y, NO_y) in overshooting plumes and the ~~possibility probability~~ that water vapour mixing ratios high enough for chlorine activation meet temperatures low enough is a matter of

debate (e.g. Schwartz et al., 2013; Homeyer et al., 2014). ~~In this study, we examined the sensitivity to different water vapour mixing ratios, temperature, content, and trajectory duration.~~

The ozone loss mechanism investigated here requires the occurrence of the heterogeneous reaction R1, which leads to enhanced ClO_x and reduced NO_x mixing ratios and thus maintains effective catalytic ozone loss cycles. Enhanced ClO and reduced NO concentrations were observed by Keim et al. (1996) and Thornton et al. (2007) close to the mid-latitude tropopause under conditions with ~~elevated both enhanced~~ water vapour and enhanced concentrations of condensation nuclei, such as sulphate particles. These observations were attributed to the occurrence of the heterogeneous reactions R1 ($\text{ClONO}_2 + \text{HCl}$) and R2 ($\text{ClONO}_2 + \text{H}_2\text{O}$, Thornton et al., 2007; Keim et al., 1996). For the temperature and the water vapour range observed in the studies of Keim et al. (1996) (15 ppmv H_2O , ~ 207 K) and Thornton et al. (2007) (15–22 ppmv H_2O , ~ 213 –215 K), a heterogeneous chlorine activation would not occur in the box-model simulation conducted here, not even in a sensitivity simulation assuming a high sulphate gas phase equivalent of 7.5 ppbv H_2SO_4 (not shown). At low temperatures ($\lesssim 196$ K), heterogeneous chlorine activation may occur in the tropical stratosphere (Solomon et al., 2016; von Hobe et al., 2011). Von Hobe et al. (2011) observed enhanced ClO mixing ratios during aircraft campaigns over Australia (SCOUT-O₃, 2005) and Brazil (TROCCINOX, 2005) in combination with low temperatures and the occurrence of cirrus clouds. Analysing the balance between chlorine activation and deactivation von Hobe et al. (2011) showed an increase of the chlorine activation rate (R1) with a higher ClO , BrO and O_3 mixing ratio. Thus, once started, R1 accelerates due to higher ClO -mixing ratios subsequently yielding a fast conversion of NO_x into HNO_3 (von Hobe et al., 2011), comparable to the NO_y repartitioning found in the present study. Von Hobe et al. (2011) found a threshold in ozone mixing ratio, which has to be exceeded for chlorine activation to occur. Hence, the water vapour threshold discussed here is expected to depend on the ozone mixing ratio, as well. Furthermore a potential occurrence of ice particles in the lowermost mid-latitude stratosphere (Spang et al., 2015) might affect the water vapour threshold due to a different heterogeneous reactivity on ice than on liquid particles (Solomon, 1999).

An ~~elevated sulphate content enhances enhanced sulphate content increases~~ the heterogeneous reaction rate caused by an ~~increased enlarged~~ liquid surface. Due to this relation, an impact of stratospheric albedo modification (by applying solar geoengineering) on the ozone loss process proposed by Anderson et al. (2012) is discussed (Dykema et al., 2014).

~~Applying solar geoengineering would also affect the temperature in the lowermost stratosphere by perturbing the Eddy-heat fluxes and would change the lower stratospheric dynamics (Visioni et al., 2017). It would also affect large scale latitudinal mixing of atmospheric tracers in the lower branch of the Brewer-Dobson-Circulation leading to a different level of isolation of the tropical pipe with mid-latitudes and would result in a different chemical composition of the lower mid-latitude stratosphere (Visioni et al., 2017)~~

~~Varying the sulphate content in this our study showed that for temperatures and water vapour conditions of the case based on observations, a moderate enhancement of $3 \times \text{H}_2\text{SO}_4$ is sufficient to yield ozone depletion. Considering the temperature and water vapour dependence of the chlorine activation line (Fig. 9, white line), a $10 \times$ enhancement of stratospheric sulphate yields a shift of chlorine activation to slightly lower water vapour mixing ratios and higher temperatures. However, even for enhanced sulphate and a water vapour mixing ratio of 20 ppmv, the temperature has to fall below 205 K for chlorine activation (and hence ozone depletion) to occur at the assumed Cl_y and NO_y conditions of the standard case.~~

After the chlorine activation step, catalytic ozone loss cycles can occur: the ClO -Dimer cycle (??), the ClO - BrO -cycle (??) and

cycles subsequent to R13 ($\text{ClO} + \text{HO}_2$, **C2**–**C3**–**C4**). Cycle **C2** is reported to have an impact on stratospheric ozone in mid-latitudes in previous studies (e.g. Johnson et al., 1995; Kovalenko et al., 2007; Ward and Rowley, 2016). Here, **C2** was found to be the dominate cycle based on R13 under standard conditions. Nevertheless, simulating the “0.5 Br_y and” and “high Cl_y ” case 5 has shown that the relevance of ~~?? ($\text{ClO} + \text{ClO}$) and ?? ($\text{ClO} + \text{BrO}$) depends on the~~ the ClO-Dimer-cycle and the ClO-BrO-cycle depends on the assumed initial values of Cl_y and Br_y . Anderson and Clapp (2018) discussed the occurrence of the ClO-Dimer cycle ~~??~~ and the ClO-BrO-cycle ~~??~~ dependent on water vapour, the Cl_y mixing ratio and temperature. They illustrate a significant increase in the rate of R17 ($\text{ClO} + \text{ClO}$) and R18 ($\text{ClO} + \text{BrO}$) if the combination of ~~elevated enhanced~~ water vapour and low temperatures is sufficient for chlorine activation to occur. If chlorine activation occurs in their model study, a higher Cl_y 10 mixing ratio yields higher catalytic ozone loss rates (R17, R18). Their finding regarding the effect of temperature, water vapour and chlorine on the ozone loss process is consistent with the results found here. The occurrence of net chlorine activation is determined by temperature and water vapour mixing ratio, while the Cl_y mixing ratio controls how much ozone is destroyed. A measure for the effect of temperature and water vapour on stratospheric chlorine activation and ozone chemistry is the temperature and water vapour dependent chlorine activation line (Fig. 9, white line). Anderson et al. (2012) ~~estimates reported that~~ 15 lower temperatures than 205 K ~~as are~~ necessary for chlorine activation to occur at a water vapour mixing ratio of 20 ppmv and a climatological non enhanced sulphate content. In comparison, assuming standard conditions for Cl_y and NO_y but a constant temperature here, temperatures lower than 203 K are required for ozone loss to occur at similar H_2O and sulphate concentrations. The standard trajectory was chosen here to hold for conditions most likely for chlorine activation based on SEAC⁴RS measurements ~~and at~~. For the temperature range of this trajectory ~~and~~ the measured water vapour mixing ratio (10.6 ppmv) ~~is~~ 20 ~~slightly lower than the water vapour threshold no significant ozone depletion occurs~~. Hence, for all SEAC⁴RS and MACPEX trajectories calculated (not only the shown examples), no trajectory produced ozone loss. A further requirement for the occurrence of chlorine activation is the maintenance of the conditions, which yield chlorine activation, during the entire time of chlorine activation. Assuming standard conditions and a water vapour mixing ratio of 20 ppmv, chlorine activation takes 5 hours, ~~but for conditions of~~. However for a water vapour content close to the water vapour threshold, low temperatures and 25 enhanced water vapour mixing ratios have to be maintained 24–36 ~~hour hours~~ for chlorine activation ~~and thus to have~~ an impact on stratospheric ozone chemistry ~~to occur~~. For the occurrence of ozone depletion, temperatures have also to remain low and water vapour mixing ratios high after the chlorine activation step.

The maximum ozone depletion at standard conditions occurs here for a water vapour mixing ratio of 20 ppmv. Final ozone ~~at assuming~~ 20 ppmv H_2O in the 7-day simulation is 11% lower than the final ozone reached under atmospheric background 30 conditions ~~of assuming~~ 5 ppmv H_2O . For the 19-day simulation ~~at assuming~~ 20 ppmv H_2O , the final ozone is 22% reduced compared to the 19-day simulation ~~at assuming~~ 5 ppmv H_2O . Anderson and Clapp (2018) calculated a similar ozone reduction of 17% in a 14-day simulation and the same potential temperature range of 380 K assuming 20 ppmv H_2O and ~~similar somewhat higer~~ Cl_y ~~conditions~~ ($\sim 0.2 \text{ ppbv}$) ~~than~~ as used here in the realistic case. In contrast assuming the high Cl_y and NO_y ~~of mixing ratios employed by~~ Anderson et al. (2012) in the case of high Cl_y would lead to an ozone loss of 85% (265 ppbv) 35 during the 7-day simulation. This ozone loss would occur in the lower stratosphere.

Borrmann et al. (1996, 1997) and Solomon et al. (1997) conducted a study about the impact of cirrus clouds on chlorine ac-

tivation and ozone chemistry in the mid-latitudes lowermost stratosphere. They found a significant impact of heterogeneous processes occurring on cirrus clouds for ozone chemistry of the lowermost stratosphere but a minor effect for column ozone. Anderson and Clapp (2018) calculated a fractional loss in the total ozone column of ~~0.25~~^{0.24}~~–0.27~~ % assuming a full Cl_y profile in the altitude range of 12–18 km with a constant water vapour mixing ratio of 20 ppmv and the mixing ratio of Cl_y ~~similar to somewhat higher (~0.2 ppbv at a potential temperature of 380 K) than in~~ our standard case. However, the simulations ~~of us and Anderson and Clapp (2018)~~ assume a constant high water vapour mixing ratio and neglect mixing with the stratospheric background, which is characterized by much lower water vapour mixing ratios and subsequent dilution of convective uplifted air masses. Ozone loss would only occur in the specific volume of stratospheric air, that is directly affected by the convectively injected additional water. Hence, the ozone loss presented here corresponds to the maximal possible ozone loss for rather realistic convective overshooting conditions.

7 Conclusions

We investigated in detail the ozone loss mechanism at mid-latitudes in the lower stratosphere occurring under enhanced water vapour conditions and the sensitivity of this ozone loss mechanism on a variety of conditions. A CLaMS box-model study was conducted including a standard assumption and a variety of sensitivity cases regarding the chemical initialisation, temperatures and the duration of the simulated period. The assumed standard conditions (155.7 pptv Cl_y, 728.8 pptv NO_y, ~~197–203~~^{197–202} K and an H₂SO₄ gas phase equivalent of 0.20 ppbv) were determined based on measurements in an H₂O environment showing strongly enhanced H₂O values compared to the stratospheric background during the SEAC⁴RS aircraft campaign in Texas 2013.

The ozone loss mechanism consists of two phases: The first step is chlorine activation due to the heterogeneous reaction ClONO₂ + HCl (R1), which yields both an increase of ClO_x and a decrease of NO_x. ~~When~~^{In} the second phase, ~~when~~ chlorine is activated, enhanced ClO_x mixing ratios lead to catalytic ozone loss cycles ~~in the second phase of the mechanism~~. Our findings show that besides the ClO-Dimer-cycle (~~??~~) and ~~and~~ the ClO-BrO-cycle (~~??~~), three ozone loss cycles (C2, C3–C4) based on the reaction ClO+HO₂ (R13) have to be taken into account. The relevance of the ~~cycles ??–C2 and C3–C4 for ozone loss depends on the different ozone loss cycles for ozone destruction depends on~~ water vapour, Cl_y and Br_y mixing ratios. Reduced NO_x mixing ratios yield a decreasing chemical net ozone formation in cycle C1. This reduced ozone formation at high water vapour mixing ratios ~~is~~ in the box-model simulation ~~amounts to~~ around 20% ~~as high as~~ the ozone destruction in catalytic ozone loss cycles. Furthermore a detailed analysis of chemical processes revealed the occurrence of pathways, which maintain high ClO_x and low NO_x mixing ratios after the chlorine activation step but do not ~~reduce~~ ~~destroy~~ ozone, similar to HCl-null-cycles in the lower stratosphere (~~Müller et al., 2018~~) in Antarctic early spring (~~Müller et al., 2018~~).

Focussing on the dependence of chlorine activation on temperature and water vapour mixing ratio, we found that the temperature has to fall below 203 K for chlorine activation to occur at a water vapour mixing ratio of 20 ppmv and Cl_y and NO_y for our standard case. Testing the water vapour dependence of ozone loss along a realistic trajectory that experienced very low

temperatures between 197 and 203 K, we observed a water vapour threshold of 11.0–11.6 ppmv H₂O, which has to be exceeded for ozone reduction chlorine activation to occur. An ozone loss occurs in these simulations for at least 12 ppmv H₂O. For our assumed standard conditions, a maximum ozone loss of 9% (27 ppbv) was calculated for a water vapour mixing ratio of 20 ppmv. In contrast, a simulation assuming the observed conditions (10.6 ppmv H₂O) yielded ozone formation; but a tripling of background sulphate gas phase equivalent (as it can be reached under geoengineering conditions or volcanic eruptions) is sufficient for a slight ozone loss to occur under these unusually cold conditions for the chosen standard trajectory. Simulating a high Cl_y case assuming initial Cl_y and NO_y based on the study of Anderson et al. (2012) results in both a lower water vapour threshold of 7–8 ppmv and a larger ozone depletion of 85% (265 ppbv) at high water vapour mixing ratios. The model runs described here assume an air parcel moving along the trajectory and, which does not mix with neighbouring air masses. In the case of water, this mixing would likely reduce the concentration. Because that mixing was neglected, the runs discussed here are likely and an extreme case, and the ozone loss modelled simulated provides an upper bound to the process described. Considering the duration for which low temperatures and high water vapour mixing ratios have to be maintained to activate chlorine and deplete stratospheric ozone, a chlorine activation time of 24 to 36 hours when the water vapour abundance is near the close to the water vapour threshold and of 5 h at assuming 20 ppmv H₂O was calculated. The water vapour threshold shifts strongly with depends strongly on a changing temperature and sulphate content as well as with on Cl_y, NO_y and Br_y mixing ratios. The dependence of the water vapour threshold is explained here by focussing on the water dependence of the heterogeneous reactivity (R1) and the balance between heterogeneous chlorine activation (R1, ClONO₂ + HCl) and gas phase chlorine deactivation (R12, Cl + CH₄).

The ozone loss mechanism was investigated here by conducting box-model simulations along a trajectory, which was calculated based on measurements of elevated enhanced water vapour. Sensitivity and case studies, which cover a range of uncertainties, illustrate the impact of the Cl_y, NO_y, Br_y and H₂O mixing ratios, the temperature, the sulphate gas equivalent and the duration of the simulated period on the ozone loss process. While the water vapour threshold which has to be exceeded for chlorine activation to occur is mainly determined by the temperature, water vapour mixing ratio and sulphate content, the intensity of ozone loss depends on Cl_y, NO_y, Br_y and the duration of the time period, for which a chlorine activation can be maintained. Our comprehensive sensitivity studies are a basis to assess the impact of enhanced water vapour mixing ratios in the lower mid-latitude stratosphere on ozone under sulphate geoengineering conditions and in a changing climate. However, for the conditions observed during SEC⁴RS (in particular H₂O = 10.6 ppmv), we did not simulate ozone depletion for the observed conditions. Further global any ozone depletion. Global modelling studies are needed to establish whether the mechanism analysed here is of concern for the future.

Code and data availability. The complete SEAC⁴RS data are available at <https://www-air.larc.nasa.gov/cgi-bin/ArcView/seac4rs>. The CLaMS box model calculations can be requested from Sabine Robrecht (sa.robrecht@fz-juelich.de).

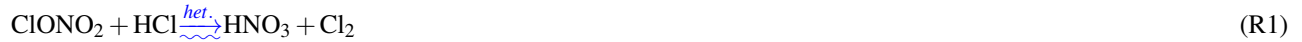
Appendix A: Maintenance of activated chlorine

In Sec. 3.2.2 chlorine catalysed ozone loss cycles are analysed and the maintenance of activated chlorine is described schematically based on Fig. 6. Here, we describe the pathways yielding the maintenance of activated chlorine and balancing the NO_x mixing

5 ratio in more detail, including all radical balancing reactions. Since the pathway balancing HCl-formation and -destruction is coupled with the pathway balancing HNO_3 -formation and -destruction, both are combined here. In total, two pathways are described here, which balance HCl-formation and -destruction as well as HNO_3 -formation and -destruction, and which mainly differ in the reaction of the methylperoxy radical ($\text{H}_3\text{COO} + \text{NO}$, R22, or $\text{H}_3\text{COO} + \text{ClO}$, R23).

At water vapour mixing ratios slightly higher than the water vapour threshold, H_3COO reacts rather with NO . Hence, pathway

10 **AC1** mainly balances HCl and ClO_x as well as HNO_3 and NO_x .



In pathway **AC1**, HCl is formed in R12. The methylradical formed in R12 reacts fastly with oxygen in AR1 yielding a methylperoxy radical H_3COO , which reacts with NO in R22. In reaction R9 ClONO_2 is formed, which reacts with HCl heterogeneously in R1 (and thus leads to an HCl depletion). HNO_3 formed in R1 is depleted in R20. These reactions constitute the balance between HCl and HNO_3 -formation and -destruction. The reactions AR3 and R16 balance the ClO_x -species, R7 and AR4 the NO_x -species, reactions R13 and R14 the HO_x -species and AR5 odd oxygen (O_x). All of these radical reactions are

significantly faster than the reactions, which constitute the balance between HCl and HNO₃ formation and destruction. Hence, the net reaction of this pathway is the oxidation of CH₄ to HCHO (formaldehyde).

In cycle AC1 the H₃COO-radical reacts with NO (R22). As an alternative the H₃COO-radical reacts with ClO (R23) at high water vapour mixing ratios yielding to cycle AC2 as balance between HCl and HNO₃ formation and destruction.



The main difference between pathway AC1 and AC2 is the reaction of the H₃COO-radical. The reactions R12, AR1, R9, R1 and R20 balance HCl and ClO_x as well as HNO₃ and NO_x. The reactions AR3, R16, R13, R14 and AR5 convert the radical species and are very fast. The net reaction of this pathway is the oxidation of methane (CH₄) into formaldehyde (HCHO) with a simultaneous ozone destruction. Since the ozone destruction due to the catalytic ozone loss cycles discussed in Sec. 3.2.2 is much faster, the ozone destruction in AC2 is negligible compared to the ozone loss cycles discussed above.

Appendix B: MACPEX case

25 The MACPEX case (Mid-latitude airborne Cirrus Properties Experiment) was conducted to complement the results obtained from the standard case as a further example for an event with high stratospheric water vapour based on airborne measurements. In this section, first the model setup for the MACPEX case is described. In a second step, the results of model calculations of the MACPEX case are presented, comprising the chosen trajectory for chemical simulations and the sensitivity of ozone chemistry to various conditions.

B1 Model Setup

Simulations are performed similar to the SEAC⁴RS case (see, Sec. 2) based on measurements with enhanced water vapour of at least 10 ppmy taken during the MACPEX campaign (Rollins et al., 2014). Chemistry is calculated for single air parcels

5 along trajectories including diabatic descent. Trajectories are calculated as described in Sec. 2.2. For chemical initialization, important trace gases for ozone chemistry – O₃, Cl_y and NO_y – are initialized based on MACPEX measurements. Ozone and water vapour were measured directly during the aircraft campaign. Cl_y and NO_y are inferred from tracer-tracer relations using N₂O measured on the aircraft employed. The initialization of all further trace gases except of water vapour were taken from the full chemistry 3D-CLaMS simulation (Vogel et al., 2015, 2016) for summer 2012 at the location of the measurement.

10 Chemistry was initialized 7 days before the measurement.

The MACPEX campaign (Rollins et al., 2014) took place during the spring 2011 and was based in Houston, Texas. The water vapour values used here were measured by the Fast In-situ Stratospheric Hygrometer (FISH), which employs the Lyman- α photofragment fluorescence technique (Meyer et al., 2015). MACPEX ozone was measured by the UAS-O₃ instrument (Gao et al., 2012). Initial Cl_y and NO_y were assumed based on tracer-tracer correlations with N₂O that was measured by the Jet Propulsion

15 Laboratory's Aircraft Laser Infrared Absorption Spectrometer (ALIAS) instrument (Webster et al., 1994).

Initial Cl_y and NO_y is calculated based on N₂O tracer-tracer correlations (Groß et al., 2014, see also App. C) with corrections considering a N₂O increase from 2009 to 2013. Cl_y is determined using the same correlation with CH₄ as for the standard case (see Sec. 2.3). Therefore CH₄ is first calculated using measured N₂O of 320.28 ppbv and a correlation based on measurements from 2009 (Groß et al., 2014). The increase of stratospheric CH₄ and N₂O is considered as described for the standard case

20 (GHG Bulletin, 2014). First, an increase in N₂O of 1.6 ppbv from 2009 to 2011 is estimated to adjust N₂O. Furthermore calculated CH₄ is adjusted considering a difference between CH₄ in 2000 and 2009 of 0.026 ppm. The annual decrease of Cl_y from 2000 to 2011 is assumed to be 0.8% (WMO, 2014). A summary of the initial values for main tracers assumed in the MACPEX case are given in Table B1. Furthermore sensitivity studies assuming only 80% of initial Cl_y (0.8 Cl_y), 80% of initial NO_y (0.8 NO_y), and an elevated H₂SO₄-background (0.6 ppbv H₂SO₄) are conducted.

25

B2 Results of MACPEX simulations

During the MACPEX campaign only few cases with enhanced stratospheric water vapour were observed. Here we present an example for a trajectory calculated based on such a case. This trajectory is used to test the sensitivity of lowermost stratospheric ozone in mid-latitudes on the water vapour, Cl_y and NO_y mixing ratio and on an enhancement of stratospheric sulphate.

30 B2.1 MACPEX Trajectory

The selected trajectory for the MACPEX case is shown in Fig. B1. It refers to a measurement on 11 April 2011 during the MACPEX campaign. In the left panel, a backward trajectory is presented in the range of –7 to 0 days from the time of measurement and a forward trajectory in the range from 0 to 7 days. In the right panel, the location of the measurement is

Table B1. Mixing ratios and sources used for initialization of relevant trace gases for the MACPEX case. Cl_y and NO_y values were determined based on tracer-tracer correlations (see text). Initial mixing ratios of ClO_x species were assumed to be zero.

Species	Value	Source
O_3	283.0 ppbv	UAS- O_3
CH_4	1.68 ppmv	CLaMS-3D
CO	19.0 ppbv	CLaMS-3D
Cl_y	55 pptv	tracer corr.
HCl	52.7 pptv	tracer corr.
ClONO_2	2.19 pptv	tracer corr.
NO_y	620 pptv	tracer corr.
HNO_3	390.3 pptv	tracer corr.
NO	114.6 pptv	tracer corr.
NO_2	114.6 pptv	tracer corr.
Br_y	1.2 pptv	CLaMS-3D
H_2O	5–20 ppmv	
H_2SO_4	0.2 ppbv, 0.6 ppbv	

shown by a red square.

The potential temperature level of this trajectory is around 380 K and above the tropopause located at \sim 350 K, which was deduced from the temperature profile measured during the flight on 11 April 2011. The forward trajectory shows a strongly

5 increasing temperature and pressure level due to a decrease in altitude. Coming from the Western Pacific, this air parcel passes the North American continent briefly. The backward trajectory reaches very low temperatures with a minimum temperature of 191 K. Because of its low temperature, which pushes the occurrence of heterogeneous reactions, the backwards trajectory is chosen to test the sensitivity of lowermost stratospheric ozone to a variety of conditions.

10 B2.2 Sensitivity studies

Chemical simulations assuming the MACPEX initialization (Tab. B1) and a water vapour mixing ratio varying between 5 and 20 ppmv are performed along the MACPEX 7-day backwards trajectory. Final ozone, reached at the end of this simulations, is

shown as blue squares in Fig. B2. The water vapour threshold necessary for chlorine activation to occur is reached at 8 ppmv H_2O . It is a lower water vapour mixing ratio than for the SEAC⁴RS case, because of the very low temperatures reached.

15 For the MACPEX trajectory and 8 ppmv H_2O , the time until chlorine is activated takes 63 h from the begin of the trajectory. Because of increasing temperatures (see Fig. B2), chlorine activation can be maintained for 14 h at this water vapour mixing ratio. Hence, no decrease of final ozone can be observed during this simulation. For higher water vapour mixing ratios, chlorine activation is maintained for a longer time and final ozone is reduced comparing with final ozone reached for low water vapour

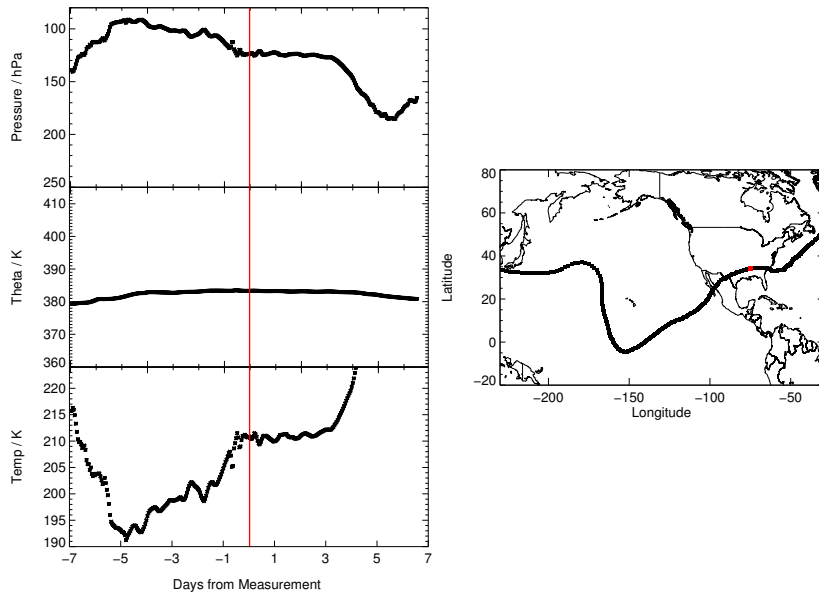


Figure B1. Pressure, potential temperature, temperature and location of the selected trajectory calculated based on measurements with enhanced water vapour during the MACPEX aircraft campaign. The red line (left panels) marks the time of measurement and the red squares (right panels) mark the location of the measurement. Since the tropopause is very low, it is not plotted here. In the right panel, the begin of the trajectory (4. April 2011) is at the left edge of the panel. In the bottom panel (left), the MACPEX trajectory consists of single squares due to a faster movement of the air parcel in that region.

mixing ratios. In general, the decrease in final ozone is much lower for the MACPEX case than for the SEAC⁴RS case. In the MACPEX initialization, Cl_y is a third of Cl_y in the SEAC⁴RS initialization. Hence, catalytic ozone loss has lower rates for MACPEX conditions and ozone is less affected by chlorine activation. Even assuming high water vapour of 20 ppmv yields

5 higher final ozone than initial ozone for MACPEX conditions. Although chlorine is activated in the MACPEX case, no net ozone destruction occurs.

The impact of changes in sulphate, Cl_y and NO_y is tested for the MACPEX case, as well. The changes affect the water vapour threshold in the same way as in the SEAC⁴RS case. An enhancement of sulphate (Fig. 7, left, yellow diamonds), and a reduction of NO_y (green triangles) shifts the water vapour threshold to lower water vapour mixing ratios. A reduction of Cl_y (black circles) shifts it to higher water vapour mixing ratios.

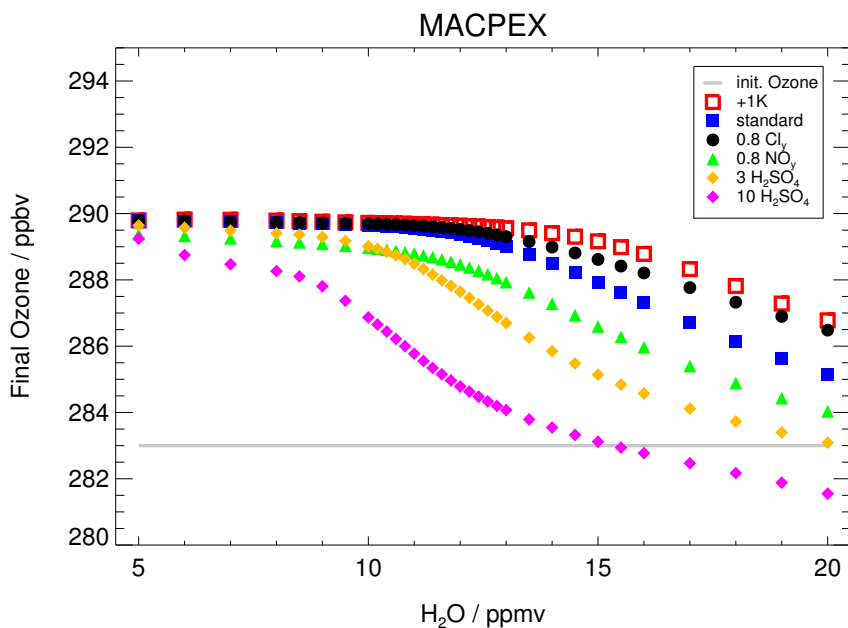


Figure B2. Impact of the water vapour content on the ozone mixing ratio (final ozone) reached at the end of the 7-day simulation along the MACPEX trajectory. The standard case is shown in blue and the initial ozone amount is marked by the grey line. An impact on the final ozone mixing ratios is observable after exceeding a critical threshold in water vapour. This threshold changes with a shift in the temperature (+1K, red), the Cl_y mixing ratio to 0.8 Cl_y (black), the NO_y mixing ratio (0.8 NO_y , green), the sulphate content (3× standard H_2SO_4 , yellow, 10× standard H_2SO_4 , pink).

Appendix C: Tracer-Tracer Correlations

The mixing ratios of Cl_y and NO_y were initialized based on stratospheric tracer-tracer correlations from Grooß et al. (2014). Cl_y and NO_y were initialized based on a CH_4 measurement during the SEAC⁴RS aircraft campaign. Initial Cl_y was calculated
5 using the tracer-tracer correlation (Grooß et al., 2014)

$$[\text{Cl}_y] = 2.510 + 3.517 \cdot [\text{CH}_4] - 3.741 \cdot [\text{CH}_4]^2 + 0.4841 \cdot [\text{CH}_4]^3 + 0.03042 \cdot [\text{CH}_4]^4. \quad (\text{C1})$$

The volume mixing ratio of Cl_y ($[\text{Cl}_y]$) is here in ppt and the mixing ratio of methane ($[\text{CH}_4]$) in ppm.

To determine NO_y based on the CH_4 measurement, first N_2O was calculated through

$$[\text{N}_2\text{O}] = -124.9 + 311.9 \cdot [\text{CH}_4] - 158.1 \cdot [\text{CH}_4]^2 + 146.6 \cdot [\text{CH}_4]^3 - 43.92 \cdot [\text{CH}_4]^4 \quad (\text{C2})$$

10 assuming $[\text{N}_2\text{O}]$ in ppbv and $[\text{CH}_4]$ in ppmv (Grooß et al., 2002). Subsequently NO_y (in ppt) was calculated in a correlation with N_2O .

$$[\text{NO}_y] = 11.57 + 0.1235 \cdot [\text{N}_2\text{O}] - 1.013 \cdot 10^{-3} \cdot [\text{N}_2\text{O}]^2 + 1.984 \cdot 10^{-6} \cdot [\text{N}_2\text{O}]^3 - 1.119 \cdot 10^{-9} \cdot [\text{N}_2\text{O}]^4 \quad (\text{C3})$$

In the MACPEX case NO_y and Cl_y were initialized based on N_2O measurements. NO_y was calculated using correlation C3. Cl_y was calculated using C1. Therefore first CH_4 (in ppmv) had to be calculated based on a correlation with N_2O (in ppbv)
15 (Grooß et al., 2014).

$$[\text{CH}_4] = 0.1917 + 0.01333 \cdot [\text{N}_2\text{O}] - 8.239 \cdot 10^{-5} \cdot [\text{N}_2\text{O}]^2 + 2.840 \cdot 10^{-7} \cdot [\text{N}_2\text{O}]^3 - 3.376 \cdot 10^{-10} \cdot [\text{N}_2\text{O}]^4 \quad (\text{C4})$$

Competing interests. The authors declare that they have no conflict of interest.

Acknowledgements. Our activities were funded by the German Science Foundation (Deutsche Forschungsgemeinschaft, DFG) under the DFG project CE-O₃ in the context of the Priority Program Climate Engineering: Risks, Challenges, Opportunities? (SPP 1689; VO 1276/4-1). We thank the European Centre for Medium-Range Weather Forecasts (ECMWF) for providing ERA-Interim data. We thank the group
20 of Steven Wofsy (Harvard University, Department Earth and Planetary Science, Cambridge, MA USA) and Jessica Smith for providing their data measured during the SEAC⁴RS aircraft campaign. [Furthermore, we thank Simone Tilmes for helpful discussions.](#)

References

Anderson, J. G. and Clapp, C. E.: Coupling free radical catalysis, climate change, and human health, *Phys. Chem. Chem. Phys.*, 20, 10 569–10 587, <https://doi.org/10.1039/C7CP08331A>, 2018.

5 Anderson, J. G., Wilmouth, D. M., Smith, J. B., and Sayres, D. S.: UV Dosage Levels in Summer: Increased Risk of Ozone Loss from Convectively Injected Water Vapor, *Science*, 337, 835–839, <https://doi.org/10.1126/science.1222978>, 2012.

Anderson, J. G., Weisenstein, D. K., Bowman, K. P., Homeyer, C. R., Smith, J. B., Wilmouth, D. M., Sayres, D. S., Klobas, J. E., Leroy, S. S., Dykema, J. A., and Wofsy, S. C.: Stratospheric ozone over the United States in summer linked to observations of convection and temperature via chlorine and bromine catalysis, *Proc. Natl. Acad. Sci.*, 114, E4905–E4913, <https://doi.org/10.1073/pnas.1619318114>, 10 2017.

Becker, G., Groß, J.-U., McKenna, D. S., and Müller, R.: Stratospheric photolysis frequencies: Impact of an improved numerical solution of the radiative transfer equation, *J. Atmos. Chem.*, 37, 217–229, <https://doi.org/10.1023/A:1006468926530>, 2000.

Berthet, G., Jégou, F., Catoire, V., Krysztofiak, G., Renard, J.-B., Bourassa, A. E., Degenstein, D. A., Brogniez, C., Dorf, M., Kreycy, S., Pfeilsticker, K., Werner, B., Lefèvre, F., Roberts, T. J., Lurton, T., Vignelles, D., Begue, N., Bourgeois, Q., Daugeron, D., Cartiert, M., 15 Robert, C., Gaubicher, B., and Guimbaud, C.: Impact of a moderate volcanic eruption on chemistry in the lower stratosphere: balloon-borne observations and model calculations, *Atmos. Chem. Phys.*, 17, 2229–2253, <https://doi.org/10.5194/acp-17-2229-2017>, 2017.

Borrmann, S., Solomon, S., Dye, J. E., and Luo, B.: The potential of cirrus clouds for heterogeneous chlorine activation, *Geophys. Res. Lett.*, 23, 2133–2136, <https://doi.org/10.1029/96GL01957>, 1996.

Borrmann, S., Solomon, S., Avallone, L., Toohey, D., and Baumgardner, D.: On the occurrence of ClO in cirrus clouds and volcanic aerosol 20 in the tropopause region, *Geophys. Res. Lett.*, 24, 2011–2014, <https://doi.org/10.1029/97GL02053>, 1997.

Brewer, A. W.: Evidence for a world circulation provided by the measurements of helium and water vapour distribution in the stratosphere, *Q. J. R. Meteorol. Soc.*, 75, 351–363, <https://doi.org/10.1002/qj.49707532603>, 1949.

Brown, P. N., Byrne, G. D., and Hindmarsh, A. C.: VODE: A variable coefficient ODE solver, *SIAM J. Sci. Stat. Comput.*, 10, 1038–1051, <https://doi.org/https://doi.org/10.1137/0910062>, 1989.

25 Crutzen, P. J., Müller, R., Brühl, C., and Peter, T.: On the potential importance of the gas phase reaction $\text{CH}_3\text{O}_2 + \text{ClO} \rightarrow \text{ClOO} + \text{CH}_3\text{O}$ and the heterogeneous reaction $\text{HOCl} + \text{HCl} \rightarrow \text{H}_2\text{O} + \text{Cl}_2$ in “ozone hole” chemistry, *Geophys. Res. Lett.*, 19, 1113–1116, <https://doi.org/10.1029/92GL01172>, 1992.

Daniel, J. S., Solomon, S., Portmann, R. W., and Garcia, R. R.: Stratospheric ozone destruction: The importance of bromine relative to chlorine, *J. Geophys. Res.*, 104, 23 871–23 880, <https://doi.org/10.1029/1999JD900381>, 1999.

30 Dee, D. P., Uppala, S. M., Simmons, A. J., Berrisford, P., Poli, P., Kobayashi, S., Andrae, U., Balmaseda, M. A., Balsamo, G., Bauer, P., Bechtold, P., Beljaars, A. C. M., van de Berg, L., Bidlot, J., Bormann, N., Delsol, C., Dragani, R., Fuentes, M., Geer, A. J., Haimberger, L., Healy, S. B., Hersbach, H., Hólm, E. V., Isaksen, L., Kállberg, P., Köhler, M., Matricardi, M., McNally, A. P., Monge-Sanz, B. M., Morcrette, J.-J., Park, B.-K., Peubey, C., de Rosnay, P., Tavolato, C., Thépaut, J.-N., and Vitart, F.: The ERA-Interim reanalysis: configuration and performance of the data assimilation system, *Q. J. R. Meteorol. Soc.*, 137, 553–597, <https://doi.org/10.1002/qj.828>, 2011.

35 Drdla, K. and Müller, R.: Temperature thresholds for chlorine activation and ozone loss in the polar stratosphere, *Ann. Geophys.*, 30, 1055–1073, <https://doi.org/10.5194/angeo-30-1055-2012>, 2012.

Dykema, J. A., Keith, D. W., Anderson, J. G., and Weisenstein, D.: Stratospheric controlled perturbation experiment: a small-scale experiment to improve understanding of the risks of solar geoengineering, *Phil. Trans. R. Soc. A*, 372, 1–22, <https://doi.org/10.1098/rsta.2014.0059>, 2014.

5 Elrod, M. J., Koch, R. E., Kim, J. E., and Molina, M.: HCl vapour pressures and reaction probabilities for ClONO₂+HCl on liquid H₂SO₄-HNO₃-HCl-H₂O solutions, *Faraday Discuss.*, 100, 269–278, 1995.

Gao, R. S., Ballard, J., Watts, L. A., Thornberry, T. D., Ciciora, S. J., McLaughlin, R. J., and Fahey, D. W.: A compact, fast UV photometer for measurement of ozone from research aircraft, *Atmos. Meas. Tech.*, 5, 2201–2210, <https://doi.org/10.5194/amt-5-2201-2012>, 2012.

GHG Bulletin, ed.: WMO Greenhouse Gas Bulletin, GHG Bulletin No.10, WMO, <http://www.wmo.int/pages/prog/arep/gaw/ghg/GHGbulletin.html>, 2014.

10 Grenfell, J. L., Lehmann, R., Mieth, P., Langematz, U., and Steil, B.: Chemical reaction pathways affecting stratospheric and mesospheric ozone, *J. Geophys. Res. A*, 111, <https://doi.org/10.1029/2004JD005713>, 2006.

Groß, J.-U., Günther, G., Konopka, P., Müller, R., McKenna, D. S., Stroh, F., Vogel, B., Engel, A., Müller, M., Hoppel, K., Bevilacqua, R., Richard, E., Webster, C. R., Elkins, J. W., Hurst, D. F., Romashkin, P. A., and Baumgardner, D. G.: Simulation of ozone depletion in spring 2000 with the Chemical Lagrangian Model of the Stratosphere (CLaMS), *J. Geophys. Res.*, 107, 8295, <https://doi.org/10.1029/2001JD000456>, 2002.

15 Groß, J.-U., Brautzsch, K., Pommrich, R., Solomon, S., and Müller, R.: Stratospheric ozone chemistry in the Antarctic: What controls the lowest values that can be reached and their recovery?, *Atmos. Chem. Phys.*, 11, 12 217–12 226, <https://doi.org/10.5194/acp-11-12217-2011>, 2011.

20 Groß, J.-U., Engel, I., Borrman, S., Frey, W., Günther, G., Hoyle, C. R., Kivi, R., Luo, B. P., Molleker, S., Peter, T., Pitts, M. C., Schlager, H., Stiller, G., Vömel, H., Walker, K. A., and Müller, R.: Nitric acid trihydrate nucleation and denitrification in the Arctic stratosphere, *Atmos. Chem. Phys.*, 14, 1055–1073, <https://doi.org/10.5194/acp-14-1055-2014>, 2014.

Haagen-Smit, A. H.: Chemistry and physiology of the Los Angeles photochemical smog, *Ind. Eng. Chem.*, 44, 1342–1346, <https://doi.org/10.1021/ie50510a045>, 1952.

25 Hanisco, T. F., Moyer, E. J., Weinstock, E. M., Clair, J. M. S., Sayres, D. S., Smith, J. B., Lockwood, R., Anderson, J. G., Dessler, A. E., Keutsch, F. N., Spackman, J. R., Read, W. G., and Bui, T. P.: Observations of deep convective influence on stratospheric water vapor and its isotopic composition, *Geophys. Res. Lett.*, 34, L04814, <https://doi.org/10.1029/2006GL027899>, 2007.

Hanson, D. R.: Reaction of ClONO₂ with H₂O and HCl in sulfuric acid and HNO₃/H₂SO₄/H₂O mixtures, *J. Phys. Chem. A*, 102, 4794–4807, 1998.

30 Hanson, D. R. and Ravishankara, A. R.: Reactive Uptake of ClONO₂ onto Sulfuric Acid Due to Reaction with HCl and H₂O, *J. Phys. Chem.*, 98, 5728–5735, 1994.

Herman, R. L., Ray, E. A., Rosenlof, K. H., Bedka, K. M., Schwartz, M. J., Read, W. G., Troy, R. F., Chin, K., Christensen, L. E., Fu, D., Stachnik, R. A., Bui, T. P., and Dean-Day, J. M.: Enhanced stratospheric water vapor over the summertime continental United States and the role of overshooting convection, *Atmos. Chem. Phys.*, 17, 6113, <https://doi.org/10.5194/acp-17-6113-2017>, 2017.

35 Homeyer, C. R., Pan, L. L., Dorsi, S. W., Avallone, L. M., Weinheimer, A. J., O'Brien, A. S., DiGangi, J. P., Zondlo, M. A., Ryerson, T. B., Diskin, G. S., and Campos, T. L.: Convective transport of water vapor into the lower stratosphere observed during double-tropopause events, *J. Geophys. Res.*, 119, 10 941–10 958, <https://doi.org/10.1002/2014JD021485>, 2014.

Johnson, D. G., Traub, W. A., Chance, K. V., Jucks, K. W., and Stachnik, R. A.: Estimating the abundance of ClO from simultaneous remote sensing measurements of HO₂, OH, and HOCl, *Geophys. Res. Lett.*, 22, 1869–1871, <https://doi.org/10.1029/95GL01249>, 1995.

Keim, E. R., Fahey, D. W., Negro, L. A. D., Woodbridge, E. L., Gao, R., Wennberg, P. O., Cohen, R. C., Stimpfle, R. M., Kelly, K. K., Hints, E. J., Wilson, J. C., Jonsson, H. H., Dye, J. E., Baumgardner, D. G., Kawa, S. R., Salawitch, R. J., Proffitt, M. H., Loewenstein, M., Podolske, J. R., and Chan, K. R.: Observations of large reductions in the NO/NO_y ratio near the mid-latitude tropopause and the role of heterogeneous chemistry, *Geophys. Res. Lett.*, 23, 3223–3226, <https://doi.org/10.1029/96GL02593>, 1996.

5 Klooster, S. L. V. and Roeber, P. J.: Surface-Based Convective Potential in the Contiguous United States in a Business-as-Usual Future Climate, *J. Climate*, 22, 3317–3330, <https://doi.org/10.1175/2009JCLI2697.1>, 2009.

Koenig, T. K., Volkamer, R., Baidar, S., Dix, B., Wang, S., Anderson, D. C., Salawitch, R. J., Wales, P. A., Cuevas, C. A., Fernandez, R. P., Saiz-Lopez, A., Evans, M. J., Sherwen, T., Jacob, D. J., Schmidt, J., Kinnison, D., Lamarque, J.-F., Apel, E. C., Bresch, J. C., Campos, T., Flocke, F. M., Hall, S. R., Honomichl, S. B., Hornbrook, R., Jensen, J. B., Lueb, R., Montzka, D. D., Pan, L. L., Reeves, J. M., Schauffler, S. M., Ullmann, K., Weinheimer, A. J., Atlas, E. L., Donets, V., Navarro, M. A., Riemer, D., Blake, N. J., Chen, D., Huey, L. G., Tanner, D. J., Hanisco, T. F., and Wolfe, G. M.: BrO and inferred Br_y profiles over the western Pacific: relevance of inorganic bromine sources and a Br_y minimum in the aged tropical tropopause layer, *Atmos. Chem. Phys.*, 17, 15 245–15 270, <https://doi.org/10.5194/acp-17-15245-2017>, 2017.

10 15 Konopka, P., Ploeger, F., Tao, M., Birner, T., and Riese, M.: Hemispheric asymmetries and seasonality of mean age of air in the lower stratosphere: Deep versus shallow branch of the Brewer-Dobson circulation, *J. Geophys. Res.*, 120, 2053–2066, <https://doi.org/10.1002/2014JD022429>, 2015.

Kovalenko, L. J., Jucks, K. W., Salawitch, R. J., Toon, G. C., Blavier, J.-F., Johnson, D. G., Kleinböhl, A., Livesey, N. J., Margitan, J. J., Pickett, H. M., Santee, M. L., Sen, B., Stachnik, R. A., and Waters, J. W.: Observed and modeled HOCl profiles in the midlatitude stratosphere: Implication for ozone loss, *Geophys. Res. Lett.*, 34, <https://doi.org/10.1029/2007GL031100>, 2007.

20 LeTexier, H., Solomon, S., and Garcia, R. R.: The role of molecular hydrogen and methane oxidation in the water vapour budget of the stratosphere, *Q. J. R. Meteorol. Soc.*, 114, 281 – 295, [https://doi.org/https://doi.org/10.1002/qj.49711448002](https://doi.org/10.1002/qj.49711448002), 1988.

Luo, B., Krieger, U. K., and Peter, T.: Densities and refractive indices of H₂SO₄/HNO₃/H₂O solutions to stratospheric temperatures, *Geophys. Res. Lett.*, 23, 3707–3710, <https://doi.org/10.1029/96GL03581>, 1996.

25 30 McElroy, M. B., Salawitch, R. J., Wofsy, S. C., and Logan, J. A.: Reductions of Antarctic Ozone due to Synergistic Interactions of Chlorine and Bromine, *Nature*, 321, 759–762, <https://doi.org/10.1038/321759a0>, 1986.

McKenna, D. S., Grooß, J.-U., Günther, G., Konopka, P., Müller, R., Carver, G., and Sasano, Y.: A new Chemical Lagrangian Model of the Stratosphere (CLaMS): 2. Formulation of chemistry scheme and initialization, *J. Geophys. Res.*, 107, 4256, <https://doi.org/10.1029/2000JD000113>, 2002a.

35 40 McKenna, D. S., Konopka, P., Grooß, J.-U., Günther, G., Müller, R., Spang, R., Offermann, D., and Orsolini, Y.: A new Chemical Lagrangian Model of the Stratosphere (CLaMS): 1. Formulation of advection and mixing, *J. Geophys. Res.*, 107, 4309, <https://doi.org/10.1029/2000JD000114>, 2002b.

Meyer, J., Rolf, C., Schiller, C., Rohs, S., Spelten, N., Afchine, A., Zöger, M., Sitnikov, N., Thornberry, T. D., Rollins, A. W., Bozóki, Z., Tátrai, D., Ebert, V., Kühnreich, B., Mackrodt, P., Möhler, O., Saathoff, H., Rosenlof, K. H., and Krämer, M.: Two decades of water vapor measurements with the FISH fluorescence hygrometer: a review, *Atmos. Chem. Phys.*, 15, 8521–8538, <https://doi.org/10.5194/acp-15-8521-2015>, 2015.

45 50 Molina, L. T. and Molina, M. J.: Production of Cl₂O₂ from the self-reaction of the ClO radical, *J. Phys. Chem.*, 91, 433–436, <https://doi.org/10.1021/j100286a035>, 1987.

Molina, M. J., Tso, T.-L., Molina, L. T., and Wang, F. C.-Y.: Antarctic Stratospheric Chemistry of Chlorine Nitrate, Hydrogen Chloride, and Ice: Release of Active Chlorine, *Science*, 238, 1253–1257, <https://doi.org/10.1126/science.238.4831.1253>, 1987.

Müller, R., Grooß, J.-U., Zafar, A., Robrecht, S., and Lehmann, R.: The maintenance of elevated active chlorine levels in the Antarctic lower stratosphere through HCl null cycles, *Atmos. Chem. Phys.*, 18, 2985–2997, <https://doi.org/10.5194/acp-18-2985-2018>, 2018.

5 Navarro, M. A., Saiz-Lopez, A., Cuevas, C. A., Fernandez, R. P., Atlas, E., Rodriguez-Lloveras, X., Kinnison, D., Lamarque, J.-F., Tilmes, S., Thornberry, T., Rollins, A., Elkins, J. W., Hintsa, E. J., and Moore, F. L.: Modeling the inorganic bromine partitioning in the tropical tropopause layer over the eastern and western Pacific Ocean, *Atmos. Chem. Phys.*, 17, 9917–9930, <https://doi.org/10.5194/acp-17-9917-2017>, 2017.

10 Pitari, G., Visioni, D., Mancini, E., Cionni, I., Di Genova, G., and Gandolfi, I.: Sulfate aerosols from non-explosive volcanoes: chemical-radiative effects in the troposphere and lower stratosphere, *Atmosphere*, 7, 85, <https://doi.org/10.3390/atmos7070085>, 2016.

Ploeger, F., Konopka, P., Günther, G., Grooß, J.-U., and Müller, R.: Impact of the vertical velocity scheme on modeling transport across the tropical tropopause layer, *J. Geophys. Res.*, 115, D03301, <https://doi.org/10.1029/2009JD012023>, 2010.

Poshyvailo, L., Müller, R., Konopka, P., Günther, G., Riese, M., Podglajen, A., and Ploeger, F.: Sensitivities of modelled water vapour in the 15 lower stratosphere: temperature uncertainty, effects of horizontal transport and small-scale mixing, *Atmos. Chem. Phys.*, 18, 8505–8527, <https://doi.org/10.5194/acp-18-8505-2018>, 2018.

Prather, M. J.: More rapid ozone depletion through the reaction of HOCl with HCl on polar stratospheric clouds, *Nature*, 355, 534–537, <https://doi.org/10.1038/355534a0>, 1992.

Randel, W. J., Wu, F., Oltmans, S. J., Rosenlof, K. H., and Nodoluha, G. E.: Interannual Changes of Stratospheric Water 20 Vapor and Correlations with Tropical Tropopause Temperatures, *J. Atmos. Sci.*, 61, 2133–2148, [https://doi.org/10.1175/1520-0469\(2004\)061<2133:ICOSWV>2.0.CO;2](https://doi.org/10.1175/1520-0469(2004)061<2133:ICOSWV>2.0.CO;2), 2004.

Ravishankara, A. R.: Water Vapor in the Lower Stratosphere, *Science*, 337, 809–810, <https://doi.org/10.1126/science.1227004>, 2012.

Rohs, S., Schiller, C., Riese, M., Engel, A., Schmidt, U., Wetter, T., Levin, I., Nakazawa, T., and Aoki, S.: Long-term changes of methane and hydrogen in the stratosphere in the period 1978–2003 and their impact on the abundance of stratospheric water vapor, *J. Geophys. 25 Res.*, 111, D14315, <https://doi.org/10.1029/2005JD006877>, 2006.

Rollins, A. W., Thornberry, T. D., Gao, R. S., Smith, J. B., Sayres, D. S., Sargent, M. R., Schiller, C., Krämer, M., Spelten, N., Hurst, D. F., Jordan, A. F., Hall, E. G., Vomel, H., Diskin, G. S., Podolske, J. R., Christensen, L. E., Rosenlof, K. H., and Fahey, D. W.: Evaluation of UT/LS hygrometer accuracy by intercomparison during the NASA MACPEX mission, *J. Geophys. Res. A*, 119, 1915–1935, <https://doi.org/10.1002/2013JD020817>, 2014.

30 Sander, S. P., Friedl, R. R., Barker, J. R., Golden, D. M., Kurylo, M. J., Wine, P. H., Abbatt, J. P. D., Burkholder, J. B., Kolb, C. E., Moortgat, G. K., Huie, R. E., and Orkin, V. L.: Chemical kinetics and photochemical data for use in atmospheric studies, JPL Publication 10-6, 2011.

Schiller, C., Grooß, J.-U., Konopka, P., Plöger, F., Silva dos Santos, F. H., and Spelten, N.: Hydration and dehydration at the tropical tropopause, *Atmos. Chem. Phys.*, 9, 9647–9660, <https://doi.org/10.5194/acp-9-9647-2009>, 2009.

Schwartz, M. J., Read, W. G., Santee, M. L., Livesey, N. J., Froidevaux, L., Lamert, A., and Manney, G. L.: Convectively injected water 35 vapor in the North American summer lowermost stratosphere, *Geophys. Res. Lett.*, 40, 2316–2321, <https://doi.org/10.1002/grl.50421>, 2013.

Shi, Q., Jayne, J. T., Kolb, C. E., Worsnop, D. R., and Davidovits, P.: Kinetic model for reaction of ClONO₂ with H₂O and HCl and HOCl with HCl in sulfuric acid solutions, *J. Geophys. Res.*, 106, 24 259–24 274, <https://doi.org/10.1029/2000JD000181>, 2001.

Smith, J. B., Wilmouth, D. M., Bedka, K. M., Bowman, K. P., Homeyer, C. R., Dykema, J. A., Sargent, M. R., Clapp, C. E., Leroy, S. S., Sayres, D. S., Dean-Day, J. M., Bui, T. P., and Anderson, J. G.: A case study of convectively sourced water vapor observed in the overworld stratosphere over the United States, *J. Geophys. Res.*, 122, 9529–9554, <https://doi.org/10.1002/2017JD026831>, 2017.

5 Solomon, S.: Stratospheric ozone depletion: A review of concepts and history, *Rev. Geophys.*, 37, 275–316, <https://doi.org/10.1029/1999RG900008>, 1999.

Solomon, S., Garcia, R. R., Rowland, F. S., and Wuebbles, D. J.: On the depletion of Antarctic ozone, *Nature*, 321, 755–758, <https://doi.org/10.1038/321755a0>, 1986.

Solomon, S., Borrmann, S., Garcia, R. R., Portmann, R., Thomason, L., Poole, L. R., Winker, D., and McCormick, M. P.: Heterogeneous chlorine chemistry in the tropopause region, *J. Geophys. Res.*, 102, 21411–21429, 1997.

10 Solomon, S., Kinnison, D., Garcia, R. R., Bandoro, J., Mills, M., Wilka, C., Neely III, R. R., Schmidt, A., Barnes, J. E., Vernier, J.-P., and Hoepfner, M.: Monsoon circulations and tropical heterogeneous chlorine chemistry, *Geophys. Res. Lett.*, 43, <https://doi.org/10.1002/2016GL071778>, 2016.

15 Spang, R., Günther, G., Riese, M., Hoffmann, L., Müller, R., and Griessbach, S.: Satellite observations of cirrus clouds in the Northern Hemisphere lowermost stratosphere, *Atmos. Chem. Phys.*, 15, 927–950, <https://doi.org/10.5194/acp-15-927-2015>, 2015.

Spang, R., Hoffmann, L., Müller, R., Groß, J.-U., Tritscher, I., Höpfner, M., Pitts, M., Orr, A., and Riese, M.: A climatology of polar stratospheric cloud composition between 2002 and 2012 based on MIPAS/Envisat observations, *Atmos. Chem. Phys.*, 18, 5089–5113, <https://doi.org/10.5194/acp-18-5089-2018>, 2018.

20 Thomason, L. W. and Peter, T., eds.: SPARC Assessment of Stratospheric Aerosol Properties, SPARC Report No. 4, WCRP-124, WMO/TD-No.1295, <http://www.atmosp.physics.utoronto.ca/SPARC/index.html>, 2006.

Thomason, L. W., Poole, L. R., and Deshler, T.: A global climatology of stratospheric aerosol surface area density deduced from Stratospheric Aerosol and Gas Experiment II measurements: 1984–1994, *J. Geophys. Res.*, 102, 8967–8976, <https://doi.org/10.1029/96JD02962>, 1997.

Thornton, B. F., Toohey, D. W., Tuck, A. F., Elkins, J. W., Kelly, K. K., Hovde, S. J., Richard, E. C., Rosenlof, K. H., Thompson, T. L., Mahoney, M. J., and Wilson, J. C.: Chlorine activation near the midlatitude tropopause, *J. Geophys. Res.*, 112, D18 306, <https://doi.org/10.1029/2006JD007640>, 2007.

25 Tilmes, S., Kinnison, D. E., Garcia, R. R., Salawitch, R., Canty, T., Lee-Taylor, J., Madronich, S., and Chance, K.: Impact of very short-lived halogens on stratospheric ozone abundance and UV radiation in a geo-engineered atmosphere, *Atmos. Chem. Phys.*, 12, 10945–10955, <https://doi.org/10.5194/acp-12-10945-2012>, 2012.

Toon, O. B., Maring, H., Dibb, J., Ferrare, R., Jacob, D. J., Jensen, E. J., Luo, Z. J., Mace, G. G., Pan, L. L., Pfister, L., Rosenlof, K. H., Redemann, J., Reid, J. S., Singh, H. B., Thompson, A. M., Yokelson, R., Minnis, P., Chen, G., Jucks, K. W., and Pszenny, A.: Planning, implementation, and scientific goals of the Studies of Emissions and Atmospheric Composition, Clouds and Climate Coupling by Regional Surveys (SEAC4RS) field mission, *J. Geophys. Res. A*, 121, 4967–5009, <https://doi.org/10.1002/2015JD024297>, 2016.

30 Trapp, R. J., Diffenbaugh, N. S., and Gluhovsky, A.: Transient response of severe thunderstorm forcing to elevated greenhouse gas concentrations, *Geophys. Res. Lett.*, 36, <https://doi.org/10.1029/2008GL036203>, 2009.

Visioni, D., Pitari, G., Aquila, V., Tilmes, S., Cionni, I., Di Genova, G., and Mancini, E.: Sulfate geoengineering impact on methane transport and lifetime: results from the Geoengineering Model Intercomparison Project (GeoMIP), *Atmos. Chem. Phys.*, 17, 11 209–11 226, <https://doi.org/10.5194/acp-17-11209-2017>, 2017.

35 Vogel, B., Feck, T., and Groß, J.-U.: Impact of stratospheric water vapor enhancements caused by CH_4 and H_2 increase on polar ozone loss, *J. Geophys. Res.*, 116, D05301, <https://doi.org/10.1029/2010JD014234>, 2011.

Vogel, B., Günther, G., Müller, R., Groß, J.-U., and Riese, M.: Impact of different Asian source regions on the composition of the Asian monsoon anticyclone and of the extratropical lowermost stratosphere, *Atmos. Chem. Phys.*, 15, 13 699–13 716, <https://doi.org/10.5194/acp-15-13699-2015>, 2015.

5 Vogel, B., Günther, G., Müller, R., Groß, J.-U., Afchine, A., Bozem, H., Hoor, P., Krämer, M., Müller, S., Riese, M., Rolf, C., Spelten, N., Stiller, G. P., Ungermann, J., and Zahn, A.: Long-range transport pathways of tropospheric source gases originating in Asia into the northern lower stratosphere during the Asian monsoon season 2012, *Atmos. Chem. Phys.*, 16, 15 301–15 325, <https://doi.org/10.5194/acp-16-15301-2016>, 2016.

von Hobe, M., Groß, J.-U., Günther, G., Konopka, P., Gensch, I., Krämer, M., Spelten, N., Afchine, A., Schiller, C., Ulanovsky, A.,
10 Sitnikov, N., Shur, G., Yushkov, V., Ravegnani, F., Cairo, F., Roiger, A., Voigt, C., Schlager, H., Weigel, R., Frey, W., Borrman, S., Müller, R., and Stroh, F.: Evidence for heterogeneous chlorine activation in the tropical UTLS, *Atmos. Chem. Phys.*, 11, 241–256, <https://doi.org/10.5194/acp-11-241-2011>, 2011.

Wales, P. A., Salawitch, R. J., Nicely, J. M., Anderson, D. C., Carty, T. P., Baidar, S., Dix, B., Koenig, T. K., Volkamer, R., Chen, D., Huey, L. G., Tanner, D. J., Cuevas, C. A., Fernandez, R. P., Kinnison, D. E., Lamarque, J.-F., Saiz-Lopez, A., Atlas, E. L., Hall, S. R., Navarro,
15 M. A., Pan, L. L., Schauffler, S. M., Stell, M., Tilmes, S., Ullmann, K., Weinheimer, A. J., Akiyoshi, H., Chipperfield, M. P., Deushi, M., Dhomse, S. S., Feng, W., Graf, P., Hossaini, R., Jöckel, P., Mancini, E., Michou, M., Morgenstern, O., Oman, L. D., Pitari, G., Plummer, D. A., Revell, L. E., Rozanov, E., Saint-Martin, D., Schofield, R., Stenke, A., Stone, K. A., Visoni, D., Yamashita, Y., and Zeng, G.: Stratospheric Injection of Brominated Very Short-Lived Substances: Aircraft Observations in the Western Pacific and Representation in Global Models, *J. Geophys. Res. A*, 123, 5690–5719, <https://doi.org/10.1029/2017JD027978>, 2018.

20 Ward, M. K. M. and Rowley, D. M.: Kinetics of the $\text{ClO} + \text{CH}_3\text{O}_2$ reaction over the temperature range $T=250\text{--}298\text{ K}$, *Phys. Chem. Chem. Phys.*, 18, 13 646–13 656, <https://doi.org/10.1039/c6cp00724d>, 2016.

Webster, C. R., May, R. D., Trimble, C. A., Chave, R. G., and Kendall, J.: Aircraft laser infrared absorption spectrometer (ALIAS) for in situ atmospheric measurements of HCl , N_2O , CH_4 , NO_2 , and HNO_3 , *Appl. Opt.*, 33, 454–472, <https://doi.org/10.1364/AO.33.000454>, 1994.

Weinstock, E. M., Smith, J. B., Sayres, D. S., Pittman, J. V., Spackman, J. R., Hintsa, E. J., Hanisco, T. F., Moyer, E. J., St Clair, J. M.,
25 Sargent, M. R., and Anderson, J. G.: Validation of the Harvard Lyman- α in situ water vapor instrument: Implications for the mechanisms that control stratospheric water vapor, *J. Geophys. Res. A*, 114, <https://doi.org/10.1029/2009JD012427>, 2009.

Werner, B., Stutz, J., Spolaor, M., Scalone, L., Raecke, R., Festa, J., Colosimo, S. F., Cheung, R., Tsai, C., Hossaini, R., Chipperfield, M. P.,
Taverna, G. S., Feng, W., Elkins, J. W., Fahey, D. W., Gao, R.-S., Hintsa, E. J., D., T. T., Lee Moore, F., Navarro, M. A., Atlas, E., Daube,
B. C., Pittman, J., Wofsy, S., and Pfeilsticker, K.: Probing the subtropical lowermost stratosphere and the tropical upper troposphere and
30 tropopause layer for inorganic bromine, *Atmos. Chem. Phys.*, 17, 1161–1186, <https://doi.org/10.5194/acp-17-1161-2017>, 2017.

WMO: Scientific assessment of ozone depletion: 2014, Global Ozone Research and Monitoring Project–Report No. 55, Geneva, Switzerland, 2014.

WMO: Scientific assessment of ozone depletion: 2018, Global Ozone Research and Monitoring Project–Report No. 58, Geneva, Switzerland, 2018.

35 Zafar, A. M., Müller, R., Groß, J.-U., Robrecht, S., Vogel, B., and Lehmann, R.: The relevance of reactions of the methyl peroxy radical (CH_3O_2) and methylhypochlorite (CH_3OCl) for Antarctic chlorine activation and ozone loss, *Tellus B*, 70, 1507391, <https://doi.org/10.1080/16000889.2018.1507391>, 2018.

Zhang, R., Jayne, J. T., and Molina, M. J.: Heterogeneous interactions of ClONO_2 and HCl with sulfuric acid tetrahydrate: Implications for the stratosphere, *J. Phys. Chem.*, 98, 867–874, 1994.